We would like to thank the editor, Dr. Corinna Hoose, and two reviewers. Your insightful comments helped improve this paper. A list of our response and the marked-up manuscript are given below. Referees' comments are in black, while our responses are written in Italic.

Response to anonymous Referee#1

General comment

This study examines characteristics of cloud phases in five, frequently occurring, overlapping configurations, over a wide area of southeast Asia. For this purpose, the authors use combined CloudSat-CALIPSO and MODIS data. The different cloud phases are examined in terms of their seasonality and relationship with meteorology, and frequency of occurrence. Their heterogeneity and spectral radiance characteristics are examined in combination with corresponding MODIS data. Associations with MJO and ENSO are also investigated.

The study is to a large extent comprehensive. The results are discussed adequately, and the findings combine verification of previously known characteristics of specific cloud phases/types and their combinations, with new insights over their future usefulness in field campaigns and GCM evaluations. For these reasons, I recommend acceptance of this manuscript for publication in ACP. I include a list of minor comments and technical corrections for the authors to consider.

Comments

Page 5, lines 25-28: it would be useful to report how often these "multi-layer, same phase" vertical structures occur, and discuss possible consequences of this simplification.

Thanks for this great question.

*First, the multi-layer, same-phase clouds occur much less frequently than one-layer cloud (see figure below). For example, **for the ice-only clouds**, the total frequency is 28.6% composed by 20% one-layer and 8.6% multi-layer cloud. **For the ice clouds above liquid clouds**, one-layer ice cloud frequency is 13.8% and multi-layer ice cloud frequency is 6.4%. Similarly, for **the liquid-only cloud** (total frequency ~16%), one-layer liquid cloud is 14.0% and multi-layer liquid cloud is only 2%.*

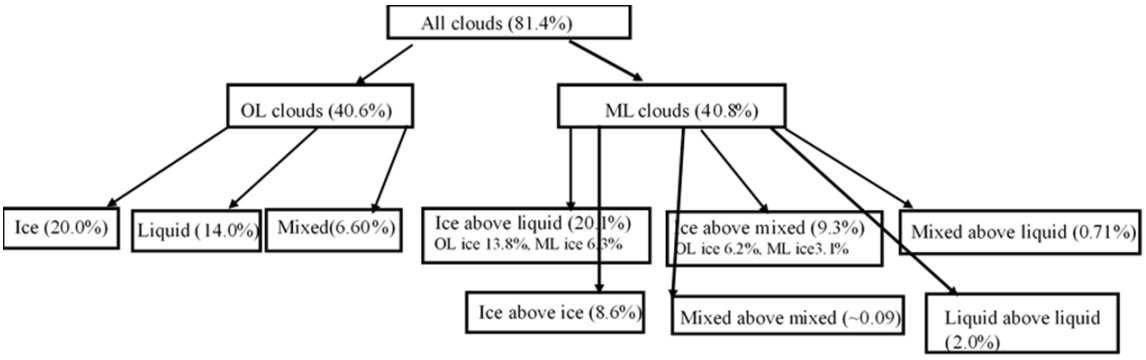

Fig. 1 cloud phase classification.

Second, though the frequency of multi-layer, same phase cloud is relatively small, we have carefully examined the biases due to our simplified classification to cloud distributions, cloud spatial heterogeneity and spectral radiative features. For example, the distributions (Fig. 2) of one-layer and multiple-layer ice clouds above liquid clouds are similar, i.e. relatively large frequency of multiple-ice clouds occurs where frequent one-layer ice clouds occur.

Third, to further check the bias to spatial heterogeneity and radiation, we have selected 10-days data in January 2007 to compare the difference between the one-layer and multiple-layer, same phase clouds. Figure 3 shows the results for ice-above-liquid clouds – the multi-layer ice cloud above liquid cloud moves the PDF a little off that of all-cloud, but the bias is small and doesn't change our analysis.

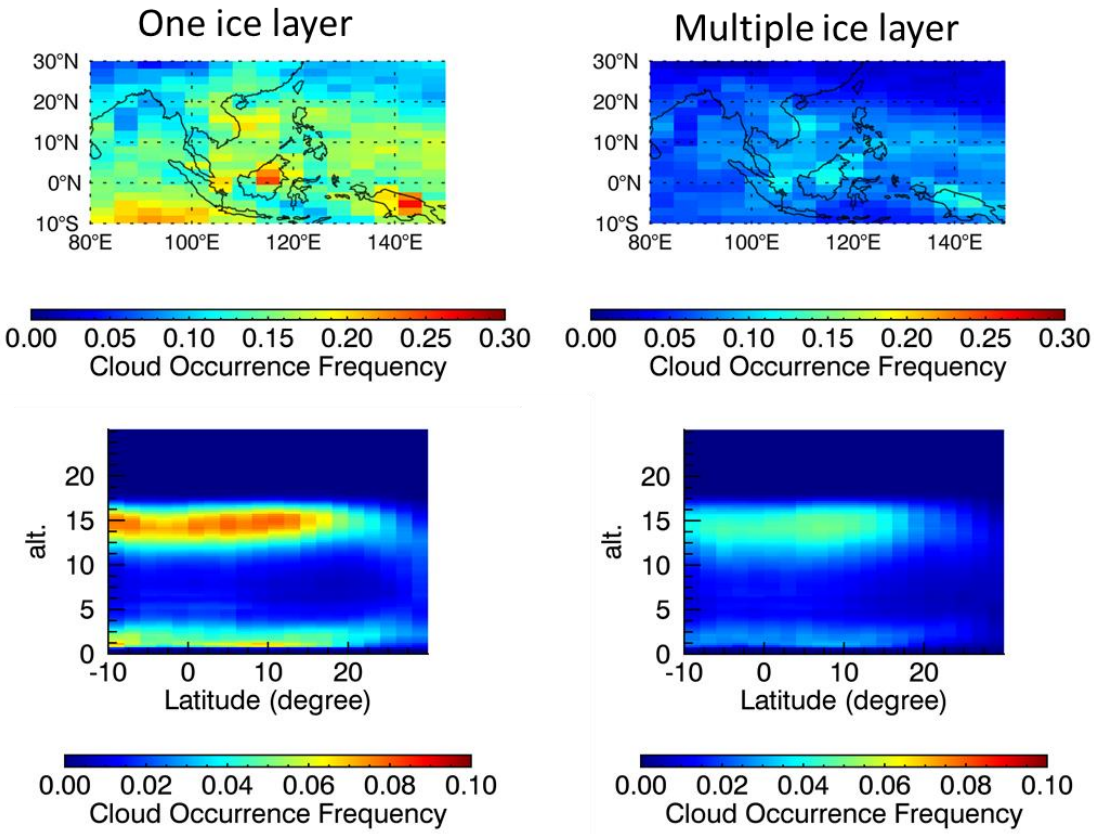

Fig.2 Distributions of ice-above-liquid clouds decomposed to two cases: one-layer ice cloud above liquid cloud (first column) and multiple-layer ice clouds (second column) above liquid clouds.

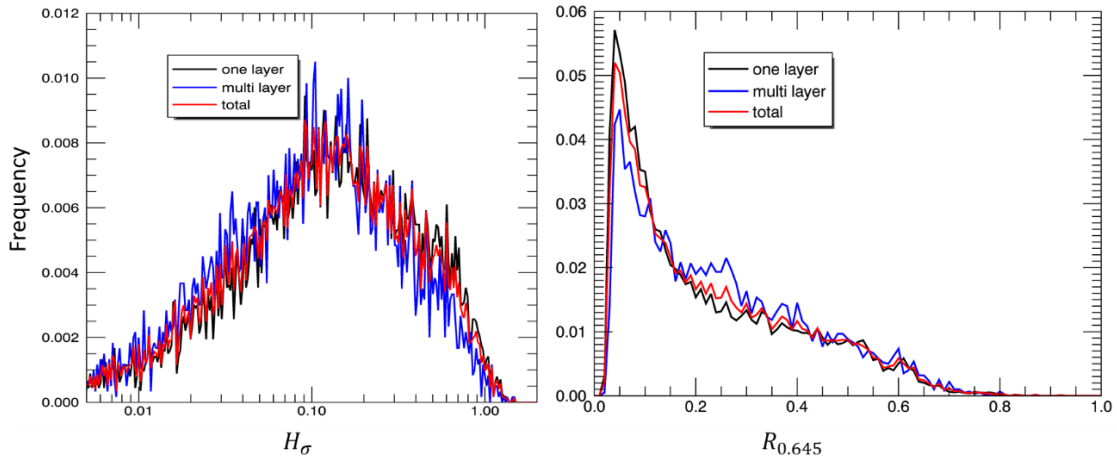

Fig. 3 H_σ *and* $R_{0.645}$ *PDF for ice-above-liquid clouds: black for one-layer ice cloud above liquid cloud, blue for multi-layer ice cloud above liquid cloud and red for all ice-above-liquid cloud.*

We have responded by summarizing these finding in Sect. 2.2 (Page8, Lines 40-41 and, Page 8, Lines 1-7 in revised version) and by adding the following statements and with appropriate additions to Table 3:

'As stated in Sect. 2.2, we classify clouds according to cloud phase and cloud layer in five main groups: ice-only, liquid-only, mixed-only, ice-above-liquid, ice-above-mixed clouds. Each group contains both single and multiple layers of the same phase. Our analysis (Table 3) shows that one-layer-one-phase clouds have much larger frequency than multi-layer-same-phase clouds. For example, multi-layer ice-only cloud (~8.6%) occurs less frequently than one-layer ice-only cloud (20%). Liquid-only clouds mostly form in a single layer (14%) and the frequency of multi-layer liquid-only cloud is only 2%. A careful comparison between single and multiple layers of the same phase clouds shows no significant difference in the properties that we're interpreting, which justifies our simpler classification.'

Page 6, lines 24-25: I don't understand how MODIS detects less clear-sky cases than CC by missing some cloudy cases. Shouldn't it be the other way around?

Yes, you're correct. MODIS detects more clear sky than CC. As displayed in Table 2, MODIS clear sky samples are 4 623 583 (32%), while CC clear sky samples are 2 587 635 (17.9%).

Now in Page 6, Lines 20-22, it is corrected as:

'We also found that 29% of CC ice-only clouds are reported as clear sky by MODIS, indicating that MODIS misses some thin cirrus in the SEA region – a point also made in Reid et al. (2013).'

Figure 5: this figure is hard to read. Please consider replacing with 2D plots.

As suggested, Figure 5 is replaced with 2D plots.

Page 16, lines 26-27: how is the frequency of occurrence related to the average reflectance? Shouldn't they be thicker to have higher R?

The averaged reflectance is not weighted by occurrence frequency, and thus you're right that thicker clouds have higher R.

Now in Page 13, Lines 30-32, it is modified as:

'The averages of the reflectance and the brightness temperature (BT) (not weighted by cloud occurrence frequency) for each cloud group are shown over SEA.'

Page 18, lines 25-27: it is hard to verify this statement based on Fig. 14d. For example, ice-above-liquid after 07/08 does not agree well.

Thanks for this comment. We have updated our results using the up-to-date CC data (R05), which show better cloud phase variation with ENSO. To verify this statement, we calculate the correlation coefficient between MODIS ice cloud anomaly and CC ice-only, ice-above-liquid, ice-above-mixed and mixed-only clouds, respectively. Results show that the CC 'ice-contained clouds' are well correlated with MODIS ice clouds as listed in the following table:

	Ice-only	*Ice-above-liquid*	*Ice-above-mixed*	*Mixed-only*
Coefficient correlations with MODIS ice cloud	*0.7*	*0.75*	*0.86*	*0.72*

Original statement: 'The MODIS ice cloud anomaly agrees with that of ice-only, ice-above-liquid, ice-above-mixed and mixed-only clouds from the CC observations (Fig. 14d), because most of these CC clouds are reported to be ice by MODIS (Table 2).'

Now in Page 17, Lines 28-30, it is revised as:

'The MODIS ice cloud anomaly correlates well with that of CC ice-only, ice-above-liquid, ice-above-mixed and mixed-only clouds (Fig. 14d) with correlation coefficients greater than 0.70 (significant at 99% confidence level).

Page 18, lines 29, 30: what is considered "abnormal" in the heterogeneity index variation?

We call the positive (negative) anomaly as abnormally high (low). To avoid this confusion, we discard the wording 'abnormal' and rephrase our results accordingly.

For example, the original statement "H_σ is observed to be abnormally small in La Niña year due to the increase of 'ice-contained clouds' and abnormally large in El Niño year because of decreased 'ice-contained clouds and the expose of liquid clouds",

Now in Page 17, Lines 32-34, it is revised as:

'H_σ anomaly is observed to be negative in La Niña year due to the increase of 'ice-contained clouds' and positive in El Niño year because 'ice-contained clouds' decrease, exposing more liquid clouds.'

Page 19, line 41: "where are relatively cold". Are you referring to the lower troposphere

conditions? Please clarify.

Yes, you're right.

It is now in Page18, Lines 38-40 corrected as:

'Liquid-only clouds appear frequently in winter and spring over southeast China and East China sea where the lower troposphere is relatively cold, dry and stable'

Figure 6: what are the vertical dashed lines?

Thanks for pointing out this issue. We now add the explanation in Figure 6 caption: The vertical dashed lines in a)-e) indicate the median values of the PDFs.

Figure 9: seasonality symbols are not clear. Please consider plotting differently or including a table.

The values of each symbols are now summarized in Table 5.

Page 2, line 14: "macrophyscial" should read "macrophysical".

Corrected

Page 2, lines 28-31: please consider rephrasing or breaking this long sentence.

Original statement: "Particularly, cloud radiative effects in the LW are reduced at the top of atmosphere (TOA) for high over low clouds compared to single-layer high clouds and much stronger than single-layer low clouds, which nicely demonstrates the importance of accurately representing cloud vertical structures in GCMs."

Now in Page 2, Lines 26-28, it is revised as:

'Particularly, the radiative effects at the TOA in the LW of high over low clouds are weaker than high clouds but much stronger than single-layer low clouds. These studies nicely demonstrate the importance of accurately representing cloud vertical structures in GCMs.'

Page 3, lines 8-9: do you mean "has not yet been examined"?

Yes, it is corrected.

Page 9, line 1: "cloud" should read "could".

Thanks, it is corrected.

Page 10, line 4: "summaries" should read "summarizes".
Thanks, it is corrected.

Page 11, line 22: “CLIPASO” should read “CALIPSO”.
Thanks, it is corrected.

Page 13, line 3: please omit “that”.
Corrected.

Page 13, line 42: “spatial” should read “spatially”.
Corrected.

Page 14, line 2: “it” should read “its”.
Corrected.

Page 14, line 35: “reflected” should read “reflective”.
Corrected.

Page 14, lines 42-43: do you mean “refractive index”?
Thanks for your correction. It is corrected.

Page 15, line 16: please consider replacing “aware” with e.g. “note that”.
As suggested, we replace ‘aware’ to ‘note that’

Page 16, line 25: “and thicker” should read “and they are thicker”.
Corrected.

Page 16, line 33: 0.546 should read 0.645.
Corrected.

Page 17, lines 18-20: please rephrase.

The original statement:

‘Area with small Hσ is surrounded by relatively large Hσ values, indicating the locations where occur suppressed MJO phase associated with more liquid clouds.’

Now in Page 16, Lines 16-18, it is revised as:

‘Areas surrounding the convective center are with relatively large H_σ values, indicating that the locations of suppressed MJO phase are associated with more liquid clouds.’

Page 17, line 22: please consider replacing “are with” with e.g. “display”.

Revised as suggested.

Page 17, line 24: “connective” should read “convective”.

Corrected.

Page 19, lines 13-14: please rephrase.

The original statement, 'As cloud phases vary interannually and hence change the spatial heterogeneity, i.e., being smoother in La Niña year than normal and vice versa in El Niño year.'

Now in Page 18, Lines 10-11, it is rephrased as:

Overall, the cloud phase varies interannually, as does H_σ , i.e., being smoother in La Niña years compared to El Niño years.

Page 19, line 15: "well correlates" should read "correlates well".
Corrected.

Page 20, line 18: "heterogenous" should read "heterogeneous".
Corrected.

Page 21, line 5: please replace "attribute" with "contribute".
Corrected.

Detailed response to reviewer #2' comments

In this paper, the authors investigate cloud properties as seen by different A-train satellites over the Southeast Asia. They further divide clouds into 5 cloud types as a function of their cloud phase and different overlapping possibilities among the cloud-type layers. In the last part of the manuscript, they study possible links between these 5 types and MJO and ENSO conditions. While the topic of this paper aligns with the scope of the journal, it is difficult to judge the novelty of the analysis since most of it is a kind of climatology rather than new results. However, I acknowledge a tremendous amount of work from the authors. Yet, the paper is too long and descriptive, which makes it difficult to follow. In addition to trimming the manuscript, I have a couple more concerns to address before recommending this paper for publication. A more detailed explanation is provided below.

The paper is indeed a climatological study, focusing on cloud phase characteristics. Since the climatological characteristics of cloud phase have not been addressed, the results are novel. The abstract highlights several of the new key results, and we note that Referee#1 commented on the novelty of our results. The length and descriptive nature of the manuscript is addressed below.

Main concerns
1) This paper is too long and descriptive. It is hard to follow and I often lost track of the goal of the sections. Every section should be reduced in size and I would recommend focusing on specific findings relevant to the topic of the study rather than describing every subplot of the figures as well as the behavior of each cloud types.
Thank you for this comment.
We have worked to reduce the length of most sections of the manuscript in response to this comment. We have also provided additional edits throughout the manuscript to improve

readability. In reducing the text, we did aim to let the figures and tables speak for themselves, but key findings from the figures do need to be discussed. We note that Referee#1 stated "The results are discussed adequately, …" so we tried to strike a balance between the referees' comments that are at odds with one another.

2) If I understand correctly there is no filtering of the data whatsoever to make them consistent with each other. I find this a little concerning. For example, in section 3.1.5 when comparing the spatial heterogeneity index with CloudSat-CALIPSO, all pixels are used including those where CC and MODIS cloud masks disagree. This may result in large biases as explained by the authors later on. It would be best to keep in the main analysis the pixels where CC and MODIS agree.

Thanks for this comment. We did examine this issue (results shown in figure below), and some of these issues are discussed in the paper (as noted by the reviewer), with results on CC and MODIS both being "clear" shown in Table 2. If we forced the analysis to be the same class consistency, then that leaves us vulnerable to carrying MODIS cloud detection and classification errors into our analysis, which we didn't want to do. The point is just to focus on CC classification as a function of H_σ, without the additional issues that MODIS cloud detection and classification would bring to the interpretation (i.e., discussion as to why the red and black curves look different below is entirely due to MODIS cloud detection and classification limitations—miss some thin or small clouds).

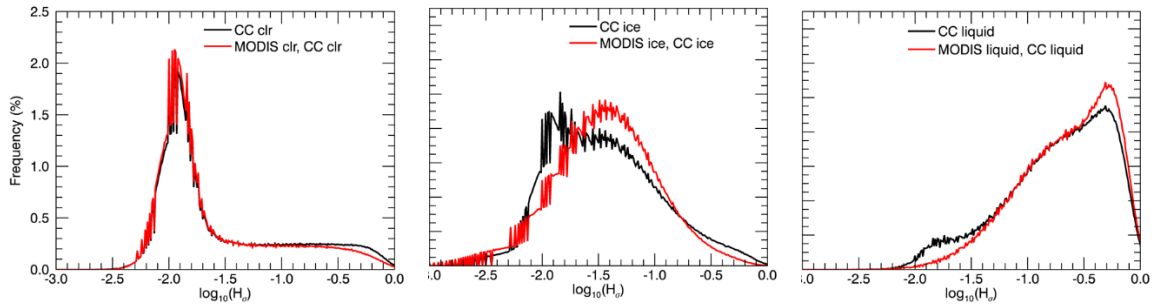

Fig. the H_σ *PDF for clear, ice and liquid cloudy skies: black for CC detections, and red for the samples agreed by both CC and MODIS.*

3) The authors use the version R04 of the 2B-CLDCLASS-LIDAR product. This version is not free of uncertainties in particular when it comes to detecting shallow cumulus clouds. It's been shown that this version overestimates the amount of shallow cumulus clouds (https://www.earth-syst-sci-data.net/11/1745/2019/essd-11-1745-2019.html). Similarly, nothing is said about any kind of uncertainty in the cloud phase retrieval of this product. For example, has this product been evaluated against other cloud phase dataset (ground-based, satellite or in situ?). I know that the cloud phase confidence considerably decreases when the lidar is totally attenuated and the decision tree only relies on the radar signal. I would suggest the authors to mention these at least.

Thanks for pointing us to the new version 2B-CLDCLASS-LIDAR data (R05), which was not available at the time of our original analysis.

1) We have updated all our results using Release 05 (R05) of both 2B-CLDCLASS-LIDAR and 2C-ICE. Compared to the R04 version, R05 shows more ice-only (0.8%↑), mixed-only (0.5%↑) and ice-above-mixed (1.9%↑) clouds, but less liquid-only (0.9%↓) and ice-above-liquid (0.8%↓) clouds in the Southeast Asia region (compare Table 3 in the revised and discussion paper). Also, the new 2B-CLDCLASS-LIDAR product displays a better interannual variations of cloud phase associated with ENSO (see subfigure in Fig. 14d between 07/08 and 07/09). Fortunately, the small changes didn't impact any of our conclusions.

2) We agree with the reviewer's concern on the uncertainties of the 2B-CLDCLASS-LIDAR cloud phase retrieval. Characterizing uncertainties in classification does require a truth to compare against, which doesn't exist for cloud phase. When such truths are lacking, the standard approach in validating cloud classification results is to validate the thresholds used in the classification algorithm (Rossow et al., 1989). The thresholds used in the classification algorithm for 2B-CLDCLASS-LIDAR cloud phase is discussed in Section 2.1 and references therein. Still, this doesn't achieve quantitative uncertainty characterization on cloud phase that a comparison to "truth" can give. To date, there are not any evaluation of the CC cloud phase against any other cloud datasets. This is why we performed a comparison of CC and MODIS cloud phase as shown in Table 2 and described in Sect. 2.3 in the paper. Overall, most of CC ice-only, ice-above-liquid, ice-above-mixed and mixed-only clouds are reported to be ice by MODIS, and most of CC liquid-only clouds are also detected to be liquid by MODIS. This comparison allows us to better interpret our results in later sections (e.g., Sect. 3.1.6 and Sect. 3.3).

3) We agree that when lidar signal is totally attenuated, confidence level of cloud phase is lowered down. We mention this information in Page 4, Lines 34-35.
'When the lidar signal is totally attenuated, the cloud phase is determined only by Ze and temperature, which lowers down the confidence level.'

4) Finally, the authors consistently mention that their results could be used for model evaluation but fail to explain how. I understand it is tempting to sell any observational result as a possible constraint for model, but if the authors want to do so, they need to explain how and why, which is not done here.

In the paper (Page20, L12-24), we added the following paragraph to make the model-observation comparison clearer.

"Finally, we note that our results may be used to evaluate a model's verisimilitude in capturing cloud properties, particularly phase and spectral characteristics. For example, we show summaries of spectral radiance at the TOA segregated by cloud phase and overlap conditions that can serve as a basis for comparing to those computed from model outputs—a similar approach given by previous research (Hashino et al., 2013; Masunaga et al., 2010; Yao et al., 2020). Since these models also use the plane-parallel assumption in computing the spectral radiation leaving the TOA, careful comparisons between model and observations can use $H\sigma$ as

a measure of departure from the plane-parallel assumption in a manner similar to (Loveridge and Davies, 2019)*, where they used Hσ within their analysis in examining GCM clouds in different sectors of southern hemisphere cyclones. The use of Hσ also extends its application to gauge biases in other satellite products used in model evaluation (e.g. Gettelman et al., 2015; Song et al., 2018), such as cloud optical depth and effective radius, since biases in these products have been noted to covary with H_σ(Fu et al., 2019; Zhang et al., 2016).”*

Minor comments
Throughout the manuscript, the authors use plural with the term cloud phase, I feel like most of the time, it would be better to use singular.

As suggested, we correct the ‘cloud phases’ to ‘cloud phase’ in most places.

P2 L35: improve GCM performance => improve climate simulations

Corrected.

P4 L8: in the lower troposphere => below 8 km

We change the statement as ‘in the lower troposphere (i.e. below 8.2 km)’

P4 L8: in the upper troposphere => above 8 km

We change the statement as ‘in the upper troposphere (i.e. above 8.2 km)’

P4 L21: Please specify the version. From your table, I believe you use the version R04.

Data version is added and now all results are updated using R05 data.

P4 second paragraph: You don’t describe how the algorithm works when the lidar signal is completely attenuated. The cloud phase is then based only on Ze and T thresholds, which substantially decreases its confidence level. Since the region under study is dominated by convective clouds, this situation may occur very often.

Yes, it is true that Ze and T threshold is used to deduce cloud phase in the radar-only region, which could lower down the confidence level.

This information is mentioned in Page 4, Lines 34-35 in the revised paper:

‘When the lidar signal is totally attenuated, the cloud phase is determined only by Ze and temperature, which lowers down the confidence level.’

P8 L13: I don’t understand the unit of LTS, it’s supposed to be in K (or ËŽC).

The unit of LTS depends on how to define it. We define static stability same as Frierson and Davis, (2011) and Li et al. (2014), i.e., $\frac{\partial \theta}{\partial z}$, which has the unit of K/km, while in some other studies such as Klein and Hartmann, (1993), they used the definition of $\Delta\theta = \theta(p = 700mb) - \theta(p = sea\ level\ pressure)$, whose unit is K.

To avoid the confusion, in Page 8, Lines 1-3, we have revised the text as:

'The lower-troposphere static stability (LTSS=$(\theta_{z=3\ km} - \theta_{z=0})/3\ km$) and the upper-troposphere static stability (UTSS = $(\theta_{z=tropopause} - \theta_{z=tropopause-3\ km})/3\ km$) are shown in Figs 2d1-d4, where the θ is potential temperature in unit of K.'

P8 L18-23: The CLDCLASS-LIDAR product provides a cloud fraction (between 0 and 1) per layer so how do you get cloud and sample numbers?

Whenever the lidar cloud fraction within a radar volume is reported to be greater than zero, we count that radar sample as cloudy. The frequency reported in Figure 3 is the frequency of these samples.

To clarify this information, we now add the text in Page 4, Lines 17-18:

'This product reports the lidar cloud fraction that records how many lidar profiles are contained in a radar resolution'

and in Page 4, Lines 39-40:

'Four years of 2B-CLDCLASS-LIDAR data, version P1_R05 (2007-2010) with lidar cloud fraction greater than zero are used.'

P8 L25: Large => large
Corrected.

Fig. 3: why do you use this particular cross section rather than a zonal mean.

We have updated the results using the zonal mean.

P8 L41: "Also: : : of cirrus". Why do you mention MISR here out of the blue? Also this sentence is confusing.

We have deleted these statements to get rid of the confusion.

P9 L1: Can you elaborate on this statement? DO you mean for that region?

The original statement: " Low-level clouds cloud have a high chance to be covered by the upper ubiquitous ice clouds (Yuan and Oreopoulos, 2013), which is further quantified in next section."

To make this clear, it has been revised in Page 8, Lines 36-38,

'As shown in Yuan and Oreopoulos, (2013), low-level clouds have a high chance to be overlapped by upper clouds in the warm pool region. In the next section, we will examine cloud overlap with a focus on cloud phase.'

P9 L19: Confusing sentence.

The original statement: "However, liquid-only clouds have very small frequencies (< 10%) between 10°S-10°N where widely distribute ice clouds, which indicates that liquid clouds occurring here are likely being covered by ice clouds, hence, they are grouped as ice-above-liquid cloud class."

Now in Page 9, Lines 19-21 , it is rephrased to make in clearer:

'Elsewhere, liquid-only clouds have very small frequencies (< 10%). The annual mean frequency of liquid-only cloud is ~16.0%.'

P11 L13: This should appear in the data section along with the other uncertainties related to the datasets.

As suggested, we mention these uncertainties due to instrument limitations in Sect. 2.1 (Page 4, Lines 35-37), where we describe the 2B-CLDCLASS-LIDAR data.

'Also, in cases of thick ice clouds attenuating lidar signals over shallow liquid clouds that are missed by the radar, only ice clouds are reported in the profiles. Biases due to instrument limitations are kept in mind in our analysis.'

P11 L22: CLIPASO => CALIPSO
Corrected.

P11 L22: attenuated by clouds with optical thickness greater than 3.
It is revised as suggested.

P12 L14: spatial => spatially
Corrected.

P12 L26: "due to the small optical thickness of the.."
It is revised as suggested.

P12 L27: It's unclear to me why the authors constantly refer to MISR for no reasons since MISR observations are used in this study.
Thanks for pointing out this. In the new version, we remove the contents related to MISR to avoid the confusion.

P12 L36: This sentence needs re-wording.

Original statements: "While these clouds are locally homogenous, hence favoring the plane-parallel assumption in radiation computation (Ham et al., 2015)."

Now in Page 12, Lines 18-19, it is revised as:

'These clouds are locally homogeneous and hence favor the plane-parallel assumption in radiation computation.'

P13 L1-2: I would strongly recommend excluding pixels in which CC and MODIS disagree in the main figures rather than only mentioning it as "not shown".

Comment addressed earlier.

P13 L2-4: There is no main verb in this sentence, please re-word.
Also, are you referring to shallow cumulus clouds? In this case it would be rather easy to validate your hypothesis by focusing on a shallow Cu dominated region, such as the Barbados. However, depending on the MODIS product used, Pincus et al 2012 reported that a substantial amount of these clouds (partially-filled pixels) are excluded of the cloud product. Another important thing to note is that, R04 over-estimate shallow Cu cloud fraction (see main concern comments).

1) Original statement:

"Indeed, many small liquid clouds with size ranging in a few tens to hundreds of meters (e.g., Koren et al., 2008) that are difficult to be measured by MODIS as reported in Zhao and Di Girolamo (2006)."

Now in Page 12, Lines 27-29

'Indeed, many small liquid clouds with size ranging in a few tens to hundreds of meters can go undetected by MODIS (Zhao and Di Girolamo 2006).'

2) Here, we are referring to small and shallow cumulus clouds undetected by MODIS--with their sizes smaller than 1 km. Pixels containing these small clouds could be reported to be clear by both CC and MODIS due to their relatively large spatial resolutions. To validate our hypothesis, we revisit the MODIS and Advanced Space Thermal Emission and Reflection Radiometer (ASTER) data (15 m resolution) used in Zhao and Di Girolamo (2006) over the tropical western Atlantic (Rain in Cumulus over the Ocean field campaign, near Barbados – check Fig. 1 in Rauber et al., (2007)). By excluding the MODIS clear sky pixels that contain ASTER reported clouds, i.e. a focus on MODIS-ASTER clear sky pixels, the long tail of the H_σ is strongly reduced (see the Cyan line in the following figure). This is consistent with our hypothesis that small liquid clouds contribute to the long tail of H_σ PDF.

To make this clear, now in Page 12, Lines 29-35, we have included the statements:

'We revisit the MODIS and Advanced Space Thermal Emission and Reflection Radiometer (ASTER) data (15-m resolution) used in Zhao and Di Girolamo (2006) over the tropical western

Atlantic. The long tail of Hσ PDF is significantly reduced, i.e. frequency change from 0.3% to 0.1% at Hσ ~ 0.1, when the ASTER data is applied to exclude the MODIS clear sky pixels that contain ASTER reported clouds. This further affirms that the undetected clouds in MODIS and CC clear sky pixels contribute to large Hσ values, which may impact at least 20% clear-sky samples whose Hσ > 0.1 (Figs. 7a,b)'

3) In terms of the concern on R04 data, we have updated our results with the R05 version data.

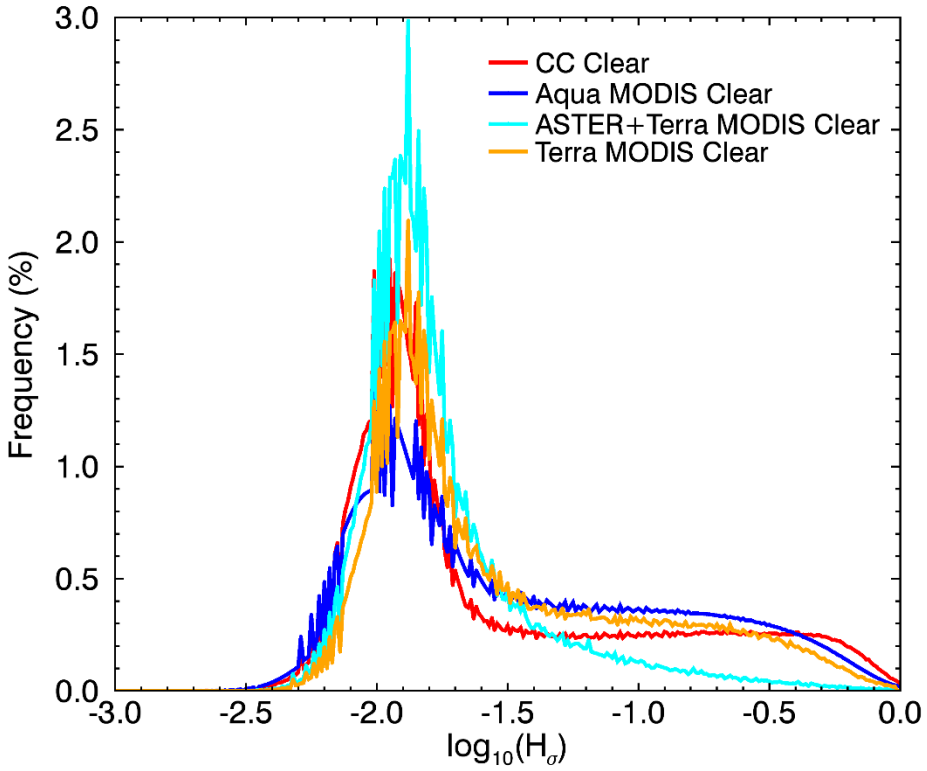

Fig. H_σ *PDF for clear skies obtained from CC and Aqua MODIS over Southeast Asia and from Terra MODIS and ASTER-Terra MODIS over the tropical western Atlantic region.*

P13 L33: Proves seems a bit strong.
We replace 'proves' as 'indicates'

P14 L35: reflecting
It is revised as 'reflective'.

P17: Why are you showing MJO phases? It's been documented in many many studies already. What does this bring to your study?

We agree that MJO is well documented in different aspects, including the related cloud type, radiative, dynamic and thermal dynamic characteristics. However, the cloud phase and the corresponding heterogeneity are less studied.

To make it clear, Page 15, Lines 40-43, we added the following statements:
'This section discusses the features of cloud phase associated with the intraseasonal 30-90 day MJO. Previous studies have provided full overviews of the radiative (in terms of OLR), dynamic and thermal dynamic characteristics of the MJO (Knutson et al., 1986; Riley et al., 2011; Wheeler and Hendon, 2004; Zhang, 2005). The purpose of this study is to focus on how the cloud phase characteristics discussed in previous sections vary with MJO phases.'

P17 L38: "suppressed"
It is corrected.

P18 L3: I don't understand the meaning of this sentence and I don't see how this could be used to validate climate models.

Original statement: 'Overall, the eastward-propagating H_σ patterns-a behavior similar to OLR pattern (e.g., Wheeler and Hendon, 2004), indicate that the H_σ could be useful for MJO studies such as serving as an observed-based parameter that are sensitive to cloud phase, to track MJO position and validate MJO simulations in climate models.'

Now in Page 17, Lines 4-6, it is revised as:
'The eastward-propagating H_σ patterns vary with MJO, indicating that H_σ could be useful for MJO studies, such as serving as an observed-based parameter to track the MJO position.'

P18 L8-20: It basically shows there are more convective clouds.

We remove the reflectance and brightness temperature from Fig. 13 and rewrite the whole paragraph to emphasize the heterogeneity variations (see Page 17, Lines 17-23).

P19 L13-14: Another sentence without meaning, please re-word.

Original statement:

'As cloud phases vary interannually and hence change the spatial heterogeneity, i.e., being smoother in La Niña year than normal and vice versa in El Niño year.'

In Page 18, Lines 10-11, It is revised as:

'the cloud phase varies interannually, as does H_σ , i.e., being smoother in La Niña years compared to El Niño years.'

P19 L36: "preferentially occur in"
It is revised as suggested.

P19 L38: occur => are
It is revised as suggested.

P21 L10: a comma is missing after ENSO L11.

It is corrected.

Overall, I would suggest rephrasing this sentence because I don't think the authors can claim the heterogeneity index captures MJO or ENSO. At best, it varies for the different ENSO/MJO phases, but it's definitely not well correlated. For the second part of the sentence, unless the authors explain how one could use this for model evaluation, I'd recommend to remove.

Original statement: "The observed H_σ values capture the MJO and ENSO features, implying that the Hσ is able to track MJO and ENSO and provides a way to validate their simulations in GCMs"

In Page 20, Line 6-7, the following sentence replaces the original statement:

'The observed Hσ varies with the ENSO index with a correlation coefficient of 0.49 (significant at confidence level 0.99).'

P21 L14-16: Here again, there is no tool to compare this to models, at least to the best of my knowledge, so unless the authors elaborate on this statement, they should remove this statement. I can envision a qualitative comparison of heterogeneity at best.

Addressed in point 4 above.

References

Frierson, D. M. W. and Davis, N. A.: The seasonal cycle of midlatitude static stability over land and ocean in global reanalyses, Geophys. Res. Lett., 38(13), 1–6, doi:10.1029/2011GL047747, 2011.

Fu, D., Di Girolamo, L., Liang, L. and Zhao, G.: Regional Biases in MODIS Marine Liquid Water Cloud Drop Effective Radius Deduced Through Fusion With MISR, J. Geophys. Res. Atmos., 124(23), 13182–13196, doi:10.1029/2019JD031063, 2019.

Gettelman, A., Morrison, H., Santos, S., Bogenschutz, P. and Caldwell, P. M.: Advanced two-moment bulk microphysics for global models. Part II: Global model solutions and aerosol-cloud interactions, J. Clim., 28(3), 1288–1307, doi:10.1175/JCLI-D-14-00103.1, 2015.

Hashino, T., Satoh, M., Hagihara, Y., Kubota, T., Matsui, T., Nasuno, T. and Okamoto, H.: Evaluating cloud microphysics from NICAM against CloudSat and CALIPSO, J. Geophys. Res. Atmos., 118, 7273–7292, doi:10.1002/jgrd.50564, 2013.

Klein, S. A. and Hartmann, D.: The seasonal cycle of low startiform clouds, J. Clim., 6, 1587–1606, doi:10.1175/1520-0442(1993)006<1587, 1993.

Li, Y., Thompson, D. W. J., Stephens, G. L. and Bony, S.: A global survey of the instantaneous linkages between cloud vertical structure and large-scale climate, J. Geophys. Res. Atmos., 119, 3770–3792, doi:10.1002/2013JD020669, 2014.

Loveridge, J. and Davies, R.: Cloud heterogeneity in the marine midlatitudes: Dependence on large-scale meteorology and implications for general circulation models, J. Geophys. Res. Atmos., 124, 3448–3463, doi:10.1029/2018JD029826, 2019.

Masunaga, H., Matsui, T., Tao, W. K., Hou, A. Y., Kummerow, C. D., Nakajima, T., Bauer, P., Olson, W. S., Sekiguchi, M. and Nakajima, T. Y.: Satellite data simulator unit: A multisensor, multispectral satellite simulator package, Bull. Am. Meteorol. Soc., 91(12), 1625–1632,

doi:10.1175/2010BAMS2809.1, 2010.
Rauber, R. M., Stevens, B., Ochs, H. T., Knight, C., Albrecht, B. a., Blyth, a. M., Fairall, C. W. and Jensen, J. B.: Over the ocean: The RICO campaign, Bull. Am. Meteorol. Soc., (December 2007), 1912–1928, doi:10.1175/BAMS-88-12-1912, 2007.
Rossow, W. B., Garder, L. C. and Lacis, A. A.: Global, Seasonal Cloud Variations from Satellite Radiance Measurements. Part I: Sensitivity of Analysis, J. Clim., 2(5), 419–458, doi:10.1175/1520-0442(1989)002<0419:gscvfs>2.0.co;2, 1989.
Song, H., Zhang, Z., Ma, P. L., Ghan, S. J. and Wang, M.: An evaluation of marine boundary layer cloud property simulations in the Community Atmosphere Model using satellite observations: Conventional subgrid parameterization versus CLUBB, J. Clim., 31(6), 2299–2320, doi:10.1175/JCLI-D-17-0277.1, 2018.
Yao, B., Liu, C., Yin, Y., Liu, Z., Shi, C., Iwabuchi, H. and Weng, F.: Evaluation of cloud properties from reanalyses over East Asia with a radiance-based approach, , 1033–1049, 2020.
Zhang, Z., Werner, F., Cho, H.-M., Wind, G., Platnick, S., Ackerman, A. S., Di Girolamo, L., Marshak, A. and Meyer, K.: A framework based on 2-D Taylor expansion for quantifying the impacts of subpixel reflectance variance and covariance on cloud optical thickness and effective radius retrievals based on the bispectral method, J. Geophys. Res. Atmos., 121, 7007–7025, doi:10.1002/2016JD024837, 2016.

Cloud Phase Characteristics Over Southeast Asia from A-Train Satellite Observations

Yulan Hong and Larry Di Girolamo

Department of Atmospheric Sciences, University of Illinois at Urbana-Champaign, Urbana, Illinois, USA

Correspondence to: Yulan Hong (yulanh@illinois.edu)

~~**Abstract.** This study examines the climatological characteristics of cloud phase over Southeast Asia (SEA) based on A-Train satellite observations. Using the combined CloudSat-CALIPSO (CC) data, five main cloud groups are investigated: ice-only, ice-above-liquid, liquid-only, ice-above-mixed and mixed-only clouds that have annual mean frequencies of 27.8%, 21.9%, 16.9%, 7.4% and 6.2%, respectively. Liquid-only clouds tend to occur in relatively cold, dry and stable environments. The other four cloud groups appear more frequently in relatively warm, humid and unstable conditions and their seasonal distributions move with large-scale climate systems: Asian monsoon and ITCZ. Liquid clouds are found to be highly inhomogeneous based on the heterogeneity index (H_{σ}) from Aqua MODIS, while ice-only and mixed-only clouds are often very smooth. Ice-above-liquid clouds are less inhomogeneous than liquid-only clouds due to the thin overlying ice clouds. Undetected subpixel liquid clouds enlarge clear sky H_{σ}, leading to some inhomogeneous clear sky pixels, which otherwise should be smooth. The reflectance at 0.645 ($R_{0.645}$) and brightness temperature at 11 μm (BT_{11}) of ice-only, liquid-only and ice-above-liquid clouds show peak frequencies near that of clear sky ($R_{0.645}$ ~ 0.02, BT_{11} ~ 294 K), implying that a large population of thin or subpixel clouds over SEA are difficult to see by MODIS. The CC data also show abundant thin clouds over SEA, which indicates 78.3% ice-only and 89.6% ice-above-liquid clouds with ice τ < 3. Mixed-only clouds in contrast are thick (top ~ 14 km), bright ($R_{0.645}$ ~ 0.61) and cold (BT_{11}~231K). The intraseasonal and interannual behaviors of all-sky H_{σ} and spectral signatures follow that of cloud phases and are able to track the MJO and ENSO phases. Climatologies of clouds over SEA provided in this study are useful for the evaluation of large-scale model simulations, as well as for the interpretation of cloud properties derived from passive satellite sensors in this region.~~

Abstract. This study examines the climatology of cloud phase over Southeast Asia (SEA) based on A-Train satellite observations. Using the combined CloudSat-CALIPSO (CC) data, five main cloud groups are investigated: ice-only, ice-above-liquid, liquid-only, ice-above-mixed and mixed-only clouds that have annual mean frequencies of 28.6%, 20.1%, 16.0%, 9.3% and 6.7%, respectively. Liquid-only clouds tend to occur in relatively cold, dry and stable lower troposphere. The other four cloud groups appear more frequently in relatively warm, humid and unstable conditions and their seasonal distributions move with the Asian monsoon and ITCZ. Liquid clouds are found to be highly inhomogeneous based on the heterogeneity index (H_{σ}) from Aqua MODIS, while ice-only and mixed-only clouds are often very smooth. Ice-above-liquid clouds are more heterogeneous than ice-only clouds owing to ice clouds being optically thin. We demonstrate that the distribution of clear-sky H_{σ} has a long tail towards heterogeneous values that are caused by undetected sub-pixel cloud within both CC and MODIS datasets. The reflectance at 0.645 ($R_{0.645}$) and brightness temperature at 11μm (BT_{11}) of CC ice-only, liquid-only and ice-above-liquid clouds show peak frequencies near that of clear sky ($R_{0.645}$ ~ 0.02, BT_{11} ~ 294 K), which explains why up to 30% of these CC cloud groups are classified as clear by MODIS. In contrast, mixed-only clouds are thick (average top ~ 13 km), bright (average $R_{0.645}$ ~ 0.6) and cold (average BT_{11} ~

Formatted: Line spacing: Multiple 1.08 li

234K). Cloud phase comparison between CC and MODIS reveals only modest agreement, with the best agreement (73%) occurring between CC ice-above-mixed and MODIS ice clouds. The intraseasonal and interannual behaviors of all-sky H_σ and spectral signatures follow that of cloud phase and vary with the MJO and ENSO phases. The climatology of cloud characteristics over SEA provided in this study may be used for evaluating large-scale model simulations, as well as in interpreting potential biases in satellite products derived from passive satellite sensors in this region.

Formatted: Font: (Asian) Times New Roman, 11 pt, Font color: Black

1. Introduction

Cloud phases and cloudtheir vertical structures are crucial to Earth's radiation budget (Hong et al., 2016; Li et al., 2011; Liou, 1986; Matus and L'Ecuyer, 2017; Oreopoulos et al., 2017), and insufficient knowledge in these areas has contributed to large uncertainties in current climate simulations. For instance, the simulated liquid and ice cloud amount and mass from global climate models (GCMs) show large discrepancies compared with observations, differing by orders of magnitudes in regions where clouds are ubiquitous such as the Western Pacific warm pool (Dolinar et al., 2014; Jiang et al., 2012; Kay et al., 2016; Waliser et al., 2009). The biases in modeled cloud properties are able to propagate and cause biases in other fields in the model, such as shortwave (SW) and longwave (LW) radiation (Li et al., 2013), sea surface temperature and precipitation (e.g., Grose et al., 2014). By examining cloud vertical structures, Cesana and Waliser (2016) found that most of the selected GCMs overestimate the frequencies of high-level clouds over tropical ocean and consistently underestimate low-level clouds. As a result, GCMs produce insufficient heating near the surface and slightly over heating near the tropopause (Cesana et al., 2018). A recent study by Berry et al. (2019) showed that the Community Atmosphere Model, version 5 (CAM5) is in good agreement with A-Train observation in terms of ice cloud radiative effect, though CAM5 generates more frequent ice clouds than satellite observations. These noted cloud and radiation biases ultimately point to an incomplete understanding of cloud phases, their vertical overlaps, and their interactions with large-scale circulations. Satellite observations continue to play important roles in furthering our understanding of cloud phases and vertical structures for future GCM evaluation (e.g. Cesana et al., 2019; Pincus et al., 2012).

The radar on CloudSat and the lidar on Cloud-Aerosol Lidar and Infrared Pathfinder Satellite Observations (CALIPSO) probing into atmosphere from space have offered unprecedented opportunities to explore cloud vertical details globally (Stephens et al., 2002; Winker et al., 2003). Using the combined CloudSat-CALIPSO (CC) observations, the vertical and horizonal structures of global hydrometeor have been first time shownexamined in Mace et al. (2009). More details of cloud characteristics including their macrophysicial properties such as cloud amount, heights and water mass, and microphysical properties such as effective radius (Re), and ice and liquid water content (IWC, LWC), have also been examined in many studies, including Eliasson et al. (2011) and Hong and Liu (2015) for ice clouds and Hu et al. (2010) for liquid clouds. With the enhancement of our understanding of different cloud phase properties, these studies have assisted to improve GCM simulations (Kay et al., 2016; Zhao et al., 2018). The CC data has also helpeds characterizeing cloud vertical overlaps, showing that multi-layer cloud occurrence frequency is greater than 50% in large-scale ascending regions such as the Western Pacific warm pool (Li et al., 2011; Matus and L'Ecuyer, 2017). Furthermore, Li et al. (2015) showed that cirrus, cumulus, altostratus and altocumulus tend to overlap with other cloud types. Oreopoulos et al. (2017) focused more on cloud altitudes by interpreting the overlap feature of high, middle and low clouds, revealing that the two most prevalent cloud classes

globally are single-layer low and high clouds (26% and 13.3%), respectively, followed by high over low clouds. Both Li et al. (2015) and Oreopoulos et al. (2017) showed distinct radiative effects between various cloud overlaps. Particularly, the~~cloud~~ radiative effects at the TOA in the LW of ~~are reduced at the top of atmosphere (TOA) for~~ high over low clouds are weaker than~~compared to single-layer~~ high clouds but ~~and~~ much stronger than single-layer low clouds. ~~,~~ These studies~~which~~ nicely demonstrate~~s~~ the importance of accurately representing cloud vertical structures in GCMs. Although vertical structures for clouds have been examined in traditional designations ~~(,~~ i.e. cloud types or cloud altitudes), ~~but not~~ cloud phase itself has not been used. Since ~~,~~ cloud phase has been demonstrated to be a sensitive parameter in GCMs that needs to be constrained (e.g., Cesana, 2016; Cesana and Storelvmo, 2017), improved ~~. Adding~~ knowledge of cloud phases and their overlaps will be beneficial to improve~~-~~ climate simulations~~GCM performance~~.

While cloud overlap or vertical heterogeneity is important in the radiative transfer, so is cloud horizontal heterogeneity (Marshak and Davis, 2005). It has long been demonstrated that the neglect of cloud horizontal heterogeneity with the plane-parallel assumption in radiative transfer can cause significant biases in computing irradiances and atmospheric heating rates (e.g., O'Hirok and Gautier, 2005), photolysis rates (e.g., Bouet et al., 2006), the emerging spectral and angular distribution of outgoing radiation field (Loeb and Davies, 1997; Song et al., 2016)~~(Loeb and Davies, 1997; Song et al. 2016)~~ and in retrieving cloud microphysical properties from passive sensors (Loeb and Davies, 1996; Marshak et al., 2006). Many studies have since examined, at least in part, the global nature of these biases by successfully associating them with measured local spatial heterogeneity in SW radiance (Di Girolamo et al., 2010; Ham et al., 2015; Liang et al., 2015). Zhang and Platnick (2011), for instance, found that the differences of the Moderate Resolution Imaging Spectroradiometer (MODIS) liquid cloud Re retrieved at 3.7 and 2.1 μm increase with heterogeneity for inhomogeneous clouds. To avoid the difficulty in interpreting satellite products whose biases co-vary with scene heterogeneity, focus on examining the spatial-temporal variability of the ~~raw~~ measured radiances in terms of their spatial heterogeneity and spectral signatures is a logical first step to understand Earth's climate systems – an approach that has successfully been carried out over the Terra satellite record over the globe (Zhao et al., 2016). However, the association of spectral and spatial heterogeneity signatures between different cloud phases and their overlap has not yet been examined, which may be possible if cloud phase can be accurately characterized from active space-based observations.

This study concentrates on cloud phase~~s~~ with an overall objective to investigate the characteristics of their climatology using the CC data with an emphasis on cloud phase overlap and the association with the spectral and spatial heterogeneity features from MODIS. We focus on South East Asia (SEA) because this region is strongly influenced by the Asian monsoon, the intertropical convergence zone (ITCZ) (As-Syakur et al., 2016; Hong and Liu, 2015), the Madden-Julian oscillation (MJO) and the El Niño-Southern Oscillation (ENSO). All of them influence cloud systems and ~~complicate~~ modulate cloud overlap structures. Also, current satellite products show wide ranging retrieval skills over SEA, in both aerosol and cloud properties, that are difficult to interpret (e.g., Reid et al., 2013). This has motivated several field campaigns in the SEA environment to better characterize aerosol, cloud properties and their interactions, including 7-SEAS (7-Southeast Asian Studies) in 2010 and 2013 (Lin et al., 2013; Reid et al., 2013) and ~~the~~ CAMP2Ex (Cloud and Aerosol Monsoonal Processes Philippines Experiment) in 2019 (white paper in https://espo.nasa.gov/CAMP2Ex_White_Paper). Enhancing our

understanding of cloud phase characteristics can help to interpreting satellite products and benefit future field campaign preparation in this area. In addition, cloud phase climatology is needed to reduced the large cloud and radiation biases in GCMs that have been noted over SEA (Cesana et al., 2018; Waliser et al., 2009). By fusing the CC-MODIS data, this study explores the following scientific questions:

1. What are the spatial patterns of cloud phases and their overlaps and how do these patterns relate to large-scale dynamics?
2. To what extent can do the spectral and spatial heterogeneity signatures tell the features ofcorrelate with cloud phases and their vertical internal overlap structures using the CC-MODIS observations?
3. How do cloud phase characteristics vary in at intraseasonal and interannual scales, i.e. their association with MJO and ENSO?

2. Data and Methodology

CloudSat, CALIPSO and Aqua are were operated together in the A-train satellite constellation, between May 2006 2XXX and Feb. 2018 YYY which is in a sun-synchronous orbit at an altitude of 705 km above Earth. The A-train is in a sun-synchronous orbit with an 's equator-crossing time is at around 1:30 pm in the daytime and 1:30 am at night. The tight orbit formation of these satellites allows the radar, lidar and MODIS to observe nearly the same point on Earth within 1 minute (Stephens et al., 2018), and thus a straightforward match between these instruments can be performed. The information of all data used in this study has beenis summarized in Table 1. The SEA region is delineated with latitudes between 10°S and 30°N and longitudes between 80°-150°E.

2.1. The Combined CloudSat-CALIPSO Data

Launched in June 2006, the CloudSat satellite carries a cloud profiling radar operated at 94 GHz with a minimum sensitivity of -28 dBZ (Stephens et al., 2002, 2008). The radar's vertical resolution is 480 m but resampled to 240 m, while its horizontal resolution is 1.8 km along track by 1.4 km cross track. The radar is able to penetrate thick clouds but misses optically thin clouds and shallow clouds lower than 1 km altitude (Stephens et al., 2008). The lidar onboard CALIPSO launched in April 2006 has vertical and horizontal resolutions of 30 m and 333 m in the lower troposphere (e.gi.e., below 8.2 km), and 60 m and 1 km in the upper troposphere (e.gi.e., above 8.2 km) (Winker et al., 2003). The lidar operates at 532 and 1064 nm and is suitable to detect optically thin clouds and aerosols, but its signal is easily attenuated, which limits its ability to penetrate optically thick clouds and to detect anything below. Nevertheless, the lidar has distinct advantages in detecting liquid clouds because 1) the backscattering (β_c) from water droplets is much less depolarized than that from ice particles and 2) water layers produce strong lidar returns that attenuate rapidly with altitude at cloud top (Hu et al., 2009; Wang and Sassen, 2001). In cases where thin clouds at any altitudes or shallow clouds near Earth's surface are missed by CloudSat, the CALIPSO lidar can detect these clouds if the lidar attenuation above these clouds is sufficiently small. Thus, combining CloudSat and CALIPSO is advantageous for detecting a wide range of cloud scenarios.

To utilize the complementary features of the CloudSat radar and the CALIPSO lidar, the CloudSat Data Processing Center provides a combined radar and lidar cloud classification product, known ascalled 2B-CLDCLASS-LIDAR (Wang, 2019). This product reports the lidar

cloud fraction that records how many lidar profiles are contained in a radar resolution. The cloud top and base heights are also reported for up to five layers in the CloudSat pixels. The cloud layer here extends from cloud top to its base, and the vertical space between two layers is more than 500 m (Sassen and Wang, 2008). Each cloud layer is assigned one thermodynamic phase, either liquid, ice or mixed. The 2B-CLDCLASS-LIDAR algorithm utilizes cloud top and base temperatures from reanalysis as a first cut for cloud phase determination. -If cloud base temperature is lower than -38.5°C, this cloud layer is regarded as ice phase. Liquid phase is determined if cloud top and base temperatures are greater than 1° and -4°C, respectively. While in the temperature range (-40° - 0°C) where supercooled and mixed clouds would exist, potential liquid layers are first located using the feature of strong vertical gradient in lidar signals near liquid tops. If a liquid layer is detected by the lidar, the radar reflectivity factor (Ze) is further adopted to discriminate supercooled liquid from mixed cloud because Ze in mixed cloud is primarily contributed by ice particles. Temperature dependent Ze thresholds were generated to judge whether ice particles occur in the cloud layer with lidar detected liquid phase~~layer~~ (Fig.2 in Zhang et al. (2010)). When the maximum Ze of the cloud layer is greater than the given threshold, the layer will be classified as mixed cloud, otherwise, it is classified as liquid cloud. When the lidar signal is totally attenuated, the cloud phase is determined only by Ze and temperature, which lowers down the confidence level. Also, ~~some~~in cases ~~such~~of ~~as~~ thick ice clouds ~~that~~ attenuatinges lidar signals over shallow liquid clouds that are missed by the radar, ~~are reported to exist~~ only ice clouds are reported in the profiles. Biases due to instrument limitations are kept in mind in our analysis.

~~Regardless~~Despite these ~~of~~ limitations, the 2B-CLDCLASS-LIDAR product provides the most comprehensive cloud phase and overlap information ~~b~~Because of the combined sensitivity of the radar to thick clouds and the lidar to thin and liquid cloudsto date~~, the vertical resolved cloud phase retrievals encompass a wide coverage of cloud thickness that range from subvisual cirrus to deep convective clouds~~. ~~The cloud phase is also used to classify cloud types (e.g., cirrus, cumulus, stratocumulus etc.) within the 2B-CLDCLASS-LIDAR product (Wang, 2019), and used for downstream CloudSat product to retrieve cloud microphysical properties (Deng et al., 2010).~~and thus this product ~~The merged CC cloud phase product is suitable for the objective of this study to characterize the overlap features of all detected cloud phases.~~ Four years of 2B-CLDCLASS-LIDAR data, version P1_R05 (2007-2010) with lidar cloud fraction greater than zero are used.

The CloudSat level-2C ice cloud property product (2C-ICE) is also used. This product~~and~~ provides ice cloud optical (extinction coefficient in the visible) and microphysical (IWC and Re) properties retrieved from combined CC measurements (Deng et al., 2010). The 2C-ICE algorithm first identifies ice clouds based on the cloud layer and phase from 2B-CLDCLASS-LIDAR. The vertical profiles of Re and IWC are retrieved based on an optimal estimation framework that minimizes a cost function linking the observed and estimated lidar backscatter and Ze via Gauss-Newton iteration. To retrieve ice cloud properties, a modified gamma particle size distribution is adopted. To estimate lidar backscatter and Ze, parameterization of ice habits from Yang et al. (2000) is employed. The 2C-ICE product was evaluated in Deng et al. (2013) by comparing ice cloud properties to field campaign measurements. It was found that the flight-measured to 2C-ICE retrieved Re ratio is about 1.05 and the extinction coefficient ratio is about 1.03, hence suggesting excellent consistency between 2C-ICE retrievals with in-situ

observations. In this study, we integrate the retrieved extinction coefficient profile over depth of the ice layer to obtain ice cloud optical depth (τ). 2C-ICE data (R05) from 2007-2010 is used.

Meteorological data is also adopted to interpret the environment for different cloud phases. Temperature, wind and moisture are from the CloudSat's European Center for Medium-Range Weather Forecasts auxiliary product (ECMWF-AUX, 2007-2010), which interpolates the ECMWF variables to each CloudSat profile (Cronk and Partain, 2017).

2.2. CC Profile Classification

The CC profiles that contain clouds are classified into five groups (Fig. 1), according to the cloud layer and thermodynamic phase information from the 2B-CLDCLASS-LIDAR product. The first group is ice-only cloud which refers to only ice phase identified in the profile. When ice layers occur above liquid layers, we classify the profile as ice-above-liquid cloud. Similarly, mixed-only, liquid-only and ice-above-mixed clouds are classified, respectively. We do not focus on liquid- above- ice, mixed- above- ice, mixed- above- liquid or liquid- above- mixed clouds, collectively referred to as 'other clouds', due to their low frequencies (~0.746%-) over SEA ~~(~0.6% in total over SEA)~~. Note that one cloud phase in each cloud category may contains ~~both single and~~ multiple layers of the same phase. For example, for ice-above-liquid group, there could be more than one ice or liquid layers. While we quantify the frequencies of same-phase overlaps in Sect.~~ion~~ 3.1.3, ~~However, the multi-layer and same-phase clouds occur much less frequently than the one-layer clouds, and these clouds don't harm the results presented in this study, and thus our~~Thisthe majority of our analysis groups them into one of the classes listed above to simplify the ~~classification~~number of classifications to work with. ~~Thus W~~we lo~~o~~se some ~~method simplifies the~~ intricate cloud vertical structures, but still ~~catches~~ capture the main features of cloud phase overlap.

2.3. The Aqua MODIS Data

The Aqua satellite, launched in May 2002, carries MODIS. MODIS has 36 discrete spectral bands, ranging from 0.415 to 14.235 μm, with spatial resolutions varying between 250 m to 1 km (Barnes et al., 1998; King et al., 1992; Platnick et al., 2003). To allow collocating CC and MODIS pixels, the MYD03 product, which includes longitude, latitude, solar zenith angle and land/sea mask, is used to obtain MODIS geolocation information. The nearest MODIS 1 km resolution pixels are assigned to the CC data from 2007-2010. The distance of the collocated CC-MODIS pixels is usually smaller than 700 m, allowing them to observe nearly the same- cloud less than a minute apart~~objectives~~. ~~No other resampling step is performed.~~ ~~Biases~~Uncertainties due to ~~dDifferences in the sensitivities and instantaneous fields of view of the instruments~~collocation are kept in mind during the analysis.

To investigate the spectral signatures of different cloud phases, the MODIS Collection 6.1 level 1B calibrated radiance data (MYD021KM) is used. The bands selected in this research have center wavelengths at 0.645, 1.375, 1.64, 2.13, 8.55 and 11.03 μm.~~, which are commonly used to distinguish cloud phase from space (e.g., Marchant et al., 2016).~~ Ice crystals are more absorptive at the shortwave infrared (SWIR) (e.g., 1.64, 2.13 μm) than liquid droplets and thus ice clouds have smaller reflectance (R) at the TOA; whereas ice and liquid clouds are about equal in reflectance ~~R at~~in the visible (0.645 μm) for the same cloud optical depth and particle size – this ~~, which~~ forms the basis for cloud optical and microphysical retrievals and cloud phase classification for MODIS (Marchant et al., 2016). $R_{1.375}$ depends on cloud optical thickness and

the amount of water vapor above the cloud, since 1.375 μm lies at the center of a strong water vapor absorption band. If cloud top is at a low altitude, the solar photons at 1.375 μm will be largely absorbed by water vapor above cloud leading to near-zero $R_{1.375}$ (Marchant et al., 2016). In the IR, we convert the radiances of 8.55 and 11.03 μm to brightness temperature (BT). $BT_{8.5}$, BT_{11} and the difference between $BT_{8.5}$ and BT_{11} (BTD) are sensitive to cloud top temperature, thickness and phases (Baum et al., 2012).

The MODIS level Level 2 cloud product (MYD06) provides cloud phase information identified according to three different IR channel pairs, i.e. 8.5 and 11 μm, 11 and 12 μm, and 7.3 and 11 μm, known as the IR-only algorithm (Baum et al., 2012). The product contains three cloud phases: ice, water and undetermined (see details in Baum et al. (2012)). Cho et al. (2009) evaluated Collection 5 CX.X MODIS IR-only cloud phase using CALIPSO observations. They found that agreements of MODIS to the CALIPSO top layers are 64% and 34.7% respectively for CALIPSO detected liquid and ice clouds over the globe. We revisited the comparisons of the latest version of MODIS IR-only cloud (C6.1, complete on Mar. 2018) to the CC cloud phase (Fig. 1) over SEA in a similar way as Cho et al. (2009). About 665% CC liquid-only clouds agree with MODIS liquid clouds, which is similar to the global results of Cho et al. (2009). About 62% of CC ice-only clouds are reported to be ice by MODIS over SEA, agreeing better than the global results of Cho et al. (2009). In addition, most of CC ice-above-liquid (556%), ice-above-mixed (734%) and mixed-only clouds (6571%) are reported to be ice phase by MODIS. We also found that 291% of CC ice-only clouds are clear sky is reported as clear sky by MODIS, indicating that MODIS misses some thin cirrus in the SEA region -- a point also made in (Reid et al., (2013). More details about the CC and MODIS cloud phase comparison is displayed in Table 2. In this study, MODIS cloud phase is also adopted to obtain additional cloud phase properties because of MODIS' wide viewingover a wider swath (2330 km) and its longer time period than the CC data.

The spatial heterogeneity index (H_σ) defined as the standard deviation over the mean of measured radiances of sixteen 250 m pixels within a 1-km pixelsample (Liang et al., 2009) is also included in the MYD06 product. The H_σ usually increases with subpixel-level inhomogeneity and correlates with radiation and remote sensing biases rooted in the plane-parallel assumption (Cho et al., 2015; Fu et al., 2019)(Cho et al., 2015). H_σ is reported at 0.645 and 0.865 μm. Here, we adopt H_σ at 0.645 μm because H_σ for 0.865 μm is reported to be zero for saturated pixels, which occurs for thick clouds under certain sun-view geometriees encountered in the MODIS data.

The matched H_σ values and MODIS radiances are assigned to cloud phase from 2B-CLDCLASS-LIDAR to investigate cloud spatial heterogeneity and spectral radiation features. Longer MODIS data (2003-2017) is used for analysis of interannual variations of cloud phase. Considering that no visible and SWIR radiances are available at night, only daytime data is considered through the paper.

2.4. Meteorological indices

The MJO (Madden and Julian, 1971) consists of large-scale coupled atmospheric circulation and deep convection in the tropical atmosphere. It forms in Indian Ocean and propagates eastward at a speed around 5 m s^{-1} across the Maritime Continent and into the equatorial western/central Pacific oceans with an intraseasonal variability of 30-90 days (Zhang,

Formatted: Not Highlight

2005). To understand cloud phase evolution with the MJO, we adopt the Real-time Multivariate MJO (RMM) index (Wheeler and Hendon, 2004), which defines eight MJO phases using two leading Empirical Orthogonal Functions (EOFs) of combined 850, 200 hPa zonal wind from NCEP reanalysis and satellite-observed outgoing longwave radiation (OLR) over the tropical belt. We only focus on strong MJO events with amplitude greater than one. The RMM index is available at http://www.bom.gov.au/climate/mjo/.

The ENSO has a interannual variability of 3-5 years, and the multivariate ENSO index (MEI) is well suited to identify ENSO events (Wolter and Timlin, 1993, 1998). The new version of MEI is created by the EOF analysis of five variables including sea level pressure, sea surface temperature, surface zonal and meridional winds, and OLR. The ENSO index is available at https://www.esrl.noaa.gov/psd/enso/mei/.

3. Results

3.1. Seasonal Variations

3.1.1 Meteorological Conditions

To better understand the linkages between cloud properties and large-scale dynamics, meteorological fields are presented in Fig. 2. It shows temperature, specific humidity, wind field, and static stability at the lower (~ 850 hPa) and upper (~ 180 hPa) troposphere ~~(~ 180 hPa)~~ over SEA in four seasons~~, that is, :~~ boreal spring (March, April and May (MAM)), summer (June, July, and August (JJA)), autumn (September, October and November (SON)) and winter (December, January and February (DJF)).

In the lower troposphere, relatively high and homogeneous temperatures are observed all year around (~290 K) corresponding to the Indo-Pacific warm pool. However, temperatures drop in boreal winter (< 285 K, Fig. 2a4) and raise in summer (> 290 K, Fig. 2a2) over Southeast China and South China Sea. In the upper troposphere, temperatures are relatively low at latitudes between 10°S-10°N (< 213 K), while temperatures over South Asia in summer are 1-3 K higher than in other seasons. Similarly, high humidity (> 10 g kg^{-1} at lower troposphere and > 0.03 g kg^{-1} at upper troposphere) is located ~~at S~~south of 10°N latitude during spring and winter (Figs. 2b1, b4), while in autumn (Fig. 2b3), the humidity pattern is quite symmetric ~~to~~ about the equator. Also, air is especially moist over South Asia during summer than other seasons at both lower and upper troposphere. The summer high temperature and humidity over South Asia are related to the heating and convection over Tibetan Plateau, which maintains a hot and humid upper troposphere, and the South Asian Anticyclone (Yeh, 1982). The summer monsoon also helps transfer a large amount of moisture from the Indian ocean to Asia (Figs. 2c2).

The seasonality of the wind field is evident (Figs. 2c1-c4). In the lower troposphere, the southwesterly wind flow brings warm and humid air to South Asia in summer when ITCZ is located at the North of equator, providing favorable conditions to form clouds and precipitation (summer monsoon). The wind direction ~~at~~ in the upper troposphere is northeasterly, which is nearly opposite to that at the lower troposphere. In DJF, the ITCZ shifts to the southern hemisphere and the wind flow reverses. The prevailing northeasterly flow near the lower troposphere (winter monsoon) is also opposite to the wind direction at the upper troposphere (southwesterly). However, the upper troposphere wind is much weaker in winter than in summer because the summer South Asian Anticyclone above Tibetan Plateau enhances the upper

troposphere wind flow (Yeh, 1982). The spring and autumn are two transition seasons of summer and winter monsoonal flows.

~~The lower-troposphere static stability (LTSS) is estimated as the difference of potential temperature between surface and around 3 km above and the upper-troposphere static stability (UTSS) is the potential temperature difference between the tropopause height and 3 km below.~~ The lower-troposphere static stability (LTSS=$(\theta_{z=3\ km} - \theta_{z=0})/3$ km) and the upper-troposphere static stability (UTSS = $(\theta_{z=tropopause} - \theta_{z=tropopause-3\ km})/3$ km) are shown in Figs. 2d1-d4, where the θ is potential temperature in unit of K. The tropopause height is defined following the World Meteorological Organization, i.e. the lowest level where lapse rate is 2° C km^{-1} or less and the average lapse rate between this level and all higher levels within 2 km is smaller than 2° C km^{-1} (Grise et al., 2010). Figures 2d1-d4 reveal that LTSS is usually smaller over land than over ocean. Small LTSS values (< 4 K km^{-1}, yellow-green color) over ocean correspond to a wetter atmosphere (Fig. 2b). Relatively larger LTSS (> 4 K km^{-1}) occurs in winter and spring such as over East and South China sea. The LTSS has been proven to be an important parameter indicating low-level cloud formations. For instance, Klein and Hartmann (1993) showed that 1°C increase in stability associates with a 6% increase in stratus cloud area coverage. The spatial pattern of UTSS is similar with that of LTSS.

3.1.2 Occurrence of All Clouds

This section focuses on cloud spatial distributions over SEA. The horizontal occurrence frequency, defined as the ratio of total cloudy number to the total observation sample in each 5° long x 2° lat grid derived from the 2B-CLDCLASS-LIDAR data, is shown in the upper panels of Fig. 3. The zonal latitude-altitude cross sections ~~centered at 115°E~~, obtained by cloudy number in each ~~each 5° long x~~ 2° lat x 250 m height cell divided by the observation sample in that cell, are displayed in the lower panels of Fig. 3.

Over SEA, the annual mean cloud frequency is about 8~~1~~0.~~49~~%, ~~the~~ being ~~the smallest~~smaller in winter and ~~the~~ large~~rst~~ in summer (Table 3). As expected, seasonal variations of ~~Large~~ cloud occurrence are ~~frequency~~ generally associated with the movement of large humidity, warm temperature and low stability in the lower and upper troposphere (Figs. 2, 3). ~~For instance, Clouds frequently occur the cloud occurrence frequency in Indochina is nearly 100% during the summer monsoon season, while in winter when the monsoon has retreated, these regions have much lower cloud occurrence (30-40%). The cloud pattern accordingly while they moves~~their frequency shifts to the Malaysia and Indonesia regions as the summer monsoon retreats and the ITCZ shifts southward. The cross sections (Figs. 3b1-b4) display prevailing high-level clouds located at around 10-15 km, matching to the ubiquitous nature of cirrus over the Warm P~~p~~ool regions (Sassen et al., 2008). These ice clouds ~~occur north of~~ have their largest frequencies centered ~1~~2~~0°N in summer, but shifts to the s~~S~~outh of the equator in winter, i.e. moving with the ITCZ and the monsoon ~~climate systems~~.

~~However, N~~~~not all~~While it is clear that clouds favor a warm, humid and unstable condition, large cloud occurrences are found in other conditions in the region. Frequent cloud occurrence (~70%) is also observed over ~~Southeast~~ southeast China and the East China Sea during winter when the atmosphere is cold, dry and stable (Figs. 2, 3a4). These winter clouds ~~at~~

Formatted: Line spacing: Multiple 1.08 li
Formatted: Font color: Dark Blue
Formatted: Font color: Auto
Formatted: Font color: Auto
Formatted: Font color: Auto
Formatted: Font color: Auto
Formatted: Font color: Auto
Formatted: Font color: Auto
Formatted: Font color: Auto
Formatted: Font color: Auto
Formatted: Font color: Auto
Formatted: Font color: Auto
Formatted: Font color: Auto
Formatted: Font color: Auto
Field Code Changed
Formatted: Font color: Blue

north of 10°N usually have low cloud heights (< 5 km) ~~without cirrus overlap~~with little cirrus above as seen from the cross section (Fig. 3b4).

While Fig. 3b displays a vertical cross section of cloud occurrence frequencies, it says little about cloud overlap frequencies. ~~However, a~~As shown in Yuan and Oreopoulos, (2013), low-level clouds have a high chance to be overlapped by ~~the~~ upper ~~ubiquitous ice~~ clouds in the warm pool region. In the next section, we will ~~display how often one cloud phase or two different cloud phases overlap occur.~~examine cloud overlap with a focus on cloud phase. ~~The cloud pattern and its seasonal variation derived from the CC observations largely agree with those reported over SEA derived from MISR, MODIS and CALIPSO, although the mean value of cloud occurrence varies among different platform due to different instrument sensitivity (Reid et al., 2013).~~

~~The cross sections centered at 115°E (Figs. 3b1-b4) display prevailing high-level clouds located at around 10-15 km, matching to the ubiquitous cirrus clouds over the Warm pool regions (Sassen et al., 2008). These ice clouds occur north of 10°N in summer but shift to the South in winter, i.e. moving with the ITCZ and monsoon climate systems. Also, low-level cloud (e.g. < 3 km) frequency can exceed 30% near the boundary and generally match to the boundary clouds derived from MISR (Reid et al., 2013), owing to MISR's ability to detect the cloud top heights of low clouds in the presence of cirrus. Low-level clouds cloud have a high chance to be covered by the upper ubiquitous ice clouds (Yuan and Oreopoulos, 2013), which is further quantified in next section.~~

3.1.3 Occurrence of Cloud Phase~~s~~

As stated in Sect. 2.2, we classify clouds according to cloud phase and cloud layer in five main groups: ice-only, liquid-only, mixed-only, ice-above-liquid, ice-above-mixed clouds. Each group contains both single and multiple layers of the same phase. Our analysis (Table 3) shows that one-layer-one-phase clouds have much larger frequency than multi-layer-same-phase clouds. For example, multi-layer ice-only cloud (~8.6%) occurs less frequently than one-layer ice-only cloud (20%). Liquid-only clouds mostly form in a single layer (14%) and the frequency of multi-layer liquid-only cloud is only 2%. A careful comparison between single and multiple layers of the same phase clouds shows no significant difference in the properties that we're interpreting, which justifies our simpler classification.

Figure 4 shows horizontal and vertical distributions of the five cloud groups as defined in Fig. 1. The mean occurrence frequency of each cloud class in four seasons over ocean and land is summarized in Table 3. The five cloud groups display visible differences in both of their mean frequencies and spatial distributions. Ice-only clouds (Fig. 4a~~s. 4a1-a4~~) occur the most frequent (~ 2~~87~~.6~~8~~%) among all cloud classes. These clouds~~-~~ widely spread in the tropical belt, and ~~with much higher frequency over ocean (~31.3%) than over land (~18.4%). These clouds appear more frequently in summer (~34.7% over ocean, ~19.6% over land) and~~ prefer the locations at north of the equator in summer but move to the south in winter~~ leading to a smaller mean frequency over SEA (~26.5% over ocean, ~16.4% over land)~~. Ice-only clouds mainly locate at high altitudes

Formatted: Indent: First line: 0.5"

Formatted: Indent: First line: 0.5"

Formatted: Indent: First line: 0.5"

between 10-15 km (Fig.4b), corresponding to the prevalent ~~ubiquitous~~ tropical cirrus discussed in many other studies (Hong and Liu, 2015; Reid et al., 2013; Sassen et al., 2008).

In contrast, l~~L~~iquid-only clouds (Fig. 4a~~s. 4b1-b4~~) ~~have an annual mean frequency of ~16.9%. They~~ are widely distributed over ~~Southeast~~ southeast China and the East China Sea and show large seasonality ~~which increase in fall, reach to a maximum in winter (> 50%) and remain ubiquitous until spring~~. These ~~L~~liquid-only clouds mostly have their cloud tops lower than 3 km (Fig. 4b). ~~These clouds~~They are the so called 'Chinese stratus' by Klein and Hartmann (1993) associated with lower-troposphere cold and dry air and large LTSS (Fig. 2). ~~However~~Elsewhere, liquid-only clouds have very small frequencies (< 10%~~). B) between 10°S-10°N where widely distribute ice clouds, which indicates that liquid clouds occurring here are likely being covered by ice clouds, hence, they are grouped as ice-above-liquid cloud class. With~~ The annual mean frequency of liquid-only cloud is ~16.0%.

Ice-above-liquid clouds have an annual mean occurrence frequency of ~ 20~~1~~.1~~9~~% (Fig. 4a~~s. 4d1-d4~~). Ice layers located at 10-15 km cover the underlying liquid clouds mostly with height below 3 km (Fig. 4b). These clouds occur frequently over South China and Indochina during the summer monsoon season and ~~(Fig. 4d2), with the mean frequency over land (~35.3%) being much larger than over ocean (22.1%) (Table 3). In winter, ice-above-liquid clouds~~ move to West Pacific Ocean and Malaysia-Indonesia regions in winter ~~(Fig. 4d4)~~.

The areas where widely distribute ice-only and ice-above-liquid clouds are also associated with relatively frequent~~Mixed phase related clouds, i.e.~~ mixed-only (annual frequency ~ 6.72%) ~~(Figs. 4c1-c4)~~ and ice-above-mixed clouds (annual frequency ~97.34%) ~~(Figs. 4e1-e4) have a higher frequency over land than ocean~~ (Table 3) such as Indochina in summer and Malaysia-Indonesia regions in winter. ~~), which is consistent with more convective activities over land in the afternoon (Eastman and Warren, 2013). The mixed-only clouds are mature convective clouds as seen from their cross sections which extend from near surface up to above 15 km. The frequency of this cloud group agrees with that of precipitation (Adler et al., 2001). Some mixed-only clouds also appear~~ Mixed-only clouds are mature convective clouds as seen from their cross sections (Fig. 4b) which extend from near surface up to above 15 km. Nevertheless, near 30°N from fall through spring where liquid-only clouds dominate, there exist relatively frequent mixed-only clouds with their top below 10 km. ~~consistent with the location of liquid-only clouds but their tops being much higher than liquid-only clouds.~~ The ice-above-mixed clouds, frequently occurring at 6 km, are more likely under development with mixed layer tops reaching to around 10 km. If the mixed layers develop higher, they would merge with the overlying ice clouds and are classified into mixed-only cloud class. ~~Both mixed-only and ice-above-mixed clouds show relatively large frequencies near the west coast of Indochina in summer and over Malaysia-Indonesia in winter that relate to the monsoon and ITCZ as well as topographical effect.~~

Overall, liquid-only clouds are~~occur~~ associated with high LTSS and lower temperature in the lower troposphere, agreeing with the relationship of low-level cloud with stability (Klein and Hartmann, 1993; Li et al., 2014). In contrast, ice-only, ice-above-liquid, ice-above-mixed and mixed-only clouds, collectively named as 'ice-contained clouds', favor a humid, warm and unstable environment.

Figure 5 further summarizes the mean and standard deviation of the meteorological variables discussed in Fig. 2 from the ECMWF-AUX ~~Aux~~ product for the five cloud groups in summer and winter seasons over ocean (to avoid the low static stability over land). In the lower troposphere, all cloud groups in summer tend to have smaller LTSS, higher temperature and humidity than in winter (Figs. 5a, b). The standard deviations in summer are also smaller, being consistent with a more homogeneous spatial pattern of the meteorological fields (Fig. 2). In winter the liquid-only clouds tend to have a much smaller humidity and colder temperature corresponding to the occurrence of the 'Chinese stratus' (Klein and Hartmann, 1993). For those 'ice-contained clouds', they are still located in a relatively warm, moist and unstable atmosphere but their standard deviations are much larger than that in summer, agreeing with the less homogeneous spatial pattern of meteorology in winter (Fig. 2).

In the upper troposphere (Figs. 5c, d), the relationship between the five cloud types and meteorology is similar in both summer and winter with liquid-only clouds deviating from 'ice-contained clouds'. The 'ice-contained clouds' relate to smaller UTSS as reported in Li et al., (2014). Also, ice-only and ice-above-liquid clouds share very similar upper tropospheric meteorology as their mean and standard deviations are nearly the same, which is not surprising because the low stability and high moisture are essential to maintain cirrus (Christensen et al., 2013; Li et al., 2014). However, the specific humidity in the upper troposphere of ice-above-mixed clouds is larger than both ice-only and ice-above-liquid clouds (Figs. 5c, d), which may reveal that convection below brings moisture to the upper troposphere.

3.1.4 Distributions of Cloud Phase Properties

Figure 6 presents the probability distribution function (PDF) of cloud properties including cloud top~~s~~ for all cloud phases, and base, geometric thickness, τ and Re for ice layers from the 2C-ICE product. The averages of the cloud properties in the four seasons are summarized in Table 4.

~~We first focus on T~~the properties of ice layers in the three categories: ice-only, ice-above-liquid and ice-above-mixed clouds are displayed in (Figs. 6a-e~~)~~. We combine both land and ocean data to investigate the distributions of ice layer properties, because their PDFs display similar shapes between that over land and ocean (Figure not shown); however, ~~, yet~~ their averages are separately summarized in Table 4. The three categories of ice layers share many similarities in their PDFs~~:.~~ t~~T~~he modes of ice top PDFs (~ 16 km) and base (~ 12.5 km) ~~are~~ slightly greater than their means and medians (Table 4 and vertical dashed lines in Fig. 6 ~~and Table 4~~)~~. .~~ ~~The samples with ice top > 15 km or ice base > 10 km account for more than 60% and 70%, respectively.~~ ~~and~~ T~~t~~The modes of geometrical thickness PDFs ~~are~~ are around 1 km, which are ~~which are also~~ smaller than their mean and median values of 2-4 km (Fig. 6c and Table 4). ~~In addition, more than 60% samples have geometrical thicknesses less than 3 km.~~ These statistics demonstrate that the distributions of ice clouds skew to higher locations and thinner thickness, corresponding well to the properties of cirrus near tropopause (Haladay and Stephens, 2009; McFarquhar et al., 2000). In addition, t~~T~~he τ PDFs show two modes for the three types of ice layers, and the Re PDFs with their modes slightly greater than 15 μm. ~~Also, the ice layers tend to be thicker, i.e. larger geometrical and optical thickness, with larger ice particles in summer and autumn than in the other two seasons (Table 4).~~

There also exist differences between the three groups of ice layers. For example, ice-only clouds tend to locate 0.4-1.4~~6~~ km lower over land than ocean, and the lower location may allow

more moisture to feed into ice clouds, which may explain the reason that ice clouds over land have mean τ values of 0.6~~1~~-1.6~~2~~ and Re of 3-5 μm larger than those over ocean (Table 4). Compared to ice-only clouds, the ice layers above liquid or mixed clouds show much less land-ocean contrast in these properties (Table 4). Also, ~~For example,~~ the ice layers above liquid clouds ~~These two groups of ice layers have similar medians and means, and~~ contain about 73.8~~0~~% samples with geometrical thickness < 3.0 km and about 91.5~~0~~% samples with ice τ < 3.0--the ~~τ~~ threshold often used to define ~~of~~ cirrus (Sassen et al., 2008) (Figs. 6 c, d). In contrast, ice-only clouds are thicker with larger means, medians, and Re (Table 4), which are ~~and less samples with τ < 3.0. This is~~ contributed by more ice-only cloud samples with geometrical thickness > 3.5 km, τ > 1.6 and Re > 60 μm (Fig. 6). ~~It should be noted that the CALIPSO lidar signals will be totally attenuated by thick ice clouds (τ > 3.0) (Sassen et al., 2008) and the CloudSat radar fails in detecting shallow cumulus.~~ Due to the fact that lidar signals are attenuated when cloud τ > 3.0 and the radar fails in detecting shallow clouds~~these instrument limitations~~, some ice-above-liquid clouds (e.g., thick ice over shallow liquid) could be classified into ice-only group, leading to some sampling biases to the mean ice τ and Re. However, in the ice τ range of 1.6-3.0 where CALIPSO can penetrate the cloud, ice-only clouds have a total frequency of ~ 0.11~~2~~ in this τ range, being higher than the frequency (~ 0.07~~14~~) of the other two groups and demonstrating a higher probability of ice-only clouds being thicker.

For liquid or mixed layers, we only focus on cloud tops, because the determination of cloud base suffers from larger uncertainties than cloud top due to the limitation of instruments, i.e. CloudSat radar has difficulty in distinguishing the cloud base near Earth's surface and the CALIP~~A~~SO lidar signal is ~~easily~~ attenuated by ~~liquid/thick~~ clouds with optical thickness greater than 3 (Hu et al., 2009; Stephens et al., 2008). For the liquid top PDFs (Fig. 6f), there are two modes for the liquid below ice clouds (green). One mode is located at 1 km for ocean (2-3 km for land), ~~agreeing with results from MISR (Reid et al., 2013),~~ and the other is located at ~ 6 km for both ocean and land. We further obtain the spatial distributions of the liquid below ice clouds with liquid top greater and lower than 5 km, respectively (Figure not shown). It is shown that liquid clouds with top < 5 km are widely distributed over SEA, while those with liquid top > 5 km are more concentrated in locations with latitude < 10°, corresponding to a more unstable environment as shown in Fig. 2. In another word, larger moisture and small LTSS allow liquid clouds to develop deeper. For liquid-only clouds, they have a much higher frequency ~~frequency than those liquid below ice clouds~~ at the PDF mode of 1 km, and the second mode is not evident. ~~for liquid-only clouds. Since the frequencies at top > 5 km of liquid below ice are much larger than liquid-only clouds,~~ T~~t~~he averaged ~~liquid~~ top value of the ~~former~~liquid below ice clouds is higher than liquid-only clouds ~~the latter~~ (Table 4). ~~The top difference is much larger in summer and fall (~ 1 km over ocean and 300 m over land).~~

For the mixed layers below ice clouds (Fig. 6g), the mode of cloud top PDF (cyan) is at around 6 km and the mean is about 8.5~~9~~ km with the values over ocean about several hundred meters higher than that over land (Table 4). Note that as the mixed layers develop deeper, e.g. top > 10 km, and merge with the upper ice layers, these clouds would be grouped as mixed-only clouds. For mixed-only clouds, the primary mode of cloud top PDF is at around 16 km and the secondary mode is at around 6 km. The primary mode is much higher over ocean than over land, while the secondary mode is higher over land, indicating that more mixed clouds over land are under development around 1:30 pm local time. This agrees with the results in Nesbitt and Zipser (2003) that convective clouds keep developing in the early afternoon and reaching to intensity

maximum in the late afternoon over land, while diurnal variation of convection intensity is insignificant over ocean.

3.1.5 Spatial Heterogeneity of Cloud Phase

Sections 3.1.1 – 3.1.4 have ~~primarily displayed~~discussed the macrophysical properties including spatial distributions, cloud thickness, top and base heights for five cloud groups~~t he different cloud phases~~ and their relationship with meteorology based only on CC data. In this section, by combining the MODIS and 2B-CLDCLASS-LIDAR data, we investigate how the~~cloud~~ spatial heterogeneity index (H_σ) relates to cloud phase.~~,~~ The H_σ ~~which~~ is not only closely related to cloud micro and macrophysical properties but also affects the accuracy of cloud retrievals from passive sensors and radiative transfer modeling (Ham et al., 2015; Zhang and Platnick, 2011). Only ocean data is considered to avoid complications with the effects of land surface heterogeneity on interpreting results.

The H_σ PDFs for the CC clear sky and the five cloud groups are shown in Fig. 7a. ~~As displayed, t~~The PDF of CC clear sky has a sharp peak at $H_\sigma \sim 0.01$, ~~suggesting~~ indicating that clear sky is usually spatially homogeneous. For cloudy sky, liquid-only clouds are the most heterogeneous among all cloud groups, ~~which have~~with H_σ ranging from 0.01 to 1 and with a peak ~~located at H_σ~~ ~ 0.5. The ice-only clouds in contrast are homogeneous as the PDF has a peak close to that of clear sky. This suggests that the biases in retrieved optical and microphysical properties of clouds from passive sensors caused by the plane-parallel assumption will be larger for water clouds compared to ice clouds in the SEA region. Indeed, MODIS liquid Re differences retrieved from three wavelengths (1.6, 2.1 and 3.7 μm) are~~is~~ especially large over this region (up to 10 μm) (Zhang and Platnick, 2011; Fu et al. 2019). Care is therefore recommended~~, and hence, it needs to be careful~~ when using the MODIS cloud microphysical products in this region, for example in interpreting the cloud-aerosol relationship over SEA ~~using the liquid cloud Re from passive sensors~~ (e.g., Ross et al., 2018)~~. considering that the large spatial heterogeneity of liquid clouds would contribute large biases to the retrieved Re~~.

~~For~~ ice-above-liquid clouds, the PDF curve moves slightly to a smaller H_σ region compared to liquid-only clouds as the overlying ice clouds have a spatial smoothing effect on the radiation emerging from the liquid clouds below. However, due to the small optical thickness ~~thin features~~ of the overlying ice clouds, radiation from underlying liquid clouds dominate (Sect. 3.1.4). ~~For this reason, MISR's stereoscopic technique, which matches spatial patterns between two views for retrieving cloud top height, often retrieves the height of the lower liquid layer rather than the height of the thin ice layer (Reid et al., 2013; Stubenrauch et al., 2013).~~ The H_σ PDF of ice-above-mixed clouds is similar with that of ice-only clouds but with some samples having H_σ smaller than clear sky (e.g., $H_\sigma < 0.01$). This feature is more obvious for the mixed-only clouds, which ~~that~~ have about 50% of its samples with $H_\sigma < 0.01$ (Fig. 7b), ~~hence~~ indicating that these clouds are extremely homogeneous. ~~We aware that t~~These cases of very smooth ice-above-mixed and mixed-only clouds correspond to high mixed layer tops and large reflectance at 0.645 μm (discussed in next section) that are~~, revealing the situations~~ associated with deep convection. ~~While t~~These clouds are locally homogeneous and~~,~~ hence favor~~ing~~ the plane-parallel assumption in radiation computation (Ham et al., 2015).

Note that CC clear sky, ice-only, ice-above-mixed and mixed-only clouds are usually homogeneous, but there exist some heterogeneous cases.~~, particularly including for clear sky,~~

whose where Tthe PDF of clear sky has a long tail of extending to large H_σ values extending up to 1 (Fig. 7a) and has about 20% samples with H_σ values greater than 0.1 (Fig. 7b). Mismatch of pixels in collocation or difference in spatial resolutions of CC (1.8 km x 1.4 km) and MODIS (1 km) can contribute uncertainties to the H_σ of CC clear sky. Yet with a focus on the clear-sky pixels that reported to be clear sky by both CC and MODIS agree(not shown), they behave nearly the same as that of CC clear sky as shown in Fig. 7a, which stands to the reasonindicating that the long tail is due to the significant amount of misdetection of small subpixel clouds by both MODIS and CCloudSat. Indeed, many small liquid clouds with size ranging in a few tens to hundreds of meters (e.g., Koren et al., 2008) that are difficult to be measuredcan go undetected by MODIS (as reported in Zhao and Di Girolamo (2006). Also,We revisitA revisit of the MODIS and Advanced Space Thermal Emission and Reflection Radiometer (ASTER) data (15 m resolution) used in Zhao and Di Girolamo (2006) Zhao and Di Giroalmo (2006) over the tropical western Atlantic showsed a the same long tail as found here. However, this The the. The long tail of H_σ PDF is significantly reduced, i.e. frequency change from 0.3% to 0.1% at H_σ ~ 0.1, when the applying the Advanced Space Thermal Emission and Reflection Radiometer (ASTER) data (15 m resolution) is applied to exclude the MODIS clear sky pixels that contain ASTER reported clouds significantly reduce the long tail of H_σ PDF but with its mode unchanged (consult with Guangyu Zhao). This , which further validates affirms that the undetected clouds in some many MODIS and CC clear sky pixels contribute to large H_σ values, which may at least impact 20% clear-sky samples whose H_σ > 0.1 (Figs. 7a,b). and the typical clear sky H_σ value of ~0.01.

MoreoverTo further investigate this last point, we calculate the MODIS liquid cloud fraction, defined as the ratio of liquid cloud samples based on the MYD06 product to the total 25 pixels in a 5 km by 5 km surrounding of the collocated CC-MODIS pixel. As shown in Fig. 7c, as H_σ increases, larger fraction of MODIS liquid clouds is observed around the CC clear sky, pixels as H_σ increases. The ubiquitous liquid clouds in the surrounding indicate a high chance of being polluted by small liquid clouds in the subpixels. Similarly, the MODIS liquid cloud fractions in the surroundings of CC ice-only, mixed-only and ice-above-mixed clouds. increase with H_σ values as well, This indicatesdemonstrating that the heterogeneous pixelscases of these clouds could also be due to undetected liquid clouds in the subpixels.

Figure 8 displays shows the spatial distributions ofmean H_σ in four seasons for CC clear sky, the five cloud groups and all sky that includes both clear and cloudy sky. As expected, ice-only, ice-above-mixed, and mixed-only clouds are homogeneous everywhere (H_σ < ~ 0.05) with some relatively large values (H_σ ~ 0.1) in the liquid-only cloud prevailing regions such as the East China sea Sea in winter (Figs. 4, 8b4, 8d4, 8f4). As liquid-only clouds are the most heterogenous, they show the largest spatial H_σ values over SEA (Figs. 8c1-c4). Also, the H_σ values over the East China sea Sea in spring, fall and winter are relatively smaller than the H_σ in other regions, implying that the 'Chinese stratus' named by (Klein and Hartmann, 1993) that favor a dry and stable meteorological conditions are less heterogenous than other liquid-only clouds (Figs. 8c1-c4). Ice-above-liquid clouds (Figs. 8e1-e4) are smoother than liquid-only clouds, and their relatively small values tend to coincide with frequent ice-above-liquid cloud occurrence frequency that associates with the monsoon and ITCZ, such as in Indonesia-Malaysia region in winter or North Indian Ocean in summer (Fig. 4). The H_σ pattern of CC clear sky (Figs. 8a1-a4) displays shows smaller values than ice-above-liquid clouds but larger values than ice-only, ice-above-mixed and mixed-only clouds. It is because H_σ PDF of clear sky has higher

frequency than the other three cloud groups when $H_\sigma > 0.2$ (Fig. 7a). Also, the places with large H_σ values of CC clear sky are consistent with those with frequent occurrence of ice-above-liquid or liquid-only clouds, which in turn indicate the high chance of undetected liquid clouds increasing the subpixel variability.

For all sky (Figs. 8g1-g4), the small H_σ values occur in North of the equator in summer, including Indian Ocean and South China sea. The pattern is quite symmetric about the equator in fall and moves to South of the equator in winter, being consistent with the shift of the monsoon and ITCZ. This is because the small H_σ values are primarily contributed by ice-only clouds due to their large occurrence frequency (Fig. 4) and spatial homogeneous features. In contrast, the pattern of large H_σ agrees more with that of liquid-only cloud occurrence (Fig. 4).

Overall, liquid clouds are spatially heterogeneous over SEA, whereas ice-only and mixed clouds are usually homogeneous. Ice-above-liquid clouds are less heterogenous than liquid-only clouds due to the smoothness of the overlying ice clouds, ice-above-liquid clouds are less heterogenous than liquid-only clouds, but their H_σ values are still large because overlying ice clouds are optically thin and the emerging radiance from underlying liquid clouds dominates. Clear sky is usually smooth with $H_\sigma \sim 0.01$, but undetected liquid clouds increase its subpixel variability. The seasonal variations of all-sky H_σ spatial patterns are in accordance with cloud movements that associated with the monsoon and ITCZ.

3.1.6 Spectral Radiative Features

The spectral differences in the complex refraction index between water and ice, as well as the differences between the macro and microphyscial properties of ice and liquid clouds, lead to differences between cloud phases in the observed spectral radiance reaching to the satellite sensor. This section examines the spectral radiance at the TOA observed by MODIS for the CC clear sky and the five cloud groups defined in Fig. 1 to investigate how their radiative features observed at the TOA relate to cloud phase. Similar to Sect. 3.1.5, only ocean data is adopted. The averages of the reflectance (R) and the brightness temperature (BT) (not weighted by cloud occurrence frequency) for each cloud group are shown over SEA in Fig. 9 and summarized in Table 5, while the PDFs and the cumulative distribution functions (CDFs) are displayed in Fig. 10.

At 0.645 μm, the averaged reflectance for clear sky is about 0.04 (Fig. 9) and the PDF of $R_{0.645}$ for clear sky shows a narrow peak at $R_{0.645} \sim 0.02$ (Fig. 10a1). The average $R_{0.645}$ of ice-only cloud is about 0.14. The location of its PDF Ice-only cloud shows its PDF peak is nearly same as near the clear sky peak and its CDF shows that that about 80% of its samples with have $R_{0.645} < 0.2$, proving the thin features of ice-only clouds over SEA and agreeing with their small optical depths in Fig. 6d. Similarly, for liquid-only cloud, the PDF also shows its mode nearly that of clear sky. A large fraction of liquid-only clouds that are optically thin clouds (e.g., more than 75% of liquid-only clouds with $R_{0.645} < 0.2$), being consistent with the findings of Leahy et al. (2012) that thin marine low-cloud fraction is greater than 80% for the SEA region. Ice-above-liquid clouds have larger mean $R_{0.645}$ are thicker than either ice-only or liquid-only clouds in the column (Table 5 and Fig. 9), have an average $R_{0.645}$ of 0.21. The peak of its PDF located at $R_{0.645} \sim 0.03$ is lower than that of ice-only and liquid-only clouds, and the corresponding $R_{0.645}$ CDF is towards to a larger reflectance region, demonstrating that ice-above-liquid clouds in the

~~column are thicker than either ice-only or liquid-only clouds.~~ ~~b~~But ice-above-liquid clouds still contains more than 60% samples with $R_{0.645} < 0.2$, further demonstrating the ubiquity of thin clouds over SEA. Many of these ~~T~~thin clouds ~~would be difficult to see~~often go undetected by MODIS as shown in Table 2, where ~~that~~ around 11~~0~~% of CC ice-above-liquid cloud, 30% of CC liquid-only and ice-only cloudy samples are reported to be ~~MODIS~~ clear sky by MODIS. The largest average $R_{0.645}$ is seen in mixed-only clouds (~ 0.59~~61~~), followed by the ice-above-mixed clouds (~0.45~~6~~). Their PDFs are broad and flat, but ~~with~~ the frequencies at $R_{0.645} > 0.4$ are evident as displayed in Fig. 10a1. Their CDFs reveal that 60% of ice-above-mixed and 80% of mixed-only clouds have $R_{0.645} > 0.4$, indicating that these clouds are geometrically deep (consistent with Fig. 4) and optically thick.

At 1.64 µm~~-~~, the average $R_{1.64}$ of ice-above-liquid clouds is nearly same as liquid-only clouds (~0.13) (Table 5 and Fig. 9). Both these cloud groups are ~~obviously~~ more reflective~~ed~~ than ice-only clouds (average $R_{1.64}$~0.06). The average $R_{1.64}$ of ice-above-mixed and mixed-only clouds is about 0.20~~19~~, implying that ice-above-mixed clouds are optically thick enough to reach the asymptotic reflectance and mixed-only clouds ~~that are geometrically thicker~~ do not increase $R_{1.64}$. Similarly, ~~at 2.13 µm,~~ the average $R_{2.13}$ of both mixed-only and ice-above-mixed clouds is also nearly equal (0.11), which in turn demonstrates their large thickness. The curve of $R_{2.13}$ across different cloud groups shows a similar shape with that of ~~-~~$R_{1.64}$ but with a smaller magnitude owing to the larger imaginary part of refra~~l~~ective index of water and ice at 2.13 µm than at ~~compared to~~ 1.64 µm. Particularly, the imaginary part of ice refra~~l~~ective index is larger than water at both wavelengths. Hence, when examining the reflectance ratio of SWIR (1.64 or 2.13 µm) to the visible (0.645 µm), we would expect that liquid-only clouds show a larger ratio than any other cloud groups. Because the Aqua MODIS 1.6 µm band has many dead detectors (King et al., 2013), we display the PDF and CDF of reflectance ratio of 2.13 to 0.645 µm ($\frac{R_{2.13}}{R_{0.645}}$) to further emphasize the spectral features of different cloud phases (Figs. 10b1 and b2). As expected, the PDF of liquid-only cloud~~s~~ extends to large reflectance ratio regions, and same as for ice-above-liquid cloud (Fig. 10b1). Moreover, there are about 60% of liquid-only cloud and 50% of ice-above-liquid cloud with reflectance ratio greater than 0.4 (Fig. 10b2), indicating that the reflectance ratio of ice-above-liquid cloud is in accord with low-level liquid cloud because of the thin features of the overlying ice clouds as discussed in Sect. 3.1.4 and 3.1.5. In contrast, ice-only clouds have very small frequencies when reflectance ratio greater than 0.4 (Fig. 10b1), and same as~~.~~ m~~M~~ixed-only and ice-above-mixed clouds~~. show even smaller reflectance ratio than ice-only clouds because more ice mass in the column results in stronger absorption at 2.13 µm and larger reflectance at 0.645 µm.~~ For CC clear sky, the PDF shows its mode at the ratio ~ 0.1 with its width ranging from 0.0 to 0.4. ~~Note that the mode of $R_{0.645}$ PDF locates at 0.02, and the mode of reflectance ratio PDF at 0.1 indicates that $R_{2.13}$ PDF peaks closely at 0.002 which agrees with our examination and conforms the darkness of ocean surface at the SWIR.~~ We also note that ~~aware~~ as the reflectance ratio of CC clear sky becomes larger, the corresponding H_σ increases as well, indicating that the undetected liquid clouds in clear sky pixels (Sect. 3.1.5) also enlarge the SWIR to the visible reflectance ratio.

At 1.375 µm, liquid-only cloud~~s~~ and clear sky show near zero average reflectance as the photons are nearly all absorbed by water vapor (Table 5). The mixed-only clouds have the largest average reflectance of 0.22~~54~~ compared to other cloud groups~~, , which is twice greater than that of ice-above-mixed clouds (~0.12). Much larger $R_{1.375}$ of mixed-only than ice-above-liquid~~

clouds could be due to the reason that the formerbecause these clouds are is much higher and thicker than the latter as shown in Fig. 4 and Table 4. Also, the average $R_{1.375}$ of ice-only clouds (~ 0.0606) is greater than that of ice-above-liquid clouds (~ 0.04). Because the specific humidity at the upper troposphere is nearly the same for both cloud groups (Fig. 5), larger $R_{1.375}$ of ice-only clouds demonstrates an average larger thickness than the ice layers above liquid clouds. This agrees with the results from the CC observations as discussed in Sect. 3.1.4 (Table 4).

At the IR, the average $BT_{8.5}$ and BT_{11} have similar magnitudes (Fig. 9 and Table 5). Because atmospheric absorption at 8.5 and 11 μm is small and hence, the radiance reaching to the sensor above Ocean largely depends on the surface temperature in clear sky and cloud property in cloudy sky. Only the PDF and CDF of BT_{11} are shown in Figs. 10c1 and c2, respectively. Note that when a cloud is opaque, the BT observed at the TOA only depends on cloud top, i.e. smaller BT for higher cloud top. As expected, the average BT_{11} of mixed-only clouds is lowest (~ 234.31 K), followed by ice-above-mixed clouds (because these clouds are thick and high (Figs. 4, 6). Ice-above-mixed clouds have average BT_{11} of ~ 247.7 K, which is larger than mixed-only clouds because ice-above-mixed clouds are optically thinner (as demonstrated by the reflectance at 0.645 μm) and have lower mixed layer tops (Table 4). The widths of BT_{11} PDF of mixed-only and ice-above-mixed clouds are broad, but the frequencies are low when $BT_{11} > 260$ K with about 20% samples at that BT_{11} region (Fig. 10c2). For liquid-only clouds, Tthe average BT_{11} (~ 289.88 K) of liquid-only cloud is only slightly smaller than that of clear sky (~ 295.24 K) due to the low liquid cloud top (mode ~1 km, Fig. 6f) and thin features. . The peak of BT_{11} PDF of liquid-only clouds is consistent with that of clear sky (BT_{11} ~ 294 K). For ice-above-liquid clouds, the average BT_{11} (~ 276.84 K) is slightly larger than ice-only clouds (~ 272.4 K). This may due to that the ice layers above liquid clouds do not absorb as strong as ice-only clouds because the former is averagely thinner than the latter over Ocean (Table 4). Also, the peaks of BT_{11} PDF of ice-only and ice-above-liquid clouds are close to that of clear sky, and 50% samples of these two cloud groups with $BT_{11} > 280$ K (Fig. 10c2), demonstrating the thin features of these clouds which agree with the conclusions from the CC data (Fig. 6) and $R_{0.645}$ analysis.

Another notable feature of the BT shown in Fig. 9 is that the average $BT_{8.5}$ is averagely larger than the average BT_{11} for ice-only, ice-above-liquid, ice-above-mixed and mixed-only clouds, i.e. 'ice-contained clouds', and vice versa for clear sky and liquid-only clouds. This is because in clear sky, absorption by the atmosphere at 8.5 μm is slightly greater than at 11 μm and hence, negative BTD between 8.5 and 11 μm ($BT_{8.5}$-BT_{11}) is observed (Fig 10d1). In cloudy sky, cloud absorption at 11 μm is larger than at 8.5 μm (Wolters et al., 2008), which decreases the BT_{11}. The absorption difference between 11 and 8.5 μm is small for water, which explains that the PDF of liquid-only clouds locates closely with that of clear sky but at larger BTD regionsbut still negative BTD regions (Fig. 10d1). That is, the PDF mode of liquid-only clouds (BTD ~ -1.8 K) is slightly larger than clear sky (BTD ~ -2.1 K), and the CDF of liquid-only clouds is very close to clear sky but slightly towards larger BTD regions (Fig. 10d2). Ice cloud has larger absorption difference between 11 and 8.5 μm than liquid cloud (Wolters et al., 2008). This explains positive BTD values for the 'ice-contained clouds'. However, For the BTD PDF of ice-above-mixed (peak at BTD ~1.2 K) and mixed-only clouds (peak at BTD ~ 1.5 K), there are only a small fraction of their samples (~20%) with BTD smaller than zero. iIce-only and ice-above-liquid clouds have their show very similar shape of BTD PDFs with their peaks located at

around BTD ~ -1.4 K. However, there are a lot of samples (> 50%) with BTD greater than zero. The negative BTDs of these ice-only or ice-above-liquid clouds also indicate their thin features over the SEA regions so that the absorption by ice clouds isare insufficiently significant to produce positive BTD.

For seasonal variations (Fig. 9 and Table 5), the change of reflectance and brightness temperature of each cloud group is associated with cloud occurrence, thickness and cloud top. For example, ice-only clouds have larger average $R_{0.645}$ and smaller BT in summer due to that these clouds occur more frequently and thicker in this season. In contrast, liquid-only clouds over ocean have similar cloud tops but occur more frequently in winter and thus they show greater average $R_{0.645}$ in winter than in summer. For ice-above-mixed or mixed-only clouds, they have larger reflectance in summer agreeing with larger frequencies but smaller BT in fall consistent with higher cloud top (Table 4).

In summary, mixed-only and ice-above-mixed clouds are bright in the visible (i.e. large $R_{0.645}$) and cold in the infrared (i.e. low BT). These clouds also have small reflectance ratio and positive BTD between 8.5 and 11 μm. Although liquid-only and ice-only clouds have similar $R_{0.546645}$, liquid-only clouds tend to have relatively larger BT_{11} and larger reflectance ratio than ice-only clouds. Ice-above-liquid clouds show slightly larger $R_{0.645}$ than either liquid-only or ice-only cloud with reflectance ratio similar to liquid-only clouds, but BT_{11} and BTD closer to ice-only clouds. The spectral radiative features of ice-only, liquid-only and ice-above-liquid clouds also demonstrate widespread thin clouds over SEA.

3.2. Cloud Phase Variations Associated with The Madden-Julian Oscillation

To connect to the seasonal variations, tThis section discusses the features of cloud phase associated with the intraseasonal 30-90 day MJO. Previous studies have provided full overviews of the radiative (in terms of OLR), dynamic and thermal dynamic characteristics of the MJO (Knutson et al., 1986; Riley et al., 2011; Wheeler and Hendon, 2004; Zhang, 2005). The purpose of this study is to , on the other hand, focuses on how the cloud phase characteristics discussed in previous sections , i.e. the spatial heterogeneity observed at the TOA, vary with MJO phases, which has not yet been documented. Satellite-observed OLR has been widely used to characterize intraseasonal oscillations either globally or regionally (e.g., Knutson et al., 1986; Wheeler and Hendon, 2004). The MJO active phase is well documented to associate with strong convection and precipitation that feature with small OLR (Zhang, 2005). Whereas in inactive phase, convective clouds and anvil cirrus are reduced as convection is suppressed and other cloud types will occur (Riley et al., 2011; Zhang, 2005), leading to larger OLR (Zhang, 2005). Because ice, liquid clouds and their overlaps have different degree of inhomogeneity as shown in Sect. 3.1.5, cloud types varying with MJO phases not only alter radiation but will also modify the spatial heterogeneity observed at the TOA, which will be examined in this section.

As seasonality is a basic feature of the MJO (Zhang and Dong, 2004), we first classify the MJO events during 2007-2010 into four seasons according to the MJO index from Wheeler and Hendon (2004) (Fig. 11). In total, 917 events with amplitude (i.e. $(RMM1^2+RMM2^2)^{0.5}>1$) greater than one (i.e. $(RMM1^2+RMM2^2)^{0.5}>1$) are selected to represent strong MJO. As shown in Fig. 11a, the occurrence of different MJO phases displays very strong seasonality. Specifically, more MJO events happen in Phase 1 and 2 in summer, while in fall, the MJO cases are concentrated in Phase 4, 5 and 6. When it moves to winter, the MJO prefers to occur in Phase

7, while in spring, more cases occur in Phase 1 and 8. Although the MJO amplitude is relatively flat across different phases, the weakest amplitude occurs in summer, while it is stronger towards winter, which is consistent with the statements in previous studies (Adames et al., 2016; Zhang and Dong, 2004).

To investigate the spatial heterogeneity associated with the MJO, Figure 12 shows the spatial distributions of all-sky H_σ over eight MJO phases. According to the spatial heterogeneity signatures derived in Sect. 3.1.5, the active MJO phase associated with deep convections and ice clouds is featured with small H_σ values. Areas surrounding the convective center are with relatively large H_σ values, ~~with small H_σ is surrounded by relatively large H_σ values,~~ indicating that the locations ~~where~~ of ~~occur~~ suppressed MJO phase are associated with more liquid clouds. As displayed by Fig. 12, the H_σ pattern well reveals the propagation of MJO. That is, the center of convection associated with small H_σ is in the Indian Ocean in Phase 1 and 2, while the West of Pacific and Maritime Continents display~~are with~~ large H_σ as convection is suppressed. The small H_σ pattern approaches to the Maritime Continent (indicated by the red dashed box in Fig. 12) in Phase 3 and centers at those regions in Phase 4, 5 and 6. After Phase 6, the con~~v~~n~~e~~ective center with small H_σ enters the West Pacific Ocean, and at the same time, H_σ becomes large over the Indian Ocean. Note that Phase 2 mainly occurs in summer, which relates to boreal summer monsoon, so the H_σ pattern here is quite similar with that in summer shown in Fig. 8g2. Similarly, the H_σ pattern of Phase 5 is in concert with the seasonal pattern in fall (Fig. 8g3) due to a high chance of Phase 5 occurring in that season. The preference of geographical location of MJO, featured by the small H_σ, moves from North of the equator in Phase 1 to the South of the Equator in Phase 6, indicating the seasonal cycle of MJO location.

To investigate more details of how H_σ pattern changes with~~and~~ cloud phase according with ~~change with~~ the MJO evolution~~s~~, Figure 12i shows the PDF of all-sky H_σ sampling over the Maritime continent for the eight MJO phases from MODIS data. Two dashed lines from left to right indicate $H_\sigma \sim 0.01$ and $H_\sigma \sim 0.4$, which are close to the mode position of H_σ PDF of CC clear sky and liquid-only clouds (Fig. 7a), respectively. Figures 12j and k show the average occurrence frequency of different cloud phases from the MYD06 and the 2B-CLDCLASS-LIDAR products in the same region. In Phase 8 (cyan) when su~~d~~pe~~p~~pressed MJO occurs over the Maritime continent, the H_σ PDF shows the largest frequency (~ 0.38%) among all MJO phases at $H_\sigma \sim 0.4$ but the smallest frequency when $H_\sigma < 0.01$ (Fig. 12i). This corresponds to the largest frequency of clear sky and liquid clouds among all MJO phases but the smallest frequency of ice clouds indicated by MODIS (Fig. 12j), and at the same time, ~~of~~ ice-only, ice-above-liquid, ice-above-mixed clouds from ~~displayed by~~ the 2B-CLDCLASS-LIDAR products occur the least frequently (Fig. 12k). In contrast, when active MJO phase locates in the Maritime continent (Phase 4, 5), the H_σ PDF has the largest frequency at $H_\sigma < 0.01$ and the smallest frequency at $H_\sigma \sim 0.4$, ~~contributing~~ due to ~~by~~ the frequent occurrence of ice or mixed clouds among all MJO phases but less frequent occurrence of clear sky and liquid clouds.

Overall, more 'ice-contained clouds' occurring during the active MJO phase ~~feature~~ ~~the~~results in smoother textures ~~active MJO a smooth texture~~, i.e., small H_σ values, ~~while~~compared to the ~~suppressed MJO phase is more inhomogeneous, i.e., larger H_σ values, due to higher occurrence frequency of liquid clouds~~. ~~Also, t~~T~~t~~he eastward-propagating H_σ patterns ~~a~~ vary with MJO~~a behavior similar to OLR pattern (e.g., Wheeler and Hendon, 2004)~~, indicating that ~~the~~ H_σ could be useful for MJO studies, such as serving as an observed-based parameter ~~that~~

~~are sensitive to cloud phase,~~ to track the MJO position ~~and validate MJO simulations in climate models.~~ ~~and~~ It can also serve as a basis for disentangling true space-time variability of cloud optical and microphysical properties associated with the MJO from space-time variability of the biases rooted in cloud retrievals from passive sensors ~~biases in passive retrievals of these cloud properties~~ that are caused by departures from the plane-parallel assumption (Di Girolamo et al., 2010). ~~(Di Girolamo et al. 2010).~~

3.3. Interannual Variations: El Niño Southern Oscillation

~~Similar to the MJO, t~~The ENSO ~~phenomenon has been~~ documented in a series of studies. It is well known that the ENSO ~~known to~~ dominates the interannual variability of precipitation and clouds over the Western equatorial Pacific (As-Syakur et al., 2016; Park and Leovy, 2004; Reid et al., 2012), and accordingly, the observed broadband radiation at the TOA varies interannually as well (e.g., Loeb et al., 2012). ~~The purpose of this section concentrates more on~~ Here we examine how the spectral radiances and spatial heterogeneity associated with cloud phase behave interannually.

~~In this section, We first display the~~The spatial distributions of all-sky spatial heterogeneity (H_σ) anomaly is shown in ~~(~~ Fig. 13) ~~the ENSO index shown in Fig. 14a is used to identify the warm (El Niño) and cold (La Niña) phase of ENSO. Anomalies of clouds, radiation and heterogeneity~~ in El Niño and La Niña years ~~are calculated~~ based on the ENSO index and MODIS data from 2003-2017. ~~The spatial distributions of theses anomalies over SEA are shown in Fig. 13 and their time series are displayed in Fig. 14. As expected, the spatial distributions show negative $R_{0.645}$ anomaly (red) in El Niño year (Figs. 13a1-a4) and positive anomaly (blue) in La Niña year (Figs. 13b1-b4). Opposite patterns are obtained for the BT_{11} (Figs. 13c, d) and~~Generally, all-sky H_σ anomaly is negative in La Ni~~-~~ña year, indicating ~~(Figs. 13e, f). The H_σ anomaly indicates that~~ that more ice and mixed clouds ~~(corresponding to positive $R_{0.645}$ and negative BT_{11} anomaly)~~ occur~~ring~~ in La Niña year causinge the spatial heterogeneity to be more homogeneous than normal and vice versa in El Niño year. Also, the anomalies over the Maritime continent tend to be stronger in winter and spring than in summer and fall (Fig. 13). This demonstrates that the H_σ varies with ENSO.

Figure 14 displays the time series of monthly anomaly of clouds, radiances and spatial heterogeneity for the areas indicated by the red-dashed box in Fig. 13a1 ~~where are~~ an area sensitive to ENSO signals. As displayed, ice clouds detected by MODIS show similar variations as MODIS all clouds with their anomalies ranging from -0.2-0.2, being positive in La Niña years and negative in El Niño years (Fig. 14b). The MODIS ice cloud anomaly correlates well~~agrees~~ with that of CC ice-only, ice-above-liquid, ice-above-mixed and mixed-only clouds ~~from the CC observations~~ (Fig. 14d), ~~as the~~with correlation coefficients greater than 0.70 (significant at 99% confidence level). ~~), because most of these CC clouds are reported to be ice by MODIS (Table 2)~~. Conversely, the anomaly of liquid cloud occurrence is positive ~~abnormally high~~ (negative~~low~~) in El Niño (La Niña) year based on both the MODIS and CC data (Figs. 14b, d). Correspondingly, H_σ anomalies~~y is~~ are observed to be negative ~~abnormally small~~ in La Niña year due to the increase of 'ice-contained clouds' and positive ~~abnormally large~~ in El Niño years because ~~of the decreased~~ 'ice-contained clouds' decrease, ~~and the expose of~~exposing more liquid clouds ~~expose~~ (Figs. 14b, d). Moreover, the correlation coefficient between H_σ and ENSO index is about 0.49 (significant at 99% confidence level), further indicating that the change of spatial

heterogeneity is associated with ENSO. Moreover, the anomaly of MODIS all and ice clouds ranges within 0.2 and their correlation is about 0.97 (significant at 99% confidence level), yet the magnitude of liquid cloud anomaly (within 0.06) seen from both MODIS and CC is much smaller than that of ice clouds, indicating that the interannual variation of clouds over SEA is dominated by the change of 'ice-contained clouds'.

Note that negative (positive) anomaly of abnormally low (high) CC liquid-only or MODIS liquid cloud s associated with La Niña (El Niño) phase does not n't mean that total liquid clouds occur less (more) in La Niña (El Niño) year. because the CC data indicates the frequency of liquid clouds with ice clouds overlying of 21.9% (Table 3). The overlying clouds can conceal liquid clouds to be observed from space by passive sensors or by lidar if the overlying clouds are optically thicker than 3. Unlike CC liquid-only or MODIS liquid clouds, the CC ice-above-liquid clouds occur abnormally high in La Niña year (Fig. 14d). When adding up the frequency of liquid-only and ice-above-liquid clouds (i.e. total CC liquid cloud frequency), the anomaly does not shows the clear relationship with ENSO less evident than the liquid-only cloud (the subfigure in Fig. 14d). For example, through the La Niña phase in 2007 winter through 2008 spring, generally accompanies abnormally high the anomaly of total CC liquid cloud occurrence is close to be zero, blurring its relationship with ENSO, but in another La Niña year of 2008 winter through 2009 spring, the anomaly is generally negative. In Park and Leovy (2004), they showed negative anomalies of low-level clouds during positive ENSO phase using ship observations reported by the Extended Edited Cloud Report Archive (EECRA), i.e. less low-level clouds in El Niño year. While in our study, it is likely that MODIS data and four-year CC data is insufficient to support the relationship between liquid cloud occurrnence and ENSO over SEA.

Overall, the interannual variations of clouds over SEA are primarily due to the change of ice clouds, which are consistent with the statements in previous studies that in El Niño year, anomalous subsidence over the Western equatorial Pacific decreases cloud amount by suppressing deep convection and reducing high clouds (Park and Leovy, 2004; Wang and Su, 2015). As a result, the observed radiation at the TOA adjust accordingly (Loeb et al., 2012). As cloud phases vary varies interannually, as does and hence change H_σ the spatial heterogeneity at the TOA change correspondingly, i.e., being smoother in La Niña years than normal and vice versa incompared to El Niño years. Also, the timeseries of all-sky H_σ anomaliesy well varyies with ENSO and it correlates well with that of $R_{0.645}$ ($r \sim -0.8$, significant at 99% confidence level) and BT_{11} ($r \sim 0.8$, significant at 99% confidence level), indicating that H_σ can be one valuable observed parameter to investigate ENSO such as tracking ENSO or validation of ENSO simulations by climate models, including its basis for indicating the disentangling true space-time variability, associated with the ENSO, of the biases of cloud optical/microphysical properties retrieved from passive sensors, caused by departures from the plane-parallel assumption. associated with the ENSO from space-time variability of biases in passive retrievals of these cloud properties caused by departures from the plane-parallel assumption.

4. Discussions and Conclusions

This work is incontributes to a series of studies that examine cloud vertical structures. Li et al. (2015) explored the vertical distributions of cloud types using the 2B-CLDCLASS-LIDAR data, while Oreopoulos et al. (2017) interpreted the overlap feature of high, middle and low clouds. Considering the need ofed cloud phase information for improving GCMs (e.g., Cesana and Storelvmo, 2017), the current study focuses on investigating the characteristics of cloud

vertical structures, spatial heterogeneity and spectral radiances from the perspective of cloud phases over Southeast Asia. Utilizing the state-of-the-art CloudSat and CALIPSO (CC) observations, five cloud groups have been classified~~: including~~ ice-only, ice-above-liquid, ice-above-mixed, liquid-only and mixed-only clouds to capture the main vertical structures of cloud phases. By collocating the CC-MODIS data, the spectral and spatial heterogeneity signatures at the TOA of each CC cloud group~~s~~ have been examined. Seasonal, intraseasonal and interannual variations of these cloud phase characteristics have also been shown in this work.

A general review on cloud spatial distributions and meteorology shows that the annual cloud occurrence frequency over SEA is about 81~~0~~.4~~9~~%, being more frequent in summer (86~~5~~.5~~8~~%) and less frequent in winter (78~~7~~.7%) based on the CC observations. Ice-only (28~~7~~.6~~8~~%), ice-above-liquid (20~~1~~.1~~9~~%), ice-above-mixed (9~~7~~.3~~4~~%) and mixed-only (6.7~~2~~%) clouds, i.e. 'ice contained clouds', preferentially occur in a warm, humid and unstable environment ~~as these clouds occur~~and are associated with the seasonal movement of the monsoon and ITCZ ~~climate systems~~. It is noted that ice-only and ice-above-liquid clouds are~~occur~~ associated with similar upper troposphere dynamics, i.e., comparable mean temperature, specific humidity and static stability, while ice-above-mixed clouds occur in an environment with larger specific humidity at the upper troposphere. Liquid-only clouds appear~~occur~~ frequently in winter and spring over s~~S~~outheast China and East China sea where the lower troposphere is~~are~~ relatively cold, dry and stable.

It is shown that ice clouds over SEA are thin with about ~~more than~~ 60% and 80% samples with geometrical thickness smaller than 3.0 km and optical depth less than 3, respectively. Ice-only clouds have larger mean thickness (geometrical and optical) and Re than the ice layers above liquid or mixed clouds. Although there could exist sampling biases due to instrument limitations, ~~yet~~ a higher frequency of ice-only clouds at $1.6 < \tau < 3.0$ demonstrates that more ice-only clouds develop thicker than either the ice layers above liquid or mixed clouds. The tops of liquid-only clouds are on average lower than that of the liquid below ice clouds. As liquid-only clouds occur more frequently with increase of LTSS, their vertical development is likely to be inhibited. However, ice-above-liquid clouds more favorably distribute in a warm, humid and unstable environment, which allows the underlying liquid clouds to grow deeper. The tops of mixed layers below ice clouds are primarily located at about 6 km. For mixed-only clouds, their tops are primarily at 16 km over ocean, but over land, a large fraction of samples have cloud top around 6 km. These results ~~indicate~~ suggest~~s~~ that ice-above-mixed and mixed-only clouds over land are under development in the early afternoon.

We also show that distinct spatial heterogeneity exists between~~-~~ the five cloud groups~~different cloud phases and their overlaps~~. Ice-only, ice-above-mixed and mixed-only clouds are usually homogeneous, i.e., small H_σ values. In contrast, liquid-only clouds show the largest H_σ among all cloud phase groups, being the most heterogeneous. Ice-above-liquid clouds have large but slightly smaller H_σ values than liquid-only clouds because the overlying homogenous and thin ice clouds slightly smooth the radiation emerging from the low-level liquid clouds. A typical H_σ value for clear sky is 0.01, however, clear sky H_σ can be as large as 1, resulting from the increase of subpixel variability due to undetected liquid clouds in the ~~some~~ MODIS and CC pixels. As large H_σ values are reported to associate with the biases of cloud τ

and Re derived from passive sensors (Di Girolamo et al., 2010; Zhang and Platnick, 2011), ~~these~~ biases resulted from plane-parallel assumption are expected to be larger for liquid than ice clouds. ~~One should be cautious to these biases when interpreting cloud-aerosol relationship.~~ The seasonal patterns of all-sky H_σ show that small values are in north of the equator over Indian and West Pacific Ocean in summer but move southward in autumn and winter, being consistent with the seasonal shift of the 'ice-contained clouds'.

Difference of cloud optical, micro and macrophysical properties leads to distinct spectral features between the five cloud groups. The liquid-only clouds show zero $R_{1.375}$, large reflectance ratio ~~of between~~ the SWIR ~~to~~and the visible, high BTs and negative BTD between 8.5 and 11 μm. Ice-only clouds in contrast show notable $R_{1.375}$, reflectance ratio generally smaller than 0.4, relatively low BTs and more than 50% samples with positive BTD. Ice-above-liquid clouds behave more like ice-only clouds in the IR because these two cloud groups have similar BT_{11} and BTD PDFs, but ice-above-liquid clouds act more like liquid-only clouds in the SW spectral due to their similar PDFs/CDFs of reflectance ratio. The average $R_{1.375}$ of ice-above-liquid clouds, which is mainly contributed by the ice layers only, is smaller than that of ice-only clouds. Similarly, ~~the average BT_{11} of~~ ice-above-liquid clouds have their average BT_{11} ~~is~~ slightly larger than that of ice-only clouds. These results demonstrate that ice-only clouds are on average thicker than the ice layers above liquid clouds, being consistent with the conclusions derived from the CC observations. Mixed-only or ice-above-mixed clouds usually have large $R_{0.64}$, small reflectance ratio, low BT_{11} and positive BTD. It is also noted that the $R_{0.645}$ and BT_{11} PDFs of ice-only, liquid-only and ice-above-liquid clouds show their frequency peak nearly same as that of clear sky, revealing ubiquitous thin clouds over SEA.

Cloud phases together with their spectral and spatial heterogeneity features have also been examined in different MJO and ENSO phases. In the MJO active phase, more frequent 'ice-contained clouds' conattribute to a smooth MJO center. On both sides of the MJO convective center, large H_σ values are observed due to increase of liquid clouds and decrease of 'ice-contained clouds'. Thus, ~~.~~ the H_σ pattern reveals the eastward-propagating MJO. Similarly, the interannual variation of clouds over SEA is primarily due to the change of 'ice-contained clouds'. Increased 'ice-contained clouds' in La Niña year result in more ~~abnormally~~ homogeneous spatial heterogeneity, stronger $R_{0.645}$ and lower BT_{11}, and vice versa in El Niño year. The observed H_σ varies with the ENSO index with ~~their~~a correlation coefficient ~~to be~~of 0.49 (significant at confidence level 0.99). The H_σ varying with the MJO and ENSO forms a basis for disentangle the true intraseasonal/interannual variability of cloud optical/microphysical properties from the space-time variability of cloud biases due to the plane-parallel assumption in cloud retrievals from passive sensors.

~~Our results showing the space-time variability of H_σ Hs with the MJO and ENSO forms the basis for disentangling true space-time variability of cloud optical microphysical properties associated with the MJO and ENSO from the space-time variability of biases in passive retrievals of these cloud properties caused by departures from the plane-parallel assumption. values capture the MJO and ENSO features, implying that the H_σ is able to track MJO and ENSO and provides a way to validate their simulations in GCMs.~~

Formatted: Indent: First line: 0"

~~As the CC observations are sensitive to a wide range of cloud scenarios, cloud patterns shown here can help interpreting the cloud product variability in SEA as discussed in Reid et al., (2013). The results also provide summaries of spectral radiation at the TOA useful for accessing model output of spectral radiance computed from modeled clear and cloud properties, such as those found within GCM or reanalysis products , providingClimatological characteristics of cloud phases provided in this study can serve as a benchmark to improve the performance of climate models in validating their simulations of cloud phases and their vertical overlap, their spatial heterogeneity and spectral signatures, including cloud. Since these models also use the plane-parallel assumption in computing the spectral radiation leaving the TOA, careful comparisons between model and observations can use H_σHs as a measure of departure from the plane-parallel assumption. Particularly, spatial heterogeneity, a direct measured variable from satellite that reveals subpixel variability of different cloud phases, is not only able to track the MJO and ENSO but is also useful to accessing the performance of GCMs in capturing cloud property variations associated with the MJO and ENSO can use the space-time behavior of H_σHs shown here in a manner similar toevaluate how well GCMs capture subpixel cloudsLoveridge and Davies (2019), where they used H_σHs in examining GCM clouds in different sectors of southern hemisphere cyclones. (e.g., Loveridge and Davies, 2019).~~

Finally, we note that our results may be used to evaluate a model's verisimilitude in capturing cloud properties, particularly phase and spectral characteristics. For example, we show summaries of spectral radiance at the TOA segregated by cloud phase and overlap conditions that can serve as a basis for comparing to those computed from model outputs—a similar approach given by previous research (e.g. Hashino et al., 2013; Masunaga et al., 2010; Yao et al., 2020). Since these models also use the plane-parallel assumption in computing the spectral radiation leaving the TOA, careful comparisons between model and observations can use Hσ as a measure of departure from the plane-parallel assumption in a manner similar to Loveridge and Davies, (2019), where they used Hσ within their analysis in examining GCM clouds in different sectors of southern hemisphere cyclones. The use of Hσ also extends its application to gauge biases in other satellite products used in model evaluation (e.g. Gettelman et al., 2015; Song et al., 2018), such as cloud optical depth and effective radius, whose biases have been noted to covary with H_σ (Fu et al., 2019; Zhang et al., 2016).

Data availability. Data used in this study are summarized in Table 1 and their availability is provided in acknowledgements.

Author contributions. YH and LD conceived this study. YH analyzed the results and wrote the manuscript. LD joined result discussions and refined this manuscript.

Competing interests. The authors declare that they have no conflict of interest.

Formatted: Font: Not Italic
Formatted: Font: Not Italic
Formatted: Font: Not Italic
Field Code Changed
Formatted: Font: Not Italic
Formatted: Font: Not Italic
Formatted: Font: Not Italic
Formatted: Font: Not Italic
Formatted: Font: Not Italic
Formatted: Font: Not Italic
Formatted: Font: Not Italic
Formatted: Font: Not Italic
Formatted: Font: Not Italic
Formatted: Indent: First line: 0.5"

Acknowledgements. This research has been supported by the Cloud, Aerosol and Monsoon Processes Philippines Experiment (CAMP^{2}Ex) ~~and by~~ under NASA Grant 80NSSC18K0144. We are grateful to Dr. Guangyu Zhao for his ~~offer~~ examination of clear sky H_σ derived from ASTER and MODIS. We acknowledge the members of the CloudSat Data Processing Center who provide CloudSat products, including 2B-CLDCLASS-LIDAR, 2C-ICE and ECMWF-AUX, available at http://www.cloudsat.cira.colostate.edu/. The MODIS products, MYD021KM, MYD03 and MYD06, are obtained via the Atmosphere Archive and Distribution System (LAADS) Distributed Active Archive Center (DAAC), which is available at https://ladsweb.modaps.eosdis.nasa.gov/. We also thank Bureau of Meteorology in Australia offering MJO index and NOAA Earth System Research Laboratory providing Multivariate ENSO index.

References

Adames, Á. F., Wallace, J. M. and Monteiro, J. M.: Seasonality of the structure and propagation characteristics of the MJO, J. Atmos. Sci., 73, 3511–3526, doi:10.1175/JAS-D-15-0232.1, 2016.

As-Syakur, A. R., Osawa, T., Miura, F., Nuarsa, I. W., Ekayanti, N. W., Dharma, I. G. B. S., Adnyana, I. W. S., Arthana, I. W. and Tanaka, T.: Maritime Continent rainfall variability during the TRMM era: The role of monsoon, topography and El Niño Modoki, Dyn. Atmos. Ocean., 75, 58–77, doi:10.1016/j.dynatmoce.2016.05.004, 2016.

Barnes, W. L., Pagano, T. S. and Salomonson, V. V.: Prelaunch characteristics of the moderate resolution, IEEE Trans. Geosci. Remote Sens., 36, 1088–1100, 1998.

Baum, B. A., Menzel, W. P., Frey, R. A., Tobin, D. C., Holz, R. E., Ackerman, S. A., Heidinger, A. K. and Yang, P.: MODIS cloud-top property refinements for collection 6, J. Appl. Meteorol. Climatol., 51, 1145–1163, doi:10.1175/JAMC-D-11-0203.1, 2012.

Berry, E., Mace, G. G. and Gettelman, A.: Using A-Train observations to evaluate cloud occurrence and radiative effects in the Community Atmosphere Model during the Southeast Asia summer monsoon, J. Clim., 32, 4145–4165, doi:10.1175/jcli-d-18-0693.1, 2019.

Bouet, C., Szczap, F., Leriche, M. and Benassi, A.: What is the effect of cloud inhomogeneities on actinic fluxes and chemical species concentrations?~~,~~ Geophys. Res. Lett., 33, L01818, doi:10.1029/2005GL024727, 2006.

Cesana, G.: Using in situ airborne measurements to evaluate three cloud phase products derived from CALIPSO, J. Geophys. Res. Atmos., 121, 5788–5808, doi:10.1002/2014JD022963, 2016.

Cesana, G. and Storelvmo, T.: Improving climate projections by understanding how cloud phase affects radiation, J. Geophys. Res. Atmos., 122, 4594–4599, doi:10.1002/2017JD026927, 2017.

Cesana, G. and Waliser, D. E.: Characterizing and understanding systematic biases in the vertical structure of clouds in CMIP5/CFMIP2 models, Geophys. Res. Lett., 43, 10,538-10,546, doi:10.1002/2016GL070515, 2016.

Cesana, G., Waliser, D. E., Henderson, D., L'Ecuyer, T. S., Jiang, X. and Li, J.-L. F.: The vertical structure of radiative heating rates: A multimodel evaluation using A-train satellite

observations, J. Clim., 32, 1573–1590, doi:10.1175/jcli-d-17-0136.1, 2018.

Cesana, G., Del Genio, A. D. and Chepfer, H.: The Cumulus And Stratocumulus CloudSat-CALIPSO Dataset (CASCCAD), Earth Syst. Sci. Data Discuss., 2667637(November), 1–33, doi:10.5194/essd-2019-73, 2019.

Cho, H. M., Nasiri, S. L. and Yang, P.: Application of CALIOP measurements to the evaluation of cloud phase derived from MODIS infrared channels, J. Appl. Meteorol. Climatol., 48, 2169–2180, doi:10.1175/2009JAMC2238.1, 2009.

Cho, H. M., Zhang, Z., Meyer, K., Lebsock, M., Platnick, S., Ackerman, A. S., Di Girolamo, L., Labonnote, L. C., Cornet, C., Riedi, J. and Holz, R. E.: Frequency and causes of failed MODIS cloud property retrievals for liquid phase clouds over global oceans, J. Geophys. Res. Atmos., 120, 4132–4154, doi:10.1002/2015JD023161, 2015.

Christensen, M. W., Carrió, G. G., Stephens, G. L. and Cotton, W. R.: Radiative impacts of free-tropospheric clouds on the properties of marine stratocumulus, J. Atmos. Sci., 70, 3102–3118, doi:10.1175/JAS-D-12-0287.1, 2013.

Cronk, H. and Partain, P.: CloudSat ECMWF-AUX auxillary data product process description and interface control document, ,–15 pp [online] Available from: http://www.cloudsat.cira.colostate.edu/sites/default/files/products/files/ECMWF-AUX_PDICD.P_R05.rev0_.pdf, 2017.

Deng, M., Mace, G. G., Wang, Z. and Okamoto, H.: Tropical composition, cloud and climate coupling experiment validation for cirrus cloud profiling retrieval using cloudsat radar and CALIPSO lidar, J. Geophys. Res., 115, D00J15, doi:10.1029/2009JD013104, 2010.

Deng, M., Mace, G. G., Wang, Z. and Lawson, R. P.: Evaluation of several A-train ice cloud retrieval products with in situ measurements collected during the SPARTICUS campaign, J. Appl. Meteorol. Climatol., 52, 1014–1030, doi:10.1175/JAMC-D-12-054.1, 2013.

Dolinar, E. K., Dong, X., Xi, B., Jiang, J. H. and Su, H.: Evaluation of CMIP5 simulated clouds and TOA radiation budgets using NASA satellite observations, Clim. Dyn., 44, 2229–2247, doi:10.1007/s00382-014-2158-9, 2014.

Eliasson, S., Buehler, S. a., Milz, M., Eriksson, P. and John, V. O.: Assessing observed and modelled spatial distributions of ice water path using satellite data, Atmos. Chem. Phys., 11, 375–391, doi:10.5194/acp-11-375-2011, 2011.

Fu, D., Di Girolamo, L., Liang, L. and Zhao, G.: Regional Biases in MODIS Marine Liquid Water Cloud Drop Effective Radius Deduced Through Fusion With MISR, J. Geophys. Res. Atmos., 124(23), 13182–13196, doi:10.1029/2019JD031063, 2019.

Gettelman, A., Morrison, H., Santos, S., Bogenschutz, P. and Caldwell, P. M.: Advanced two-moment bulk microphysics for global models. Part II: Global model solutions and aerosol-cloud interactions, J. Clim., 28(3), 1288–1307, doi:10.1175/JCLI-D-14-00103.1, 2015.

Di Girolamo, L., Liang, L. and Platnick, S.: A global view of one-dimensional solar radiative transfer through oceanic water clouds, Geophys. Res. Lett., 37, L18809, doi:10.1029/2010GL044094, 2010.

Grise, K. M., Thompson, D. W. J. and Birner, T.: A global survey of static stability in the stratosphere and upper troposphere, J. Clim., 23, 2275–2292, doi:10.1175/2009JCLI3369.1, 2010.

Grose, M. R., Brown, J. N., Narsey, S., Brown, J. R., Murphy, B. F., Langlais, C., Gupta, A. Sen, Moise, A. F. and Irving, D. B.: Assessment of the CMIP5 global climate model simulations of the western tropical Pacific climate system and comparison to CMIP3, Int. J. Climatol., 34, 3382–3399, doi:10.1002/joc.3916, 2014.

Haladay, T. and Stephens, G.: Characteristics of tropical thin cirrus clouds deduced from joint CloudSat and CALIPSO observations, J. Geophys. Res., 114, D00A25, doi:10.1029/2008JD010675, 2009.

Ham, S.-H., Kato, S., Barker, H. W., Rose, F. G. and Sun-Mack, S.: Improving the modelling of short-wave radiation through the use of a 3D scene construction algorithm, Q. J. R. Meteorol. Soc., 141, 1870–1883, doi:10.1002/qj.2491, 2015.

Hashino, T., Satoh, M., Hagihara, Y., Kubota, T., Matsui, T., Nasuno, T. and Okamoto, H.: Evaluating cloud microphysics from NICAM against CloudSat and CALIPSO, J. Geophys. Res. Atmos., 118, 7273–7292, doi:10.1002/jgrd.50564, 2013.

Hong, Y. and Liu, G.: The characteristics of ice cloud properties derived from CloudSat and CALIPSO measurements, J. Clim., 28, 3880–3901, doi:10.1175/JCLI-D-14-00666.1, 2015.

Hong, Y., Liu, G. and Li, J.-L. F.: Assessing the radiative effects of global ice clouds based on CloudSat and CALIPSO measurements, J. Clim., 29, 7651–7674, doi:10.1175/JCLI-D-15-0799.1, 2016.

Hu, Y., Winker, D., Vaughan, M., Lin, B., Omar, A., Trepte, C., Flittner, D., Yang, P., Nasiri, S. L., Baum, B., Sun, W., Liu, Z., Wang, Z., Young, S., Stamnes, K., Huang, J., Kuehn, R. and Holz, R.: CALIPSO/CALIOP cloud phase discrimination algorithm, J. Atmos. Ocean. Technol., 26, 2293–2309, doi:10.1175/2009JTECHA1280.1, 2009.

Hu, Y., Rodier, S., Xu, K. M., Sun, W., Huang, J., Lin, B., Zhai, P. and Josset, D.: Occurrence, liquid water content, and fraction of supercooled water clouds from combined CALIOP/IIR/MODIS measurements, J. Geophys. Res., 115, D00H34, doi:10.1029/2009JD012384, 2010.

Jiang, J. H., Su, H., Zhai, C., Perun, V. S., Del Genio, A., Nazarenko, L. S., Donner, L. J., Horowitz, L., Seman, C., Cole, J., Gettelman, A., Ringer, M. A., Rotstayn, L., Jeffrey, S., Wu, T., Brient, F., Dufresne, J.-L., Kawai, H., Koshiro, T., Watanabe, M., LÉcuyer, T. S., Volodin, E. M., Iversen, T., Drange, H., Mesquita, M. D. S., Read, W. G., Waters, J. W., Tian, B., Teixeira, J. and Stephens, G. L.: Evaluation of cloud and water vapor simulations in CMIP5 climate models using NASA “A-Train” satellite observations, J. Geophys. Res., 117, D14105, doi:10.1029/2011jd017237, 2012.

Kay, J. E., Bourdages, L., Miller, N. B., Morrison, A., Yettella, V., Chepfer, H. and Eaton, B.: Evaluating and improving cloud phase in the Community Atmosphere Model version 5 using spaceborne lidar observations, J. Geophys. Res. Atmos., 121, 4162–4176, doi:10.1002/2015JD024699, 2016.

King, M. D., Kaufman, Y. J., Menzel, W. P. and Tanré, D.: Remote sensing of cloud, aerosol, and water vapor properties from the Moderate Resolution Imaging Spectrometer (MODIS), IEEE Trans. Geosci. Remote Sens., 30, 2–27, doi:10.1109/36.124212, 1992.

King, M. D., Platnick, S., Menzel, W. P., Ackerman, S. A. and Hubanks, P. A.: Spatial and temporal distribution of clouds observed by MODIS onboard the Terra and Aqua satellites, IEEE Trans. Geosci. Remote Sens., 51, 3826–3852, doi:10.1109/TGRS.2012.2227333, 2013.

Klein, S. A. and Hartmann, D.: The seasonal cycle of low startiform clouds, J. Clim., 6, 1587–1606, doi:10.1175/1520-0442(1993)006<1587, 1993.

Knutson, T. R., Weickmann, K. M. and Kutzbach, J. E.: Global-scale intraseasonal oscillations of outgoing longwave radiation and 250 mb zonal wind during northern hemisphere summer, Mon. Weather Rev., 114, 605–623, 1986.

Leahy, L. V., Wood, R., Charlson, R. J., Hostetler, C. A., Rogers, R. R., Vaughan, M. A. and Winker, D. M.: On the nature and extent of optically thin marine low clouds, J. Geophys. Res., 117, D22201, doi:10.1029/2012JD017929, 2012.

Li, J.-L. F., Waliser, D. E., Stephens, G., Lee, S., L'Ecuyer, T., Kato, S., Loeb, N. and Ma, H.-Y.: Characterizing and understanding radiation budget biases in CMIP3/CMIP5 GCMs, contemporary GCM, and reanalysis, J. Geophys. Res. Atmos., 118, 8166–8184, doi:10.1002/jgrd.50378, 2013.

Li, J., Yi, Y., Minnis, P., Huang, J., Yan, H., Ma, Y., Wang, W. and Kirk Ayers, J.: Radiative effect differences between multi-layered and single-layer clouds derived from CERES, CALIPSO, and CloudSat data, J. Quant. Spectrosc. Radiat. Transf., 112, 361–375, doi:10.1016/j.jqsrt.2010.10.006, 2011.

Li, J., Huang, J., Stamnes, K., Wang, T., Lv, Q. and Jin, H.: A global survey of cloud overlap based on CALIPSO and CloudSat measurements, Atmos. Chem. Phys., 15, 519–536, doi:10.5194/acp-15-519-2015, 2015.

Li, Y., Thompson, D. W. J., Stephens, G. L. and Bony, S.: A global survey of the instantaneous linkages between cloud vertical structure and large-scale climate, J. Geophys. Res. Atmos., 119, 3770–3792, doi:10.1002/2013JD020669, 2014.

Liang, L., Di Girolamo, L. and Platnick, S.: View-angle consistency in reflectance, optical thickness and spherical albedo of marine water-clouds over the northeastern Pacific through MISR-MODIS fusion, Geophys. Res. Lett., 36, L09811, doi:10.1029/2008GL037124, 2009.

Liang, L., Di Girolamo, L. and Sun, W.: Bias in MODIS cloud drop effective radius for oceanic water clouds as deduced from optical thickness variability across scattering angles, J. Geophys. Res. Atmos., 120, 7661–7681, doi:10.1002/2015JD023256, 2015.

Lin, N. H., Tsay, S. C., Maring, H. B., Yen, M. C., Sheu, G. R., Wang, S. H., Chi, K. H., Chuang, M. T., Ou-Yang, C. F., Fu, J. S., Reid, J. S., Lee, C. Te, Wang, L. C., Wang, J. L., Hsu, C. N., Sayer, A. M., Holben, B. N., Chu, Y. C., Nguyen, X. A., Sopajaree, K., Chen, S. J., Cheng, M. T., Tsuang, B. J., Tsai, C. J., Peng, C. M., Schnell, R. C., Conway, T., Chang, C. T., Lin, K. S., Tsai, Y. I., Lee, W. J., Chang, S. C., Liu, J. J., Chiang, W. L., Huang, S. J., Lin, T. H. and Liu, G. R.: An overview of regional experiments on biomass burning aerosols and related

pollutants in Southeast Asia: From BASE-ASIA and the Dongsha Experiment to 7-SEAS, Atmos. Environ., 78, 1–19, doi:10.1016/j.atmosenv.2013.04.066, 2013.

Liou, K.-N.: Influence of cirrus clouds on weather and climate processes: A global perspective, Mon. Weather Rev., 114, 1167–1199, doi:10.1175/1520-0493(1986)114<1167:IOCCOW>2.0.CO;2, 1986.

Loeb, N. G. and Davies, R.: Observational evidence of plane parallel model biases : Apparent dpendence of cloud optical depth on solar zenith angle, J. Geophys. Res., 101, 1621–1634, 1996.

Loeb, N. G. and Davies, R.: Angular dependence of observed reflectances: A comparison with plane parallel theory, J. Geophys. Res. Atmos., 102(D6), 6865–6881, doi:10.1029/96JD03586, 1997.

Loeb, N. G., Kato, S., Su, W., Wong, T., Rose, F. G., Doelling, D. R., Norris, J. R. and Huang, X.: Advances in understanding top-of-atmosphere radiation variability from satellite observations, Surv. Geophys., 33, 359–385, doi:10.1007/s10712-012-9175-1, 2012.

Mace, G. G., Zhang, Q., Vaughan, M., Marchand, R., Stephens, G., Trepte, C. and Winker, D.: A description of hydrometeor layer occurrence statistics derived from the first year of merged Cloudsat and CALIPSO data, J. Geophys. Res., 114, D00A26, doi:10.1029/2007JD009755, 2009.

Madden, R. A. and Julian, P. R.: Detection of a 40-50 Day Oscillation in the Zonal Wind in the Tropical Pacific, J. Atmos. Sci., 28, 702–708, doi:https://doi.org/10.1175/1520-0469(1971)028<0702:DOADOI>2.0.CO;2, 1971.

Marchant, B., Platnick, S., Meyer, K., Thomas Arnold, G. and Riedi, J.: MODIS Collection 6 shortwave-derived cloud phase classification algorithm and comparisons with CALIOP, Atmos. Meas. Tech., 9, 1587–1599, doi:10.5194/amt-9-1587-2016, 2016.

Marshak, A. and Davis, A. B.: Horizontal fluxes and radiative smoothing, in 3D Radiative Transfer in Cloudy Atmospheres, pp. 543–586., 2005.

Marshak, A., Platnick, S., Várnai, T., Wen, G. and Cahalan, R. F.: Impact of three-dimensional radiative effects on satellite retrievals of cloud droplet sizes, J. Geophys. Res., 111, D09207, doi:10.1029/2005JD006686, 2006.

Masunaga, H., Matsui, T., Tao, W. K., Hou, A. Y., Kummerow, C. D., Nakajima, T., Bauer, P., Olson, W. S., Sekiguchi, M. and Nakajima, T. Y.: Satellite data simulator unit: A multisensor, multispectral satellite simulator package, Bull. Am. Meteorol. Soc., 91(12), 1625–1632, doi:10.1175/2010BAMS2809.1, 2010.

Matus, A. V. and L'Ecuyer, T. S.: The role of cloud phase in Earth's radiation budget, J. Geophys. Res. Atmos., 122, 2559–2578, doi:10.1002/2016JD025951, 2017.

McFarquhar, G. M., Heymsfield, A. J., Spinhirne, J. and Hart, B.: Thin and subvisual tropopause tropical cirrus: Observations and radiative impacts, J. Atmos. Sci., 57, 1841–1853, doi:10.1175/1520-0469(2000)057<1841:TASTTC>2.0.CO;2, 2000.

Nesbitt, S. W. and Zipser, E. J.: The diurnal cycle of rainfall and convective intensity according to three years of TRMM measurements, J. Clim., 16, 1456–1475, doi:10.1175/1520-0442-

16.10.1456, 2003.

O'Hirok, W. and Gautier, C.: The impact of model resolution on differences between independent column approximation and monte carlo estimates of shortwave surface irradiance and atmospheric heating rate, J. Atmos. Sci., 62, 2939–2951, doi:10.1175/jas3519.1, 2005.

Oreopoulos, L., Cho, N. and Lee, D.: New insights about cloud vertical structure from CloudSat and CALIPSO observations, J. Geophys. Res. Atmos., 122, 9280–9300, doi:10.1002/2017JD026629, 2017.

Park, S. and Leovy, C. B.: Marine low-cloud anomalies associated with ENSO, J. Clim., 17, 3448–3469, doi:10.1175/1520-0442(2004)017<3448:MLAAWE>2.0.CO;2, 2004.

Pincus, R., Platnick, S., Ackerman, S. A., Hemler, R. S. and Patrick Hofmann, R. J.: Reconciling simulated and observed views of clouds: MODIS, ISCCP, and the limits of instrument simulators, J. Clim., 25(13), 4699–4720, doi:10.1175/JCLI-D-11-00267.1, 2012.

Platnick, S., King, M. D., Ackerman, S. A., Menzel, W. P., Baum, B. A., Riédi, J. C. and Frey, R. A.: The MODIS cloud products : Algorithms and examples from Terra, IEEE Trans. Geosci. Remote Sens., 41, 459–473, doi:10.1109/TGRS.2002.808301, 2003.

Reid, J. S., Xian, P., Hyer, E. J., Flatau, M. K., Ramirez, E. M., Turk, F. J., Sampson, C. R., Zhang, C., Fukada, E. M. and Maloney, E. D.: Multi-scale meteorological conceptual analysis of observed active fire hotspot activity and smoke optical depth in the Maritime Continent, Atmos. Chem. Phys., 12, 2117–2147, doi:10.5194/acp-12-2117-2012, 2012.

Reid, J. S., Hyer, E. J., Johnson, R. S., Holben, B. N., Yokelson, R. J., Zhang, J., Campbell, J. R., Christopher, S. A., Di Girolamo, L., Giglio, L., Holz, R. E., Kearney, C., Miettinen, J., Reid, E. A., Turk, F. J., Wang, J., Xian, P., Zhao, G., Balasubramanian, R., Chew, B. N., Janjai, S., Lagrosas, N., Lestari, P., Lin, N. H., Mahmud, M., Nguyen, A. X., Norris, B., Oanh, N. T. K., Oo, M., Salinas, S. V., Welton, E. J. and Liew, S. C.: Observing and understanding the Southeast Asian aerosol system by remote sensing: An initial review and analysis for the Seven Southeast Asian Studies (7SEAS) program, Atmos. Res., 122, 403–468, doi:10.1016/j.atmosres.2012.06.005, 2013.

Riley, E. M., Mapes, B. E. and Tulich, S. N.: Clouds associated with the Madden–Julian Oscillation: A new perspective from CloudSat, J. Atmos. Sci., 68, 3032–3051, doi:10.1175/JAS-D-11-030.1, 2011.

Ross, A. D., Holz, R. E., Quinn, G., Reid, J. S., Xian, P., Joseph Turk, F. and Posselt, D. J.: Exploring the first aerosol indirect effect over Southeast Asia using a 10-year collocated MODIS, CALIOP, and model dataset, Atmos. Chem. Phys., 18, 12747–12764, doi:10.5194/acp-18-12747-2018, 2018.

Sassen, K. and Wang, Z.: Classifying clouds around the globe with the CloudSat radar: 1-year of results, Geophys. Res. Lett., 35, L04805, doi:10.1029/2007GL032591, 2008.

Sassen, K., Wang, Z. and Liu, D.: Global distribution of cirrus clouds from CloudSat/Cloud-Aerosol Lidar and Infrared Pathfinder Satellite Observations (CALIPSO) measurements, J. Geophys. Res., 113, D00A12, doi:10.1029/2008JD009972, 2008.

Savtchenko, A., Ouzounov, D., Ahmad, S., Acker, J., Leptoukh, G., Koziana, J. and Nickless,

D.: Terra and Aqua MODIS products available from NASA GES DAAC, Adv. Sp. Res., 34, 710–714, doi:10.1016/j.asr.2004.03.012, 2004.

Song, H., Zhang, Z., Ma, P. L., Ghan, S. J. and Wang, M.: An evaluation of marine boundary layer cloud property simulations in the Community Atmosphere Model using satellite observations: Conventional subgrid parameterization versus CLUBB, J. Clim., 31(6), 2299–2320, doi:10.1175/JCLI-D-17-0277.1, 2018.

Song, S., Sebastian Schmidt, K., Pilewskie, P., King, D. M., Heidinger, K. A., Walther, A., Iwabuchi, H., Wind, G. and Coddington, M. O.: The spectral signature of cloud spatial structure in shortwave irradiance, Atmos. Chem. Phys., 16(21), 13791–13806, doi:10.5194/acp-16-13791-2016, 2016.

Stephens, G., Winker, D., Pelon, J., Trepte, C., Vane, D., Yuhas, C., L'Ecuyer, T. and Lebsock, M.: Cloudsat and CALIPSO within the A-train: Ten years of actively observing the earth system, Bull. Am. Meteorol. Soc., 99, 569–581, doi:10.1175/BAMS-D-16-0324.1, 2018.

Stephens, G. L., Vane, D. G., Boain, R. J., Mace, G. G., Sassen, K., Wang, Z., Illingworth, A. J., O'Connor, E. J., Rossow, W. B., Durden, S. L., Miller, S. D., Austin, R. T., Benedetti, A. and Mitrescu, C.: The cloudsat mission and the A-Train: A new dimension of space-based observations of clouds and precipitation, Bull. Am. Meteorol. Soc., 83, 1771–1790, doi:10.1175/BAMS-83-12-1771, 2002.

Stephens, G. L., Vane, D. G., Tanelli, S., Im, E., Durden, S., Rokey, M., Reinke, D., Partain, P., Mace, G. G., Austin, R., L'Ecuyer, T., Haynes, J., Lebsock, M., Suzuki, K., Waliser, D., Wu, D., Kay, J., Gettelman, A., Wang, Z. and Marchand, R.: CloudSat mission: Performance and early science after the first year of operation, J. Geophys. Res., 113, D00A18, doi:10.1029/2008JD009982, 2008.

Waliser, D. E., Li, J.-L. F., Woods, C. P., Austin, R. T., Bacmeister, J., Chern, J., Del Genio, A., Jiang, J. H., Kuang, Z., Meng, H., Minnis, P., Platnick, S., Rossow, W. B., Stephens, G. L., Sun-Mack, S., Tao, W.-K., Tompkins, A. M., Vane, D. G., Walker, C. and Wu, D.: Cloud ice: A climate model challenge with signs and expectations of progress, J. Geophys. Res., 114, D00A21, doi:10.1029/2008JD010015, 2009.

Wang, Z.: CloudSat 2B-CLDCLASS-LIDAR Product Process Description and Interface Control Document,~~,~~ 1–59 [online] Available from: http://www.cloudsat.cira.colostate.edu/sites/default/files/products/files/2B-CLDCLASS-LIDAR_PDICD.P1_R05.rev0_.pdf, 2019.

Wang, Z. and Sassen, K.: Cloud type and macrophysical property retrieval using multiple remote sensors, J. Appl. Meteorol., 40, 1665–1682, doi:10.1175/1520-0450(2001)040<1665:CTAMPR>2.0.CO;2, 2001.

Wang, Z., Vane, D. and Staphens, G.: Level 2 Combined Radar and Lidar Cloud Scenario Classification Product Process Description and Interface Control document. [online] Available from: http://scholar.google.com/scholar?hl=en&btnG=Search&q=intitle:Level+2+Combined+Radar+and+Lidar+Cloud+Scenario+Classification+Product+Process+Description+and+Interface+Control+Document#1, 2012.

Wheeler, M. C. and Hendon, H. H.: An all-season real-time multivariate MJO index : Development of an index for monitoring and prediction, Mon. Weather Rev., 132, 1917–1932, 2004.

Winker, D. M., Pelon, J. R. and McCormick, M. P.: The CALIPSO mission: Spaceborne lidar for observation of aerosols and clouds, Lidar Remote Sens. Ind. Environ. Monit. III, 4893, 1–11, doi:10.1117/12.466539, 2003.

Wolter, K. and Timlin, M. S.: Monitoring ENSO in COADS with a seasonality adjusted principal component index, in Proc. of the 17th Climate Diagnostics Workshop, Norman, OK, NOAA/NMC/CAC, NSSL, Oklahoma Clim. Survey, CIMMS and the School of Meteor., Univ. of Oklahoma, pp. 52–57., 1993.

Wolter, K. and Timlin, M. S.: Measuring the strength of ENSO events: How does 1997/1998 rank?, Weather, 53, 315–324, 1998.

Wolters, E. L. A., Roebeling, R. A. and Feijt, A. J.: Evaluation of cloud-phase retrieval methods for SEVIRI on Meteosat-8 using ground-based lidar and cloud radar data, J. Appl. Meteorol. Climatol., 47, 1723–1738, doi:10.1175/2007JAMC1591.1, 2008.

Yang, P., Liou, K. N., Wyser, K. and Mitchell, D.: Parameterization of the scattering and absorption properties of individual ice crystals, J. Geophys. Res., 105, 4699–4718, doi:10.1029/1999JD900755, 2000.

Yao, B., Liu, C., Yin, Y., Liu, Z., Shi, C., Iwabuchi, H. and Weng, F.: Evaluation of cloud properties from reanalyses over East Asia with a radiance-based approach, , 1033–1049, 2020.

Yeh, T. C.: Some aspects of the thermal influences of the Qinghai-Tibetan plateau on the atmospheric circulation, Arch. Meteorol. Geophys. Bioclimatol. Ser. A, 31, 205–220, doi:10.1007/BF02258032, 1982.

Zhang, C.: Madden-Julian Oscillation, Reviews, 43, RG2003, doi:10.1029/2004RG000158, 2005.

Zhang, C. and Dong, M.: Seasonality in the Madden-Julian oscillation, J. Clim., 17, 3169–3180, doi:10.1175/1520-0442(2004)017<3169:SITMO>2.0.CO;2, 2004.

Zhang, D., Wang, Z. and Liu, D.: A global view of midlevel liquid-layer topped stratiform cloud distribution and phase partition from CALIPSO and CloudSat measurements, J. Geophys. Res., 115, D00H13, doi:10.1029/2009JD012143, 2010.

Zhang, Z. and Platnick, S.: An assessment of differences between cloud effective particle radius retrievals for marine water clouds from three MODIS spectral bands, J. Geophys. Res. Atmos., 116, D20215, doi:10.1029/2011JD016216, 2011.

Zhang, Z., Werner, F., Cho, H.-M., Wind, G., Platnick, S., Ackerman, A. S., Di Girolamo, L., Marshak, A. and Meyer, K.: A framework based on 2-D Taylor expansion for quantifying the impacts of subpixel reflectance variance and covariance on cloud optical thickness and effective radius retrievals based on the bispectral method, J. Geophys. Res. Atmos., 121, 7007–7025, doi:10.1002/2016JD024837, 2016.

Zhao, G. and Di Girolamo, L.: Cloud fraction errors for trade wind cumuli from EOS-Terra

instruments, Geophys. Res. Lett., 33, L20802, doi:10.1029/2006GL027088, 2006.

Zhao, G., Di Girolamo, L., Diner, D. J., Bruegge, C. J., Mueller, K. J. and Wu, D. L.: Regional changes in Earth's color and texture as observed from space over a 15-year period, IEEE Trans. Geosci. Remote Sens., 54, 4240–4249, doi:10.1109/TGRS.2016.2538723, 2016.

Zhao, W., Peng, Y., Wang, B., Yi, B., Lin, Y. and Li, J.: Comparison of three ice cloud optical schemes in climate simulations with community atmospheric model version 5, Atmos. Res., 204, 37–53, doi:10.1016/j.atmosres.2018.01.004, 2018.

Tables

Table 1. Summary of datasets used in this study.

Products	Version	Parameters	Resolution (km)	Period	References
2B-CLDCLASS-LIDAR	P1_R054	Cloud layers, phases	1.4 x 1.8	2007-2010	(Wang et al., 2012)
2C-ICE	P1_R054	Extinction coefficient, effective radius	1.4 x 1.8 x 0.24	2007-2010	(Deng et al., 2010)
ECMWF-AUX	P_R05	Meteorology	1.4 x 1.8 x 0.24	2007-2010	(Cronk and Partain, 2017)
MYD021KM	C6.1 L1B	Reflectance, BT	1	2003-2017	(Savtchenko et al., 2004)
MYD03	C6.1 L2	Geolocation, Ocean/land Mask	1	2003-2017	(Savtchenko et al., 2004)
MYD06	C6.1 L2	Cloud Phase, spatial heterogeneity	1	2003-2017	(Savtchenko et al., 2004)
--		MJO index	--	2007-2010	(Wheeler and Hendon, 2004)
--		ENSO index	--	2003-2017	(Wolter and Timlin, 1998)

Table 2. Comparison of MODIS and CC cloud phase. Number in parentheses represents the percentage (%) of CC phase reported as to be MODIS phase.

	CloudSat-CALIPSO cloud phase						
MODIS cloud phase	Clear	Ice only	Liquid only	Mixed only	Ice above liquid	Ice above mixed	sum
Clear	2 408 080 (93.1)	1 218 244 (29.2)	642 659 (28.6)	12 609 (1.23)	333 723 (11.1)	8 268 (0.59)	4 623 583
Liquid	168 625 (6.52)	265 985 (6.38)	1 485 900 (66.1)	144 441 (14.09)	854 024 (28.5)	90 234 (6.49)	3 009 209
ice	9 058 (0.35)	2 594 258 (62.21)	87 895 (3.91)	668 181 (65.2)	1 650 626 (55.1)	1 017 196 (73.2)	6 027 214
undetermined	1 872 (0.07)	91 511 (2.19)	32 207 (1.43)	200 050 (19.5)	158 352 (5.28)	274 433 (19.7)	758 425
sum	2 587 635	4 169 998	2 248 661	1 025 281	2 996 725	1 390 131	14 418 431

~~CloudSat-CALIPSO cloud phase~~

MODIS cloud phase	Clear	Ice only	Liquid only	Mixed only	Ice above liquid	Ice above mixed	sum
Clear	2 193 923 (91.2)	1 059 415 (29.2)	597 838 (28.4)	11 903 (1.40)	305 350 (10.5)	5 813 (0.6)	4 174 242
Liquid	185 470 (7.71)	227 625 (6.28)	1 380 378 (65.6)	67 412 (7.91)	783 585 (27.0)	40 179 (4.1)	2 684 649
ice	23 576 (0.98)	2 259 465 (62.31)	87 086 (4.14)	603 590 (70.9)	1 636 624 (56.4)	720 588 (74.3)	5 330 929
undetermined	2 741 (0.11)	79 482 (2.19)	38 450 (1.83)	168 921 (19.8)	177 710 (6.12)	202 513 (20.9)	669 817
sum	2 405 710	3 625 987	2 103 752	851 826	2 903 269	969 093	12 859 637

Table 3. Cloud occurrence frequency (%) derived from 2B-CLDCLASS-LIDAR. In ocean-vs-land section, t~~T~~he number outside parentheses represents both land and ocean. First number in parentheses is for ocean and the second one is for land. In the single-vs-multiple cloud layers section, first number in parentheses represents single layer and the second number is for multiple layer.

	~~Ice only~~	~~Liquid only~~	~~Mixed only~~	~~Ice above liquid~~	~~Ice above mixed~~	~~Others~~	~~All clouds~~
~~MAM~~	~~28.8(32.0,19.8)~~	~~17.4(15.5,22.0)~~	~~5.5(4.6,7.3)~~	~~20.7(20.2,23.6)~~	~~6.2(5.9,7.0)~~	~~0.71(0.58,1.1)~~	~~79.3(78.8,80.7)~~
~~JJA~~	~~30.5(34.7,19.6)~~	~~12.8(10.9,17.4)~~	~~7.3(6.9,7.9)~~	~~25.0(22.1,35.3)~~	~~9.5(8.9,11.4)~~	~~0.66(0.53,1.0)~~	~~85.8(84.1,92.7)~~
~~SON~~	~~28.1(32.9,17.8)~~	~~15.9(12.4,22.8)~~	~~6.6(6.1,6.9)~~	~~21.7(22.5,23.0)~~	~~7.8(8.3,7.7)~~	~~0.70(0.54,1.0)~~	~~80.8(82.8,79.2)~~
~~DJF~~	~~23.8(26.5,16.4)~~	~~21.5(20.5,22.9)~~	~~5.4(5.2,5.0)~~	~~20.3(21.8,19.1)~~	~~6.0(6.4,5.7)~~	~~0.74(0.72,0.69)~~	~~77.7(81.2,69.7)~~
~~Annual~~	~~27.8(31.3,18.4)~~	~~16.9(14.8,21.3)~~	~~6.2(5.7,6.8)~~	~~21.9(21.7,25.3)~~	~~7.4(7.4,8.0)~~	~~0.70(0.60,0.94)~~	~~80.9(81.7,80.6)~~
	Ice only	Liquid only	Mixed only	Ice above liquid	Ice above mixed	Others	All clouds
				Ocean vs. Land			
MAM	29.2(32.1, 20.7)	16.5(15.2, 20.0)	5.9(4.8, 8.1)	18.8(18.5, 21.1)	7.6(7.2, 8.8)	0.74(0.59, 1.1)	78.7(78.4, 79.9)
JJA	31.5(35.6, 20.8)	12.2(10.6, 15.8)	7.7(7.1, 8.7)	22.5(20.0, 31.5)	11.9(11.1, 14.9)	0.68(0.53, 1.1)	86.5(85.0, 92.9)
SON	29.0(33.9, 18.3)	15.2(12.5, 20.5)	6.9(6.2, 7.8)	20.4(20.9, 21.9)	10.0(10.4, 10.5)	0.72(0.57, 1.1)	82.4(84.4, 80.0)
DJF	24.5(27.2, 17.1)	20.2(19.6, 21.2)	6.1(5.6, 5.9)	18.7(20.1, 17.1)	7.7(8.1, 7.5)	0.80(0.80, 0.74)	78.0(81.5, 69.6)
Annual	28.6(32.2, 19.2)	16.0(14.5, 19.4)	6.7(5.9, 7.6)	20.1(19.9, 22.9)	9.3(9.2, 10.4)	0.74(0.62, 1.0)	81.4(82.3, 78.1)
				Single vs. multiple cloud layers			
Annual	28.6 (20.0, 8.6)	16.0(14.0, 2.0)	6.7(6.6, 0.1)	20.1(13.8, 6.3)[1]	9.3(6.2, 3.1)[1]	0.74 (--, 0.74)	81.4(40.6, 40.8)[2]

1: The single and multiple layers are for the overlying ice clouds only.

2: All single-layer clouds are the summation of single-layer ice-only (20.0%), liquid-only (14.0%), and mixed-only (6.6%) clouds, while all multi-layer clouds include multi-layer ice-only (8.6), liquid-only (2.0), mixed-only (0.1), ice-above-liquid (20.1), ice-above-mixed (9.3) and others (0.74) clouds.

Table 4. Average of cloud properties for the five cloud groups over ocean and land.

	~~Ice only~~					~~Liquid only~~		~~Ice above liquid~~					~~Ice above mixed~~						~~Mixed only~~
	~~T_c~~[1]	~~B_c~~[2]	~~H_c~~[3]	~~τ_c~~	~~Re_c~~	~~T_w~~	~~T_c~~	~~B_c~~	~~H_c~~	~~τ_c~~	~~Re_c~~	~~T_w~~	~~T_c~~	~~B_c~~	~~H_c~~	~~τ_c~~	~~Re_c~~	~~T_m~~	~~T_m~~
											Ocean								

Formatted: Centered

Formatted: Centered

Formatted: Centered

MAM	14.9	11.5	2.9	2.4	31.3	2.0	14.8	11.8	2.4	1.8	28.5	2.9	15.0	12.0	2.5	1.9	27.9	9.4	13.1
JJA	14.9	10.9	3.5	3.0	32.6	2.2	14.9	11.5	2.7	2.1	29.2	3.2	15.2	11.9	2.7	1.9	27.4	9.4	14.2
SON	15.1	11.1	3.4	2.8	31.6	2.1	15.1	11.6	2.8	2.1	28.6	3.2	15.3	12.0	2.8	1.9	27.3	9.5	14.1
DJF	15.3	11.4	3.4	2.4	29.7	2.2	15.2	11.9	2.7	1.7	27.1	3.1	15.4	11.9	2.9	1.8	26.6	9.3	13.2
Land																			
MAM	13.7	10.1	3.1	4.3	36.8	3.4	14.3	11.4	2.2	1.8	29.5	3.6	14.3	11.7	2.1	1.7	28.9	8.8	10.3
JJA	14.9	10.4	3.9	4.7	35.8	3.6	15.0	11.9	2.5	1.6	28.0	3.9	15.1	12.3	2.2	1.4	27.1	9.3	12.3
SON	14.5	10.6	3.4	3.8	34.1	3.4	14.8	11.7	2.5	1.9	28.3	3.7	15.0	12.0	2.4	1.8	27.8	9.2	11.1
DJF	13.7	10.0	3.2	3.5	33.5	2.9	14.8	11.5	2.6	1.5	26.9	3.6	15.0	11.8	2.6	1.5	26.0	8.9	9.3

	Ice only					Liquid only	Ice above liquid						Ice above mixed						Mixed only
	T_i[1]	B_i[2]	GH_i[3]	τ_i	Re_i	T_w	T_i	B_i	GH_i	τ_i	Re_i	T_w	T_i	B_i	GH_i	τ_i	Re_i	T_m	T_m
Ocean																			
MAM	14.9	11.4	2.9	2.5	31.1	1.9	14.8	11.9	2.3	1.6	27.4	2.7	15.0	11.5	2.8	2.5	29.8	8.7	12.6
JJA	14.9	10.8	3.5	3.1	32.4	2.1	14.9	11.6	2.6	1.8	28.1	2.9	15.1	11.5	3.0	2.5	29.1	8.7	13.8
SON	15.1	11.1	3.4	2.9	31.4	2.0	15.0	11.7	2.6	1.8	27.6	2.9	15.3	11.5	3.1	2.5	29.1	8.7	13.8
DJF	15.2	11.3	3.4	2.5	29.5	2.1	15.1	12.0	2.5	1.5	26.0	2.9	15.3	11.5	3.2	2.4	28.3	8.5	12.1
Land																			
MAM	13.6	10.0	3.1	4.1	36.6	3.3	14.2	11.4	2.2	1.6	28.6	3.5	14.2	11.3	2.3	2.2	30.6	8.2	9.7
JJA	14.9	10.4	3.9	4.7	35.5	3.4	15.0	11.9	2.4	1.5	27.3	3.7	15.1	11.9	2.5	1.9	28.8	8.5	11.7
SON	14.5	10.6	3.4	3.7	33.9	3.3	14.8	11.7	2.4	1.6	27.3	3.4	14.9	11.6	2.7	2.4	29.4	8.4	10.5
DJF	13.7	10.0	3.2	3.1	33.1	2.9	14.8	11.6	2.5	1.4	26.0	3.3	14.9	11.4	2.9	2.0	27.8	8.0	8.4

1: T for cloud top
2: B for cloud base
3: GH for geometric thickness
Subscripts: i for ice, w for water and m for mixed

Table 5. Average reflectance at 0.645, 1.375, 1.64 and 2.13 μm (unit: %) and brightness temperature at 8.55 and 11.03 μm (unit: K).

	Clear						Ice only						Liquid only					
	$R_{0.645}$	$R_{1.375}$	$R_{1.64}$	$R_{2.13}$	$BT_{8.55}$	$BT_{11.03}$	$R_{0.645}$	$R_{1.375}$	$R_{1.64}$	$R_{2.13}$	$BT_{8.55}$	$BT_{11.03}$	$R_{0.645}$	$R_{1.375}$	$R_{1.64}$	$R_{2.13}$	$BT_{8.55}$	$BT_{11.03}$
MAM	3.83	.08	1.28	.93	293.5	295.5	13.1	5.44	5.98	3.70	275.7	274.9	15.9	.27	13.2	9.11	289.1	290.8
JJA	3.42	.08	1.13	.85	293.4	295.2	15.3	6.58	7.02	4.31	271.8	270.6	12.4	.22	9.8	6.66	289.6	291.1
SON	3.44	.09	1.04	.75	293.4	295.2	14.1	6.11	6.43	3.92	272.5	271.3	13.7	.21	10.7	7.21	289.2	290.7

Formatted: Centered
Formatted: Centered
Formatted: Centered
Formatted: Centered
Formatted: Centered
Formatted: Centered
Formatted: Centered
Formatted: Centered
Formatted: Centered

DJF	3.48	.07	1.07	.77	293.0	294.9	13.3	5.73	6.30	3.91	273.8	272.6	19.1	.41	15.3	10.2	286.0	287.5
Annual	3.57	.08	1.15	.84	293.4	295.2	14.0	5.99	6.46	3.97	273.4	272.3	15.7	.29	12.7	8.57	288.3	289.8
	Mixed only						Ice above liquid						Ice above mixed					
MAM	59.9	21.3	21.6	12.6	239.2	238.3	18.9	3.38	12.9	8.46	278.9	278.7	46.4	11.9	20.2	11.7	250.2	248.5
JJA	62.3	25.1	19.4	10.9	232.8	231.5	19.0	3.88	12.4	8.00	277.0	276.5	45.6	11.9	19.8	11.4	249.7	248.0
SON	58.7	23.6	18.4	10.3	232.3	230.9	18.6	3.89	12.0	7.73	276.5	275.9	43.7	11.7	18.5	10.6	248.7	247.0
DJF	55.4	19.0	20.5	11.8	239.1	238.1	20.0	3.49	13.4	8.60	276.7	276.1	44.7	11.3	19.5	11.1	249.0	247.2
Annual	59.3	22.5	19.9	11.3	235.5	234.3	19.1	3.67	12.6	8.18	277.3	276.8	45.0	11.7	19.5	11.2	249.4	247.7

Figures

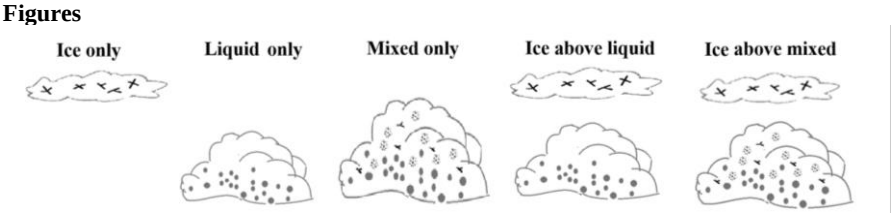

Figure 1. Schematic of cloud classification based on the 2B-CLDCLASS-LIDAR product.

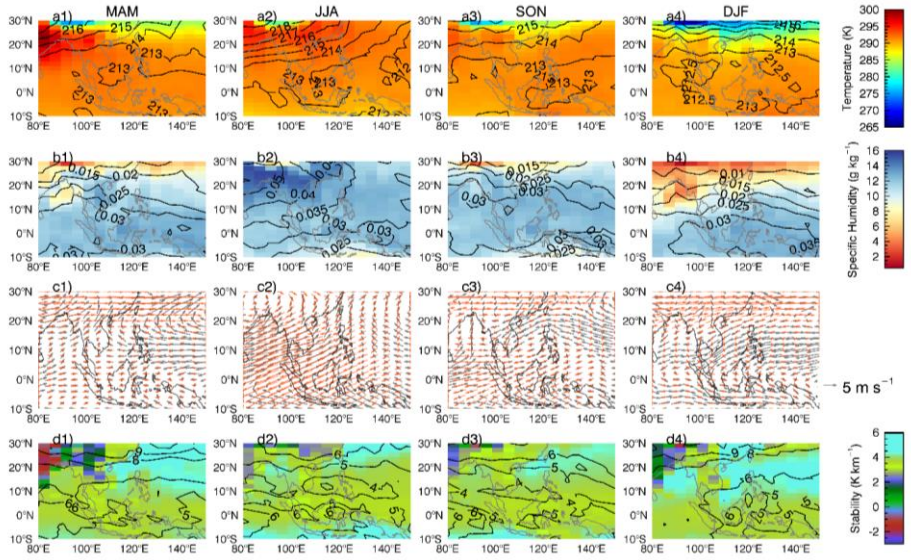

Figure 2. Temperature (a1-a4), specific humidity (b1-b4), wind field (c1-c4), and static stability (d1-d4) derived from the ECMWF-AUX data: shade for 850 hPa, contour for 180 hPa, grey vectors for wind field at 850 hPa and red vectors for 180 hPa.

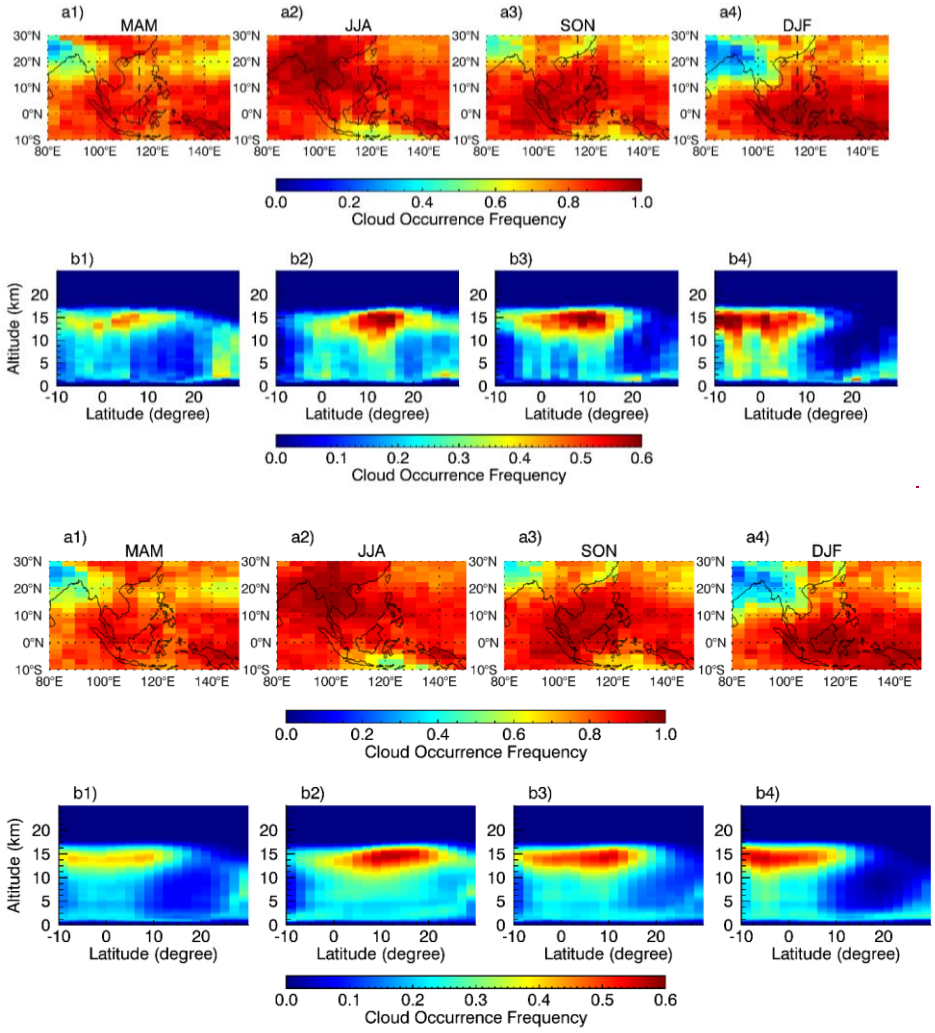

Figure 3. Cloud occurrence frequency derived from 2B-CLDCLASS-LIDAR: a1) -a4) for horizonal distribution and b1-b4) for zonal latitude-altitude cross section~~. at the longitude of 115°E, indicated by the dashed line at the upper panels.~~

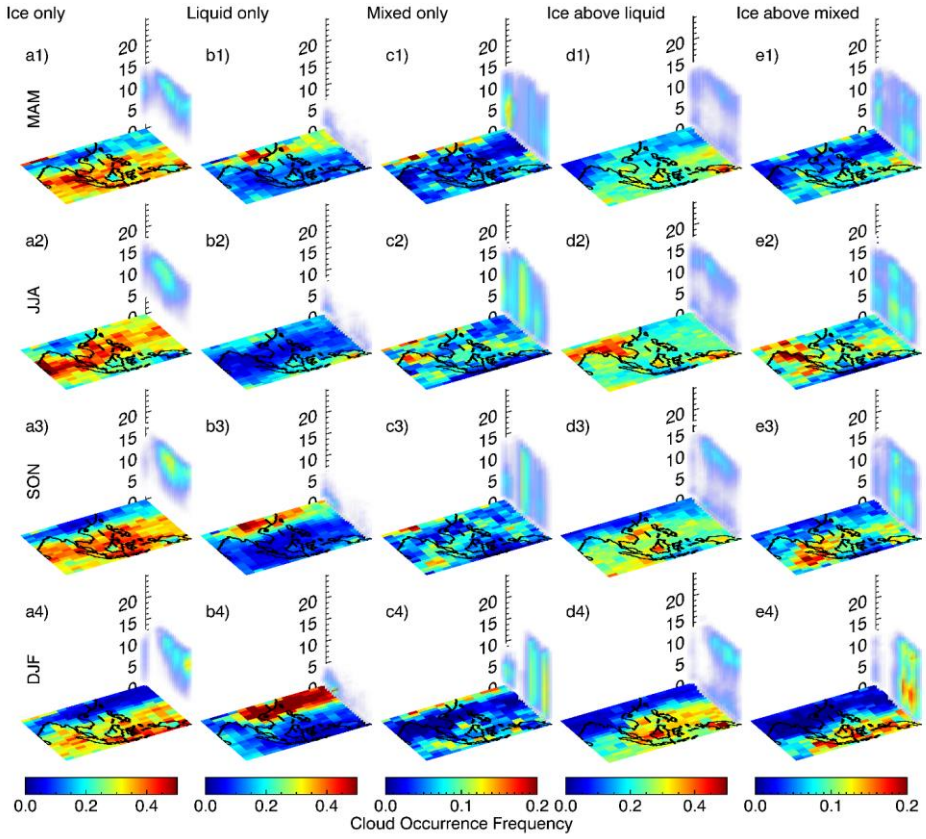
Ice only
Liquid only
Mixed only
Ice above liquid
Ice above mixed
a1)
b1)
c1)
d1)
e1)
a2)
b2)
c2)
d2)
e2)
a3)
b3)
c3)
d3)
e3)
a4)
b4)
c4)
d4)
e4)
MAM
JJA
SON
DJF
20
15
10
5
0.0
0.2
0.4
0.1
Cloud Occurrence Frequency

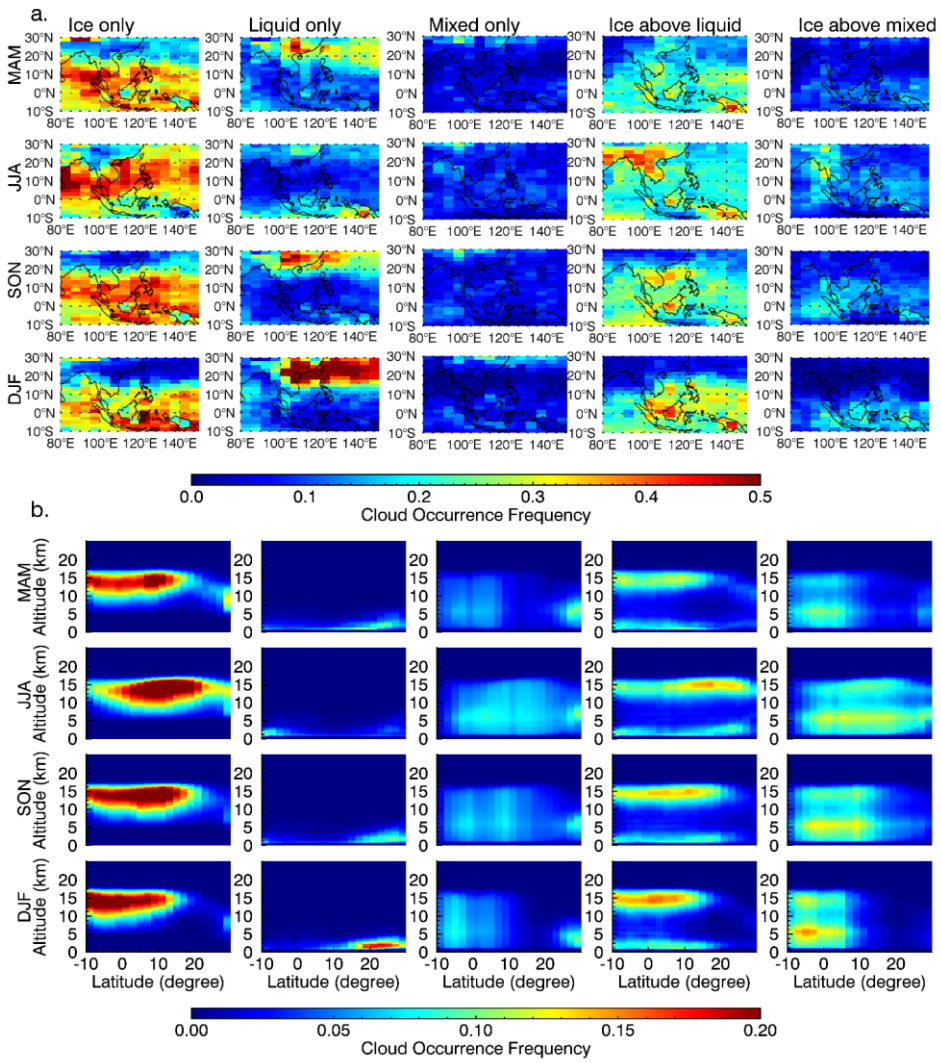

Figure 4. Occurrence frequency of the five cloud groups derived from 2B-CLDCLASS-LIDAR: a) for horizonal distribution and b) for zonal latitude-altitude cross section. ~~Note that colorbar scale is different for the five cloud groups. Cross-section is for the longitude centered at 115°E indicated by the black dashed line. Zero values of vertical frequency are set to be transparent for a better view.~~

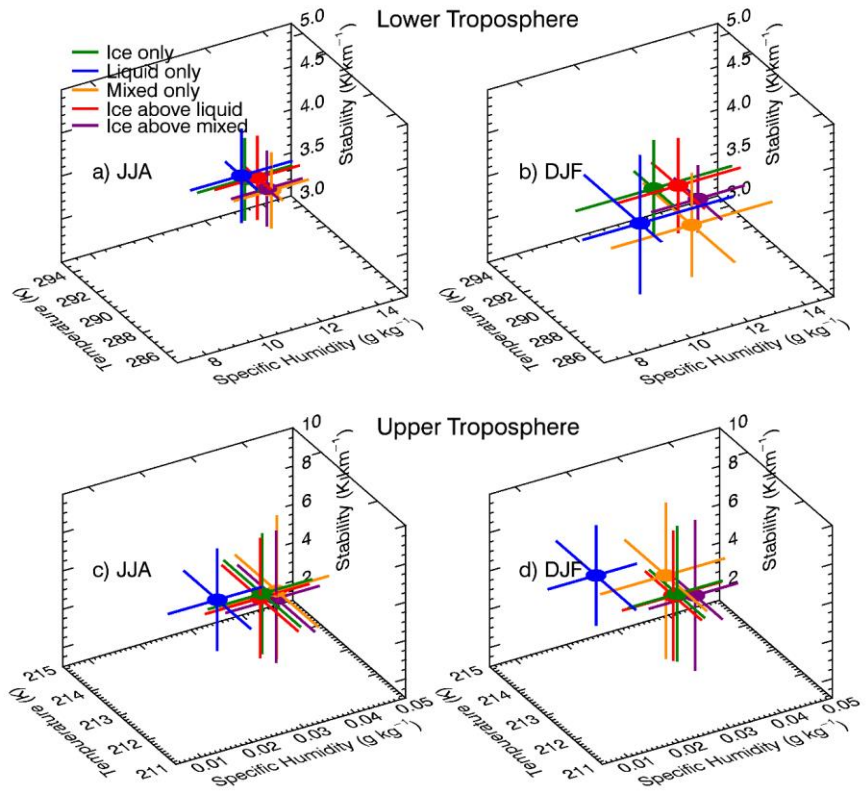
Lower Troposphere
Ice only
Liquid only
Mixed only
Ice above liquid
Ice above mixed
a) JJA
b) DJF
Stability (K km⁻¹)
Temperature (K)
Specific Humidity (g kg⁻¹)
Upper Troposphere
c) JJA
d) DJF

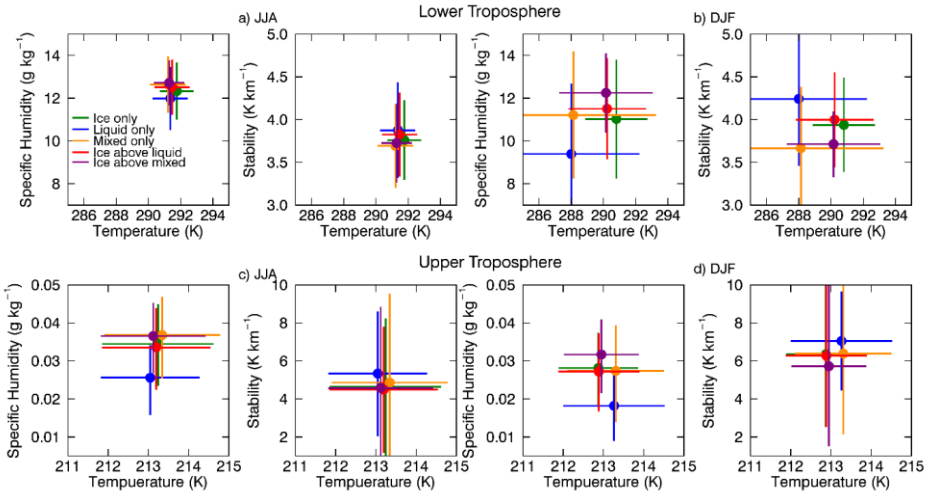

Figure 5. Mean and standard deviation of meteorological variables over ocean for the five cloud groups.

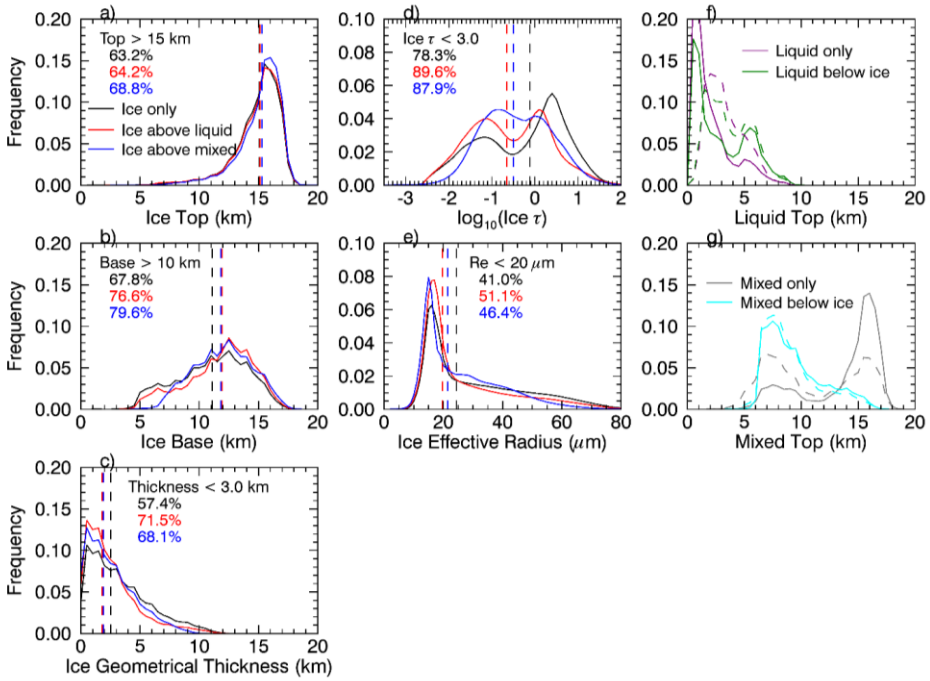
a)
Top > 15 km
63.2%
64.2%
68.8%
Ice only
Ice above liquid
Ice above mixed
Frequency
Ice Top (km)
d)
Ice τ < 3.0
78.3%
89.6%
87.9%
log10(Ice τ)
f)
Liquid only
Liquid below ice
Liquid Top (km)
b)
Base > 10 km
67.8%
76.6%
79.6%
Ice Base (km)
e)
Re < 20 μm
41.0%
51.1%
46.4%
Ice Effective Radius (μm)
g)
Mixed only
Mixed below ice
Mixed Top (km)
c)
Thickness < 3.0 km
57.4%
71.5%
68.1%
Ice Geometrical Thickness (km)

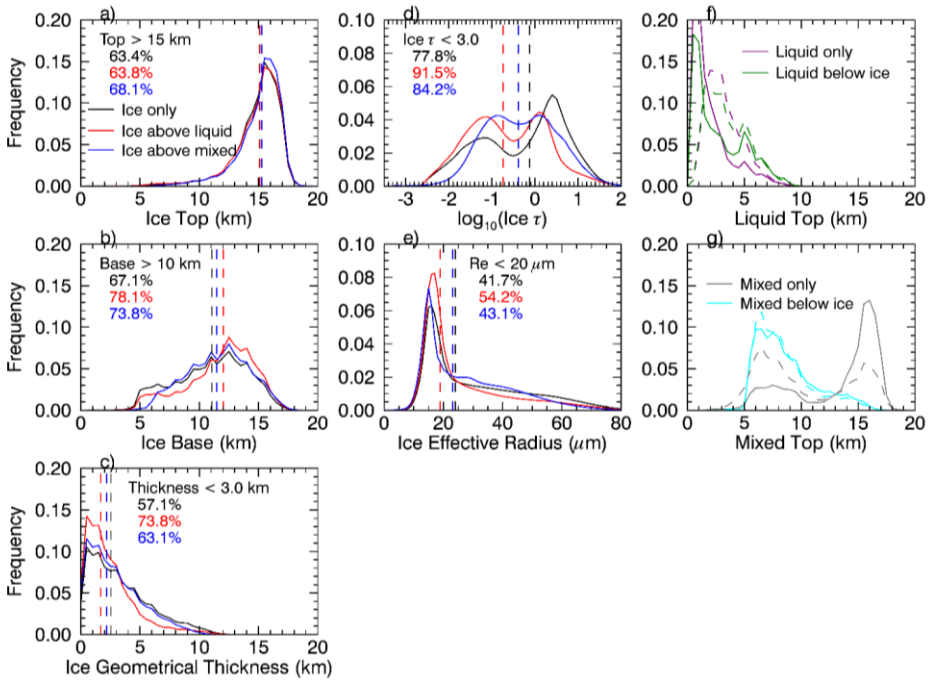

Figure 6. Annual PDFs of a) cloud top, b) base, c) geometric thickness, d) optical depth and e) effective radius for ice clouds including both ocean and land; The vertical dashed lines in a)-e) indicate the median values of the PDFs; f) cloud top for liquid-only cloud and the liquid below ice and g) cloud top for mixed-only ~~cloud~~ and the mixed cloud below ice. In f) and g), solid and dashed ~~line~~curves are for ocean and land, respectively. Cloud top and base bins adopt an interval of 0.5 km. Ice τ and Re bins use an interval of 0.1 in logscale and 1 μm, respectively.

Formatted: Centered

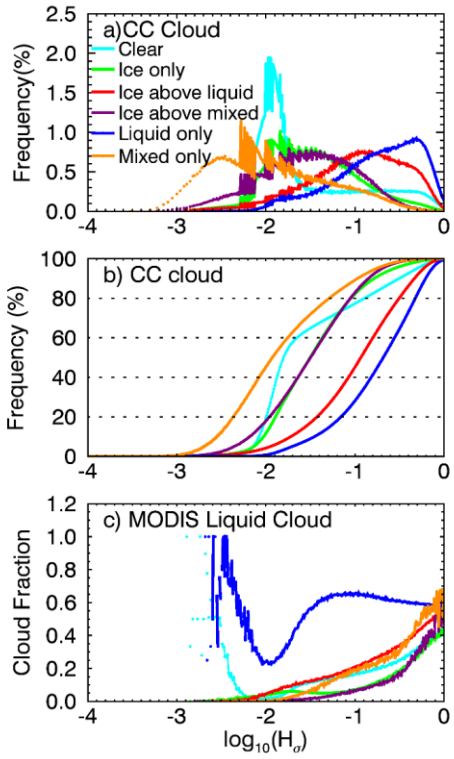
a)CC Cloud
Clear
Ice only
Ice above liquid
Ice above mixed
Liquid only
Mixed only
Frequency(%)
b) CC cloud
Frequency (%)
c) MODIS Liquid Cloud
Cloud Fraction
log10(Ha)

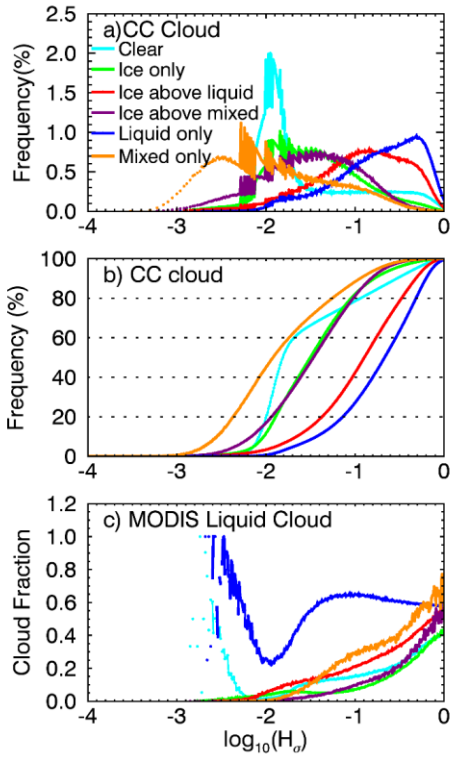

Figure 7. a) Annual PDFs of spatial heterogeneity for CC clear sky and the five cloud groups; b) same as a) but for CDF; c) liquid cloud fraction in the 5 km x5 km surrounding of the collocated CC-MODIS pixel derived from the MYD06 IR cloud phase retrievals. H_σ bin interval is 0.01 in log scale.

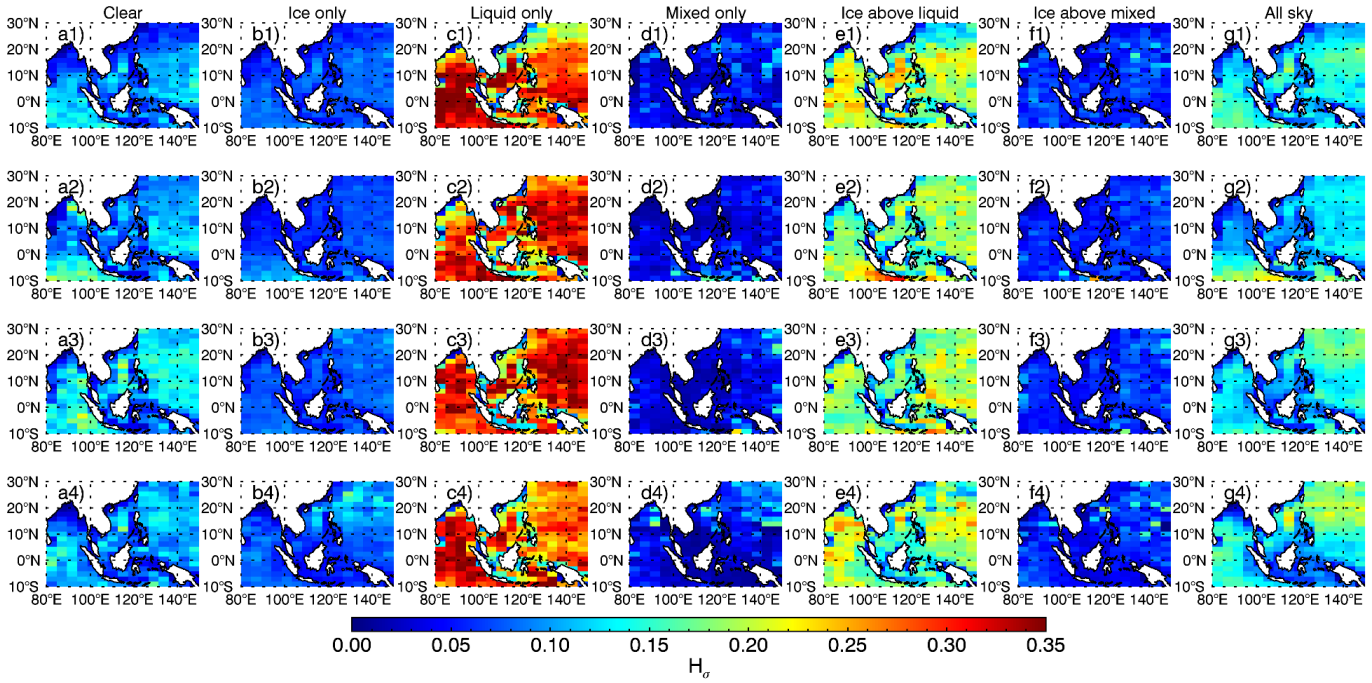
Clear
Ice only
Liquid only
Mixed only
Ice above liquid
Ice above mixed
All sky
a1)
b1)
c1)
d1)
e1)
f1)
g1)
a2)
b2)
c2)
d2)
e2)
f2)
g2)
a3)
b3)
c3)
d3)
e3)
f3)
g3)
a4)
b4)
c4)
d4)
e4)
f4)
g4)
30°N
20°N
10°N
0°N
10°S
80°E 100°E 120°E 140°E
0.00 0.05 0.10 0.15 0.20 0.25 0.30 0.35
H_σ

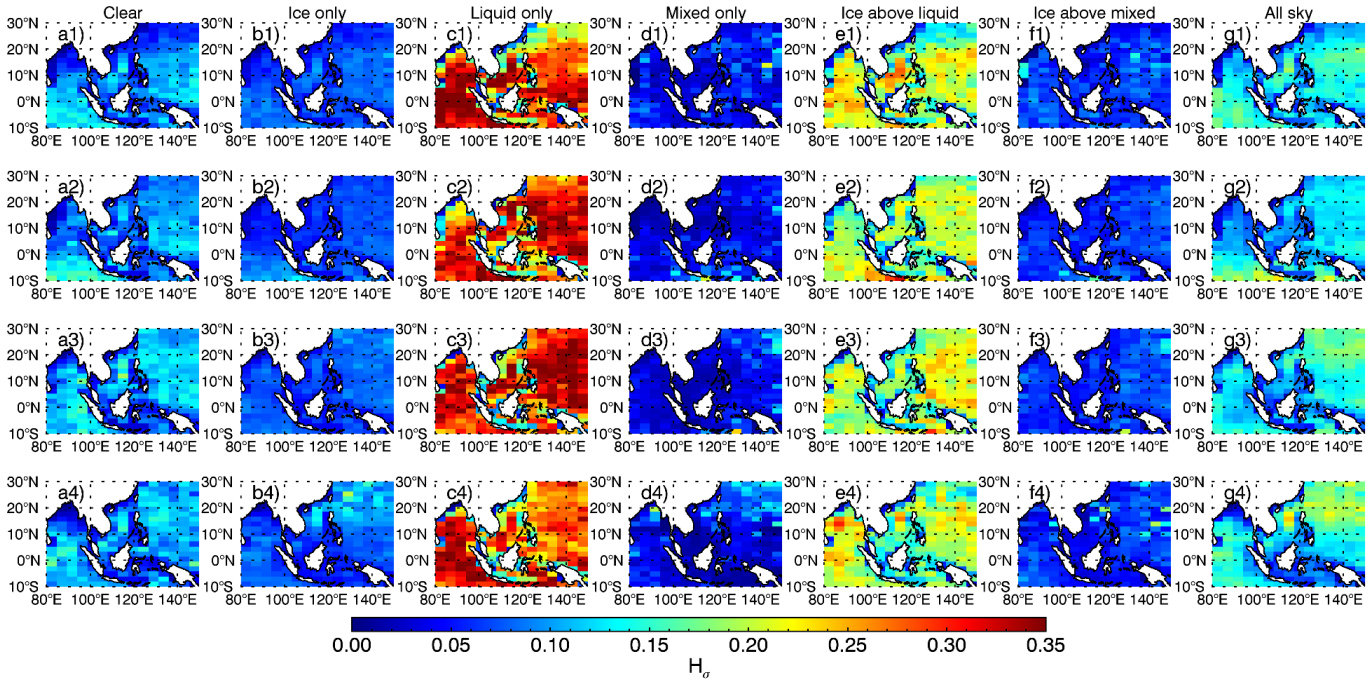

Figure 8. Spatial distributions of H_σ for clear sky, the five cloud groups and all sky: from top to bottom panels for MAM, JJA, SON and DJF, respectively.

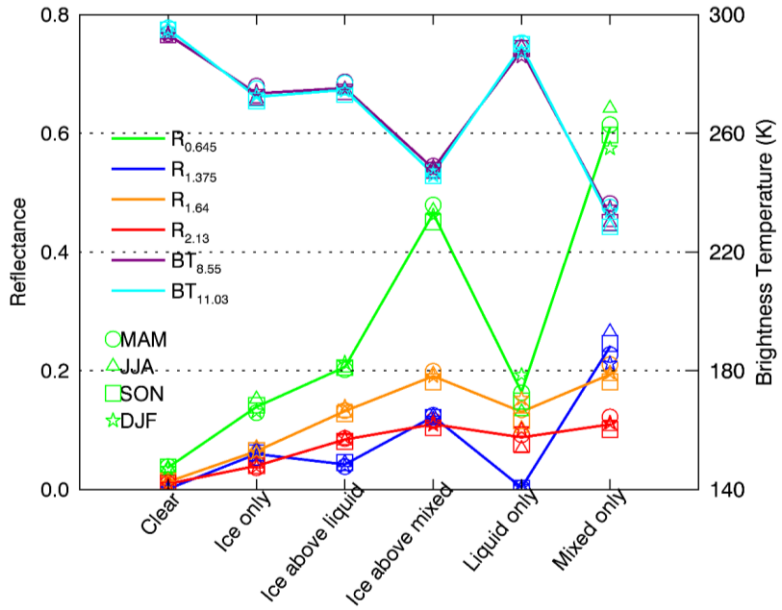
0.8
0.6
0.4
0.2
0.0
300
260
220
180
140
Reflectance
Brightness Temperature (K)
$R_{0.645}$
$R_{1.375}$
$R_{1.64}$
$R_{2.13}$
$BT_{8.55}$
$BT_{11.03}$
MAM
JJA
SON
DJF
Clear
Ice only
Ice above liquid
Ice above mixed
Liquid only
Mixed only

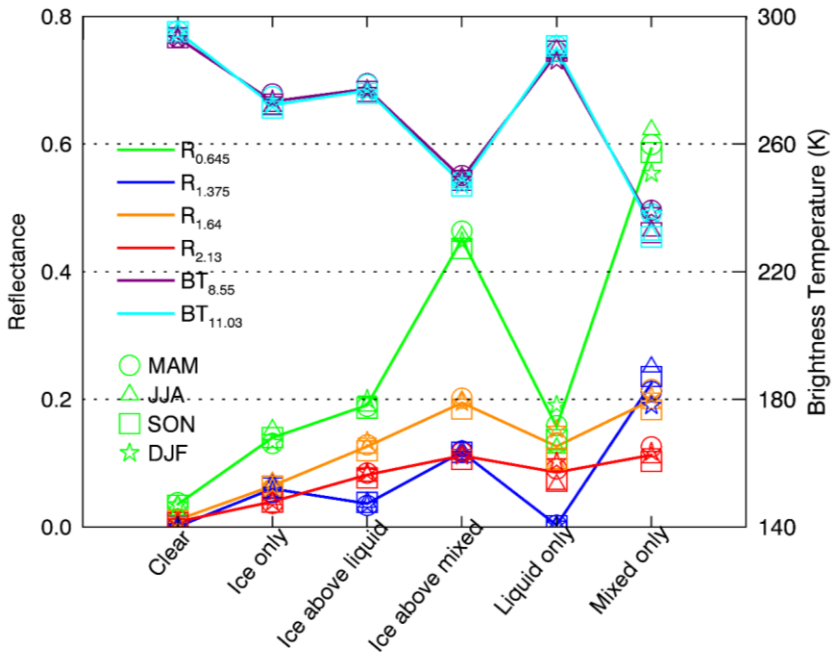

Figure 9. Average reflectance and brightness temperatures over ocean for clear sky and the five cloud groups, including all solar zenith angles. The sold lines represent annual mean and symbols denote seasonal averages.

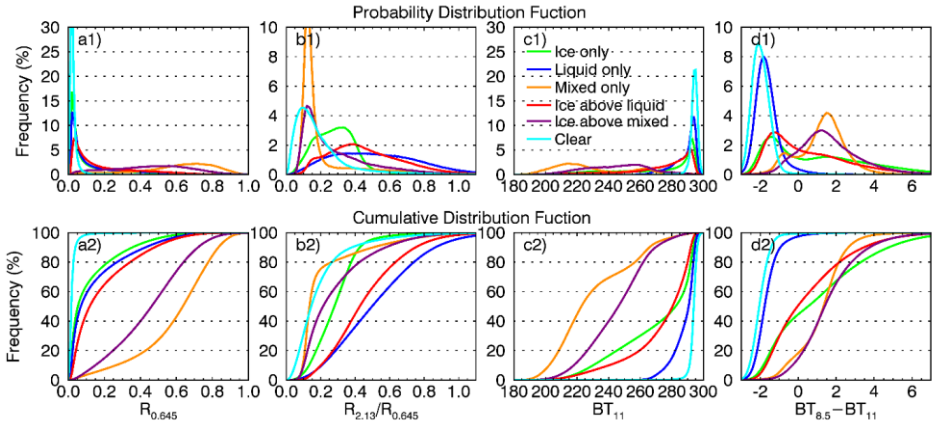

5

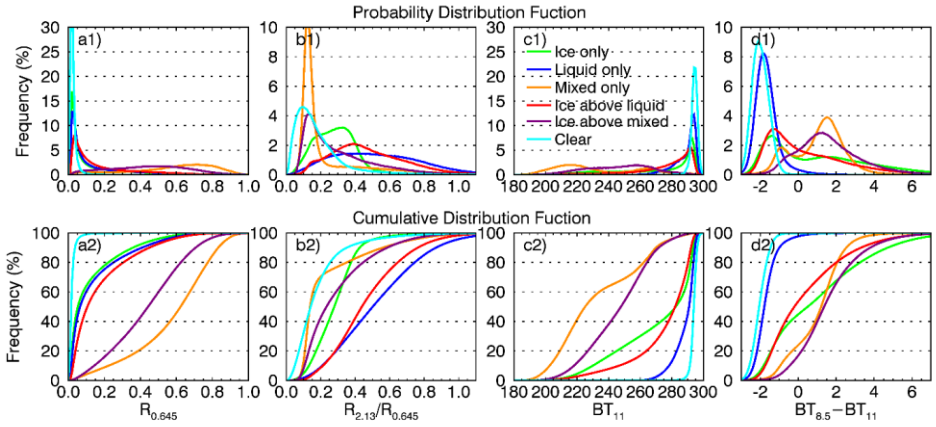

Figure 10. The annual PDFs and CDFs of reflectance at 0.645 μm, reflectance ratio, BT at 11 μm and BTD between 8.5 and 11 μm. The intervals for reflectance, reflectance ratio, BT and BTD are 0.01, 0.01, 1 K and 0.1 K, respectively.

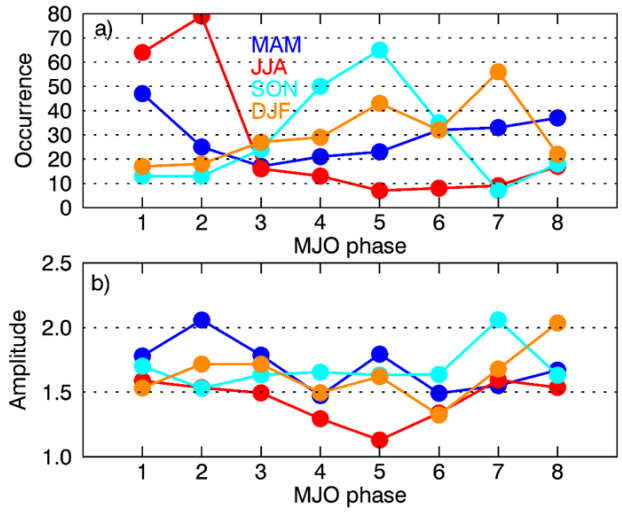

Figure 11. A statistical summary of strong MJO phases with amplitude > 1 from 2007-2010.

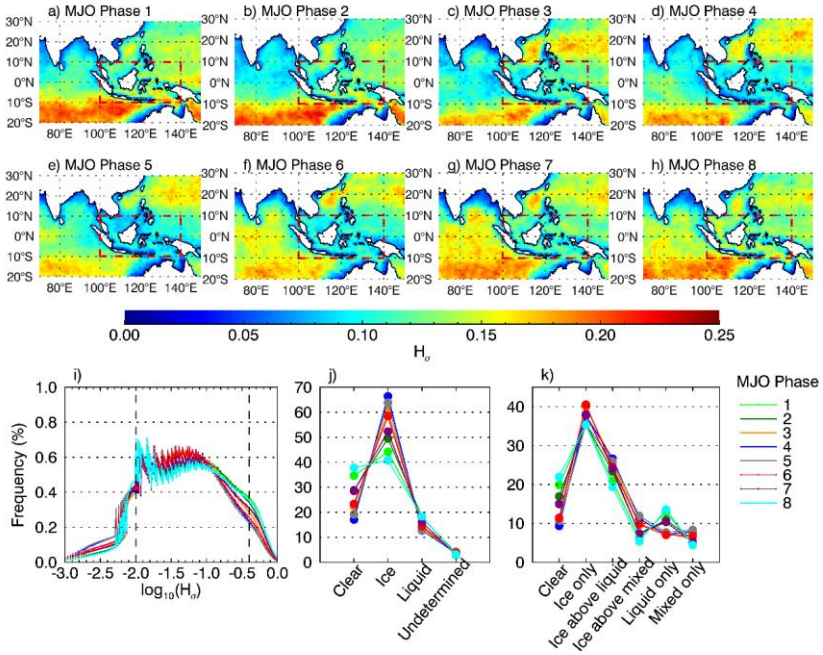
a) MJO Phase 1
b) MJO Phase 2
c) MJO Phase 3
d) MJO Phase 4
e) MJO Phase 5
f) MJO Phase 6
g) MJO Phase 7
h) MJO Phase 8
30°N
20°N
10°N
0°N
10°S
20°S
80°E 100°E 120°E 140°E
0.00 0.05 0.10 0.15 0.20 0.25
H_σ
i)
j)
k)
Frequency (%)
$\log_{10}(H_\sigma)$
Clear
Ice
Liquid
Undetermined
Ice only
Ice above liquid
Ice above mixed
Liquid only
Mixed only
MJO Phase
1
2
3
4
5
6
7
8

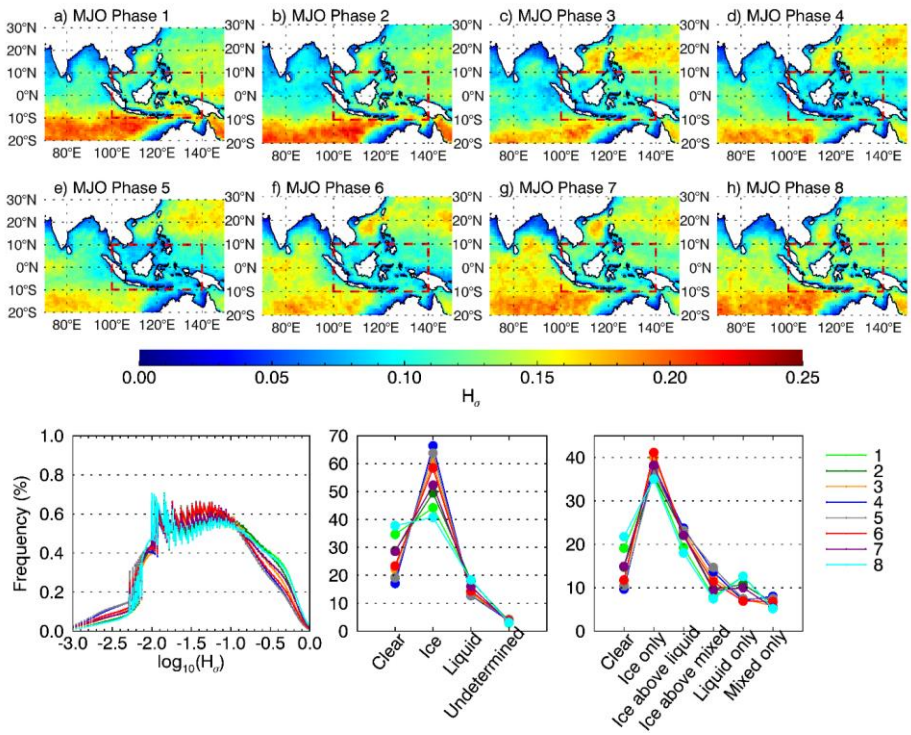

Figure 12. Cloud phase characteristics in different MJO Phases: a)-h) spatial distributions of all-sky H_σ derived from MYD06; i) PDF of all-sky H_σ derived from MYD06 over the Maritime continents (the red dashed box in each panel); j) occurrence frequency of clear sky, ice, liquid and undetermined clouds from MYD06 (unit:%); k) same as j) but for clear sky and five groups derived from the 2B-CLDCLASS-LIDAR product.

Formatted: Centered

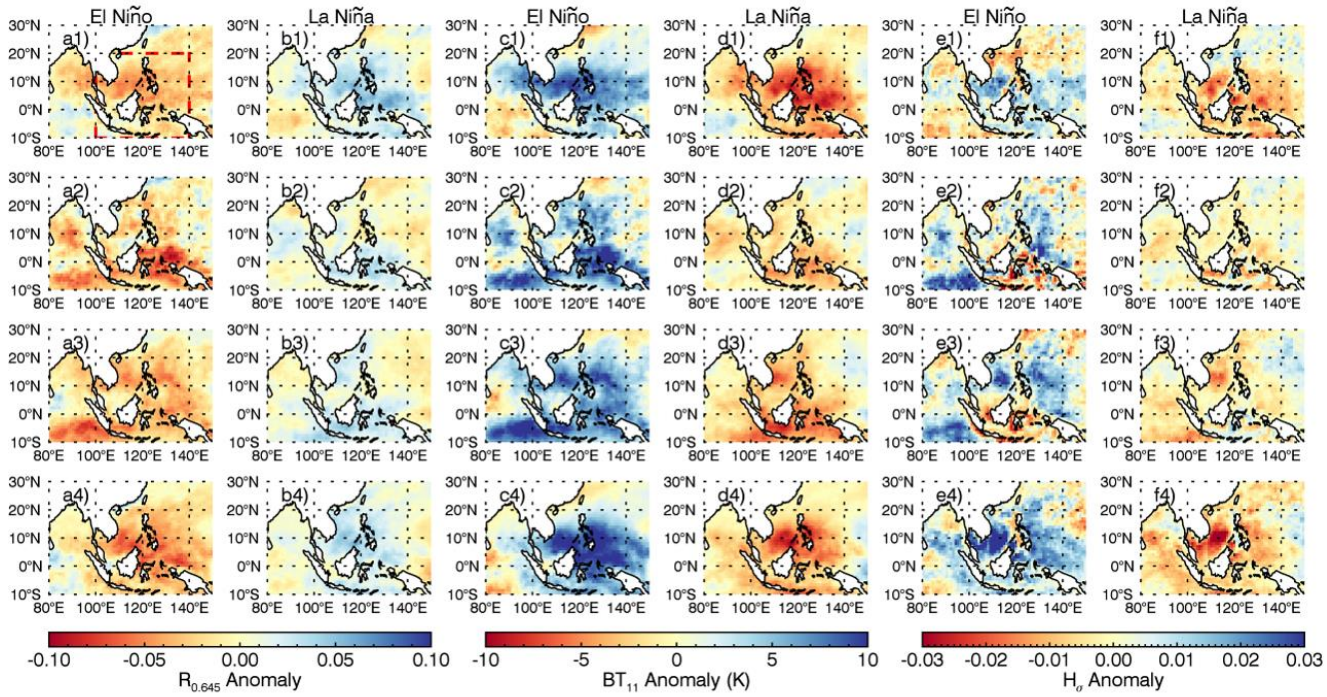
El Niño
La Niña
El Niño
La Niña
El Niño
La Niña
a1)
b1)
c1)
d1)
e1)
f1)
a2)
b2)
c2)
d2)
e2)
f2)
a3)
b3)
c3)
d3)
e3)
f3)
a4)
b4)
c4)
d4)
e4)
f4)
30°N
20°N
10°N
0°N
10°S
80°E
100°E
120°E
140°E
-0.10
-0.05
0.00
0.05
0.10
R0.645 Anomaly
-10
-5
0
5
10
BT11 Anomaly (K)
-0.03
-0.02
-0.01
0.00
0.01
0.02
0.03
Ho Anomaly

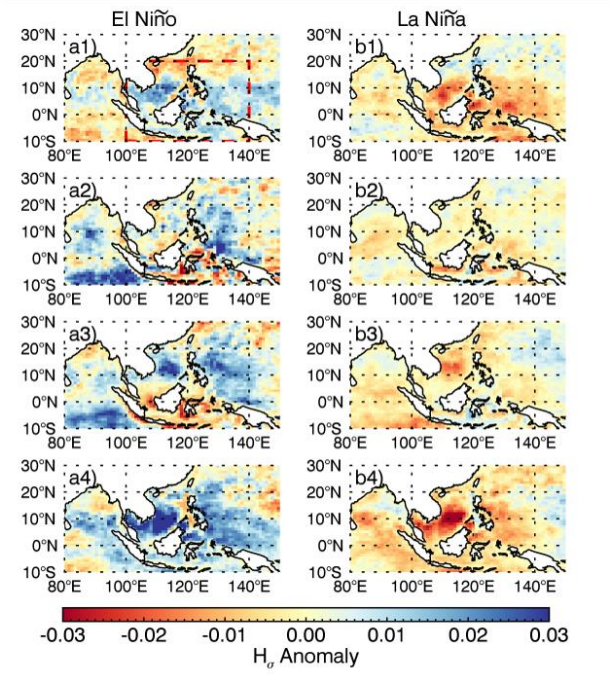

Figure 13. ~~Reflectance, brightness temperature and~~ Sspatial heterogeneity anomaly in El Niño and La Niña year: from top to bottom for MAM, JJA, SON and DJF.

Formatted: Width: 8.5", Height: 11"

Formatted: Centered

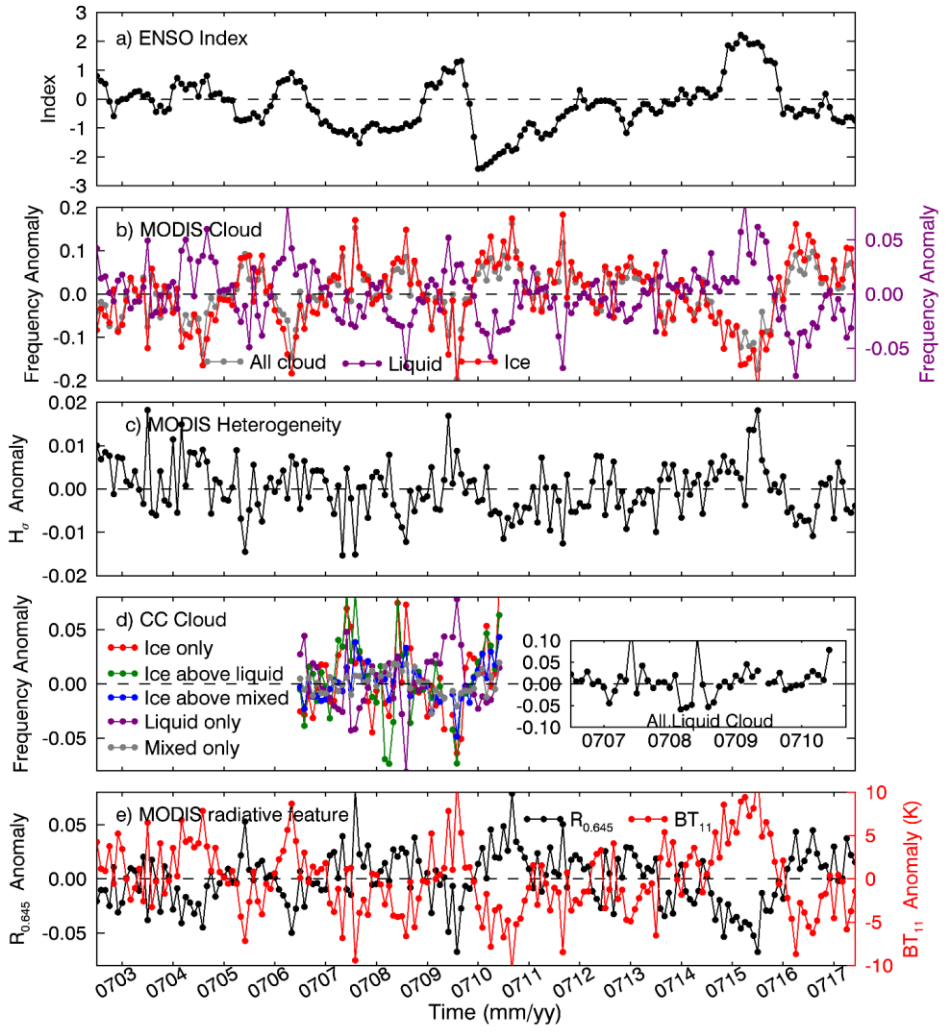
a) ENSO Index
Index
b) MODIS Cloud
Frequency Anomaly
All cloud
Liquid
Ice
c) MODIS Heterogeneity
H_σ Anomaly
d) CC Cloud
Ice only
Ice above liquid
Ice above mixed
Liquid only
Mixed only
All Liquid Cloud
e) MODIS radiative feature
$R_{0.645}$ Anomaly
$R_{0.645}$
BT_{11}
BT_{11} Anomaly (K)
0703 0704 0705 0706 0707 0708 0709 0710 0711 0712 0713 0714 0715 0716 0717
Time (mm/yy)

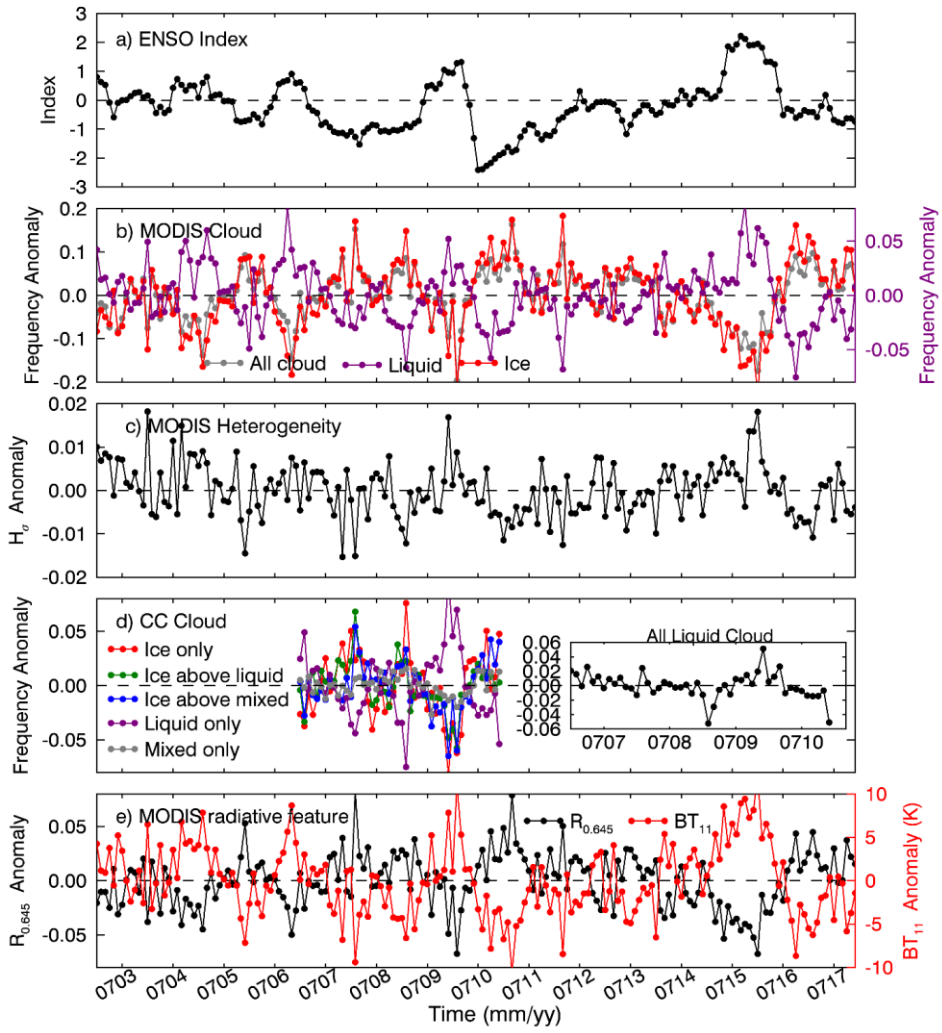

Figure 14. ENSO index and monthly anomaly of cloud, spatial heterogeneity and radiation in the region represented by the dashed-red box in Fig. 13a1.